Neural correlates of performance monitoring during discrete and continuous tasks

THÈSE N^{O} 8269 (2018)

PRÉSENTÉE LE 2 FÉVRIER 2018
À LA FACULTÉ DES SCIENCES ET TECHNIQUES DE L'INGÉNIEUR
CHAIRE FONDATION DEFITECH EN INTERFACE DE CERVEAU-MACHINE
PROGRAMME DOCTORAL EN GÉNIE ÉLECTRIQUE

ÉCOLE POLYTECHNIQUE FÉDÉRALE DE LAUSANNE

POUR L'OBTENTION DU GRADE DE DOCTEUR ÈS SCIENCES

PAR

Michael Eric Anthony PEREIRA

acceptée sur proposition du jury:

Prof. D. N. A. Van De Ville, président du jury
Prof. J. D. R. Millán Ruiz, directeur de thèse
Prof. R. Knight, rapporteur
Prof. F. Vidal, rapporteur
Prof. F. Hummel, rapporteur

ÉCOLE POLYTECHNIQUE
FÉDÉRALE DE LAUSANNE

Suisse
2018

"Also, I'm not completely convinced that a PC-mouse tracking task [...] is the most ecological scenario one could have thought of."

Anonymous reviewer

Acknowledgements

I was extremely lucky during these five years to be surrounded by the most incredible people, both in terms of scientific knowledge and human qualities. I hope I will be worthy of the time and effort they spent helping me and that I can pay them back even if only a little.

First of all, I would like to sincerely thank my supervisor, **Prof. José del R. Millán** for guiding me while allowing me to explore my own research direction(s) and for being optimistic, supportive and always excited by new findings. I am also immensely grateful to my mentor **Dr. Aleksander Sobolewski**, who spent countless hours patiently demolishing my flawed analyses, shaky claims, bad presentations and naive writing. He tought me how to think like a scientist, for the good or for the bad and is also a good friend with whom I shared beers and skiing adventures. I am also indebted to my friend and colleague **Dr. Iñaki Iturrate**, with whom I spent countless hours discussing ideas of new experiments over coffee. He allowed me to jump into some great projects and was available night and day to correct, support and orient me during my writing of the thesis. Lately, I was honored to work with **Dr. Nathan Faivre**, who introduced me to the field of metacognition, gave a whole new insight to our EEG-fMRI project and seems to be willing to devote an unlimited time from his busy schedule to correct my elucubrations on metacognition. I also wish to thank **Dr. Stéphanie Martin**. She was also especially helpful in improving (or at least she tried) my writing skills and supported me during the ups and downs of the end of the thesis. I am sorry for abusing her kindness by recording her for eight different experiments.

I benefitted from the support of great undergrad students who undoubtedly helped me with my different projects and side-projects: **Arnaud Desvachez, Frédéric Giraud, Luana Serafini, Gisong Kim, Marie Duc, Damien Jones and Ruslan Aydarkhanov**. I am also very grateful to **Prof. Dimitri Van De Ville** for our collaboration on the EEG-fMRI project. He providing us with his immense knowledge of fMRI, making the study what it is and surely further improving it before it is published. Thank you also Dimitri for accepting to be the president of the jury when you already had three other PhD defenses that week. The EEG-fMRI project would not have been possible without the devoted help of **Loan Mattera** and **Dr. Roberto Martuzzi**. Furthermore, I am very grateful to **Prof. Robert Knight**, for believing in my research to the point of providing me with invaluable ECoG and intracranial data which I unfortunately did not have enough time to torture but which I have the firm intention to crunch (and squeeze) further in the following months. Thank you Bob also for accepting me in your lab for a stay to learn the dos and don'ts of ECoG analyses and for accepting to read this thesis… Thank you also to all the **Knightlab** at UC Berkeley for a great stay and interesting discussions, and especially to **Colin Hoy** who spent countless hours sharing his impressive data analysis skills and scientific insight. It was also nice to put a face on the people who went through the burden of recording data with my buggy protocol: **Katarina** and **Arjen**. I also want to thank **Prof. Franck Vidal** for changing his busy schedule and making the trip from Marseilles to be part of my thesis committee and **Prof. Friedhelm** Hummel for accepting to be the internal expert. Finally, I wish to thank **Thomas Kemp** and **Dietmar Schill** from Sony Deutschland GmbH for funding my first six months of PhD, which allowed me to switch from music and sound signal processing and machine learning to neuroscience.

At a more personal level, I wish to thank all my colleagues for making the lab such a great working place. I truly enjoyed endless scientific discussions with **Tiffany**, **Marija** and **Christoph**, the boundless good mood of Luca, travelling to Romania with **Robert** to go to **Tom**'s wedding, teasing **Bastien**, frightening **Sareh**, unwillingly smelling **Zahra's** perfume, drinking with **Arnaud**, hearing **Kyuhwa**'s near-to-death experiences in the mountains. Life would have also been much less enjoyable without the great company and support of my friends **Pit**, **Jul**, **Marco**, **Mélina**, **Lucien**, **Delphine**, **Jérome**, **Max**, **Flavio** and **Amédé**. I am also very grateful for the support of **Silvia** during the toughest days of the last years and for her diligently reviewing my last chapter while I am writing this acknowledgment. Finally, thank you to my **family** and **family-in-law** for their support and most importantly, to my **mother**, **grandmother** and **father** for being such great persons and pushing me to study. Lastly, thank you to my life companion **Vanessa**, for sharing my life, providing me with the necessary emotional support, convincing me about the sense of pursuing a PhD and especially not divorcing while I was writing this thesis. I wish to dedicate her this thesis.

Lausanne, le 9 octobre 2017

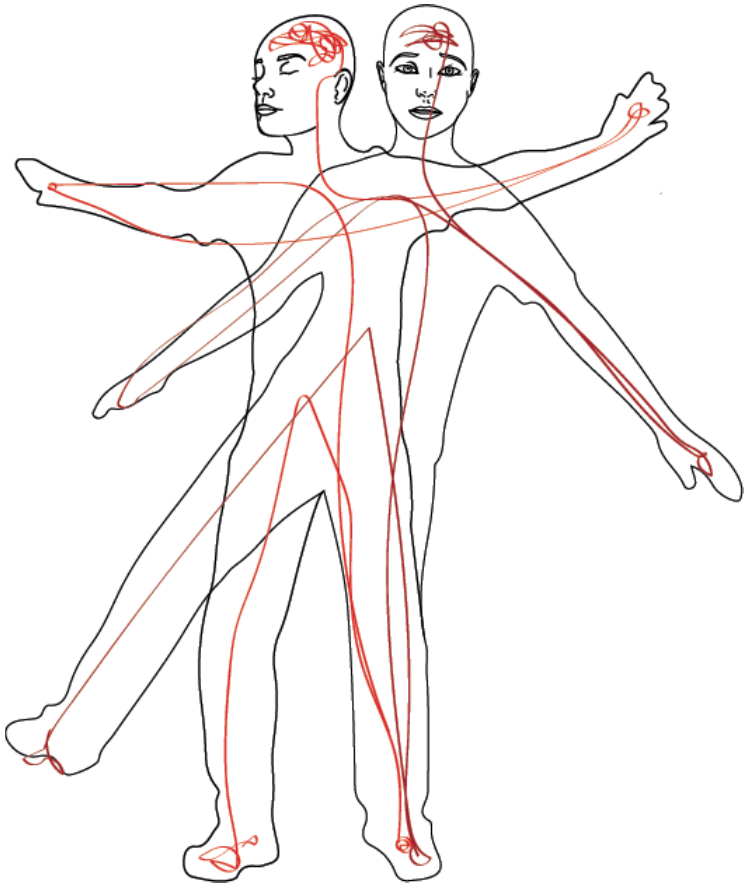

Vanessa Lorenzo, 2017

How my life companion sees my research after reading the introduction.

Abstract

Monitoring our actions is a key function of the brain for adaptive and successful behavior. Actions can be discrete such as when pressing a button, or continuous, such as driving a car. Moreover, we evaluate our actions as correct or erroneous (*performance monitoring*) and this appraisal of performance comes with various levels of confidence (*metacognition*). However, studies of performance monitoring have focused on discrete actions and are mostly agnostic to metacognitive judgments. The objective of this thesis was to extend the study of performance monitoring to more ecological conditions, in which monitoring occurs during continuous motor tasks under various degrees of error and confidence level.

We first investigated the role of actions in performance monitoring together with metacognitive judgments, using simultaneous EEG and fMRI recordings. To dissociate the role of motor actions, we designed an experimental paradigm in which subjects had to rate their confidence level about an action that they had either performed themselves (a button press) based on a decision or passively observed (a virtual hand displayed). We found correlates of confidence in both condition, in the EEG and in the supplementary motor area (SMA). Furthermore, we found that subject showed better metacognitive performances when they were the agents of the action. This difference was further emphasized for subjects that showed higher activations of a network previously linked to motor inhibition and comprising the pre-SMA and inferior frontal gyrus (IFG). Our results imply that the SMA plays a primary role in the monitoring of performance, irrespectively of a commitment to a decision and the resulting action. Our findings also suggest that the additional neural processes leading to decisions and actions can inform the metacognitive judgments.

In the following chapters, we ask whether electrophysiological correlates of performance monitoring can be found in less experimentally constrained paradigms for which motor output continuous unfolds and visual feedback is not segregated into discrete events. By decomposing the unfolding hand kinematics during a visuo-motor tracking task into periodic acceleration pulses –henceforth referred to as sub-movements, we found three electrophysiological markers that could possibly be linked to performance monitoring. Firstly, we found an ERP in the SMA, time-locked to sub-movements which encoded the deviation of the hand, 110 ms before. Secondly, we found high-gamma activity in the ACC and SMA of epileptic patients, that was phase-locked to sub-movements. Thirdly, we found a transient modulation of mu oscillations over the ipsilateral sensorimotor cortices that depended on sub-movement amplitude.

Altogether, these results provide a strong contribution in the understanding of the neurophysiological processes underlying performance monitoring. Our work proposes a methodological framework to study electrophysiological correlates of performance monitoring in less controlled paradigms during which continuous visual feedback has to be constantly integrated into motor corrections. In the conclusion chapter, we propose a way of extending current models of performance monitoring and decision making to explain the findings of this thesis by considering continuous motor tasks as a succession of decision making processes under time pressure and uncertainty.

Keywords

Brain, monitoring, performance, action, metacognition, EEG, ERP, fMRI, ECoG, SMA.

Résumé

Le suivi de la performance (SP) de nos actions est une fonction clé du cerveau pour un comportement adaptatif et réussi. Les actions peuvent être discrètes, par exemple lorsque l'on appuie sur un bouton, ou continues, comme conduire une voiture. De plus, nous évaluons nos actions comme correctes ou erronées (*SP*) et cette évaluation de la performance s'accompagne de divers niveaux de confiance (*métacognition*). Cependant, les études de SP ont mis l'accent sur des actions discrètes et sont essentiellement agnostiques des jugements métacognitifs. L'objectif de cette thèse était d'étendre l'étude de SP à des conditions plus écologiques, dans lesquelles le suivi se produit lors de tâches motrices continues avec différents degrés d'erreur et de niveau de confiance.

Nous avons d'abord étudié le rôle des actions lors du SP combinés à des jugements métacognitifs, en utilisant des enregistrements simultanés EEG et IRMf. Pour dissocier le rôle des actions motrices, nous avons conçu un paradigme expérimental dans lequel les sujets devaient évaluer leur niveau de confiance à propos d'une action qu'ils avaient réalisée eux-mêmes (en appuyant sur un bouton) ou observée passivement. Nous avons trouvé des corrélats des jugements de confiance dans les potentiels évoqués (PE) dans l'aire motrice supplémentaire (AMS). Fait intéressant, l'AMS était également activé lorsque les sujets étaient incertains des actions qu'ils avaient commises ou observées. De plus, nous avons trouvé que les sujets présentaient de meilleures performances métacognitives quand ils étaient les agents de leurs actions. Cette amélioration était plus marquée pour les sujets présentant des activations plus élevées d'un réseau précédemment lié à l'inhibition motrice et comprenant le pré-AMS et le gyrus frontal inférieur. Nos résultats impliquent que l'AMS joue un rôle prépondérant dans le SP, indépendamment d'une prise de décision et de l'action qui en résulte. Nos résultats suggèrent également que les processus neuronaux complémentaires menant à des décisions et des actions peuvent améliorer les jugements métacognitifs.

Dans les chapitres suivants, cherché des corrélats électrophysiologiques du SP dans des paradigmes moins restreints expérimentalement pour lesquels l'action est continue et le retour visuel n'est pas divisé en événements discrets. En décomposant la cinématique de la main au cours d'une tâche de tracking visuo-moteur en impulsions d'accélération périodiques - appelées ci-après sous-mouvements, nous avons trouvé trois marqueurs électrophysiologiques qui pourraient être liés au SP. Tout d'abord, nous avons trouvé un PE dans l'AMS, couplé aux sous-mouvements et qui encodait la déviation de la main, 110 ms auparavant. Deuxièmement, nous avons trouvé une activité gamma dans le cortex cingulaire antérieur et l'AMS de patients épileptiques, qui était couplée en phase aux sous-mouvements. Troisièmement, nous avons trouvé une modulation transitoire de l'amplitude des oscillations mu au dessus des cortex sensorimoteurs ipsilatéraux par l'accéleration des sous-movements.

En résumé, ces résultats apportent une contribution importante à la compréhension des processus neurophysiologiques sous-jacents au SP. Notre travail propose un cadre méthodologique pour étudier les corrélats électrophysiologiques du SP dans des paradigmes moins contrôlés au cours desquels le retour visuel continu doit être constamment intégré à des corrections motrices. Dans la conclusion, nous proposons un moyen d'étendre les modèles actuels de SP et de prise de décision pour expliquer les résultats de cette thèse en considérant les tâches motrices continues comme une succession de processus décisionnels sous pression temporelle et incertitude.

Mots-clés

Cerveau, suivi, performance, action, metacognition, EEG, ERP, IRMf, ECoG, SMA

Contents

List of Figures

List of Tables

Chapter 1 Introduction

Our daily life is full of difficult choices we make by accumulating evidence in a changing environment. While we can take time to accumulate as much evidence as possible for some choices such as career paths or investments, other choices such as which street to take at an intersection need to be carried out within seconds with very limited evidence. After such fast choices, we typically get a sense of confidence concerning our actions. Arguably, confidence depends on the strength of the signal used for the decision: in broad daylight, we might quickly realize we made the wrong turn, leading to the sense of confidence of making the wrong decision and do a U-turn. On a rainy night however, even if we slow down before the intersection, we might not know whether we made the right or wrong turn. We then have a feeling of uncertainty and might for example stop to check the map. This ability to reflect over the accuracy of our own actions is referred to as metacognition (Koriat, 2006).

Until recently, two types of metacognitive abilities have been mainly studied separately: performance monitoring –the ability to detect our errors, and confidence judgments –the ability to reflect on our decisions (Yeung and Summerfield, 2012). Performance monitoring studies have mostly used speeded response tasks in which subjects appraise errors in a binary manner (i.e., a response is either correct or wrong). On the other hand, research on confidence judgments has relied on difficult perceptual tasks in which subjects were given enough time to answer in order to assume that the state of evidence accumulation at the decision time is sufficient to fully explain confidence. It is only recently that electrophysiological (Charles et al., 2013; Boldt and Yeung, 2015; Murphy et al., 2015) and computational modelling studies (Resulaj et al., 2009; Van Den Berg et al., 2016; Fleming and Daw, 2017) have started to integrate performance monitoring and confidence judgments.

Furthermore, both fields rely on highly controlled paradigms with experimentally segregated events that are convenient to combine with neuroimaging techniques. Such discrete paradigms usually comprise a decision task (type 1 task) leading to a response action in the form of a button press, followed by a (type 2) task in which subjects are asked to report their confidence on a scale. These studies have undoubtedly uncovered much of the neurophysiology of the performance monitoring system. However, they do not capture the full scope of our interactions with a continuous environment. In real-life situations, actions and sensory feedback have to be constantly monitored and cannot necessarily be broken down into sequences of well-defined events. When driving a car for example, one has to continuously adjust for small drifts. Such situations are more challenging to study due to the continuous flow of visual feedback that is constantly integrated into the ongoing action. Moreover, since errors trigger some adaptive mechanisms such as a slowing of the response time in the next trial (Danielmeier and Ullsperger, 2011), most studies of performance monitoring are confounded by such post-error adaptive mechanisms. One notable exception is when subjects passively observe errors committed by external agents (van Schie et al., 2004).

The objective of this thesis is to extend the study of performance monitoring to more ecological conditions, in which monitoring occurs under various degrees of error and confidence and during continuous motor task. Firstly, using combined EEG-fMRI, we measured ERPs and BOLD activation related to a signed measure of confidence ranging from error certainty to correctness certainty and passing through various levels of uncertainty. By including trials in which the subject was the agent of the error and trials in which the subject was only a passive observer, we could study the importance of action on confidence judgments and isolate a common neural substrate of performance monitoring independent from motor action and post-error adaptive changes. Secondly, using EEG and invasive recordings in epileptic patients, we went beyond traditional discrete paradigms and found neural correlates of performance monitoring during continuous movements under visual-guidance by segregating

the kinematics into series of overlapping sub-movements. Finally, we report an electrophysiological correlate of corrections in the ipsilateral cortex during continuous movements.

Before presenting and discussing the empirical results in the next chapters, we review the neurophysiological findings on performance monitoring (section 1.1), decision making and confidence judgments (section 1.2) as well as some recent work linking both (section 1.3). We then go a step further towards performance monitoring during continuous movements by giving a short overview of performance monitoring during reaching movements (section 1.4), which are less strictly experimentally segregated than button presses but still (arguably) unfold in a rather feedforward manner. Finally, we review what is known about performance monitoring during continuous movements during which feedfoward and feedback mechanisms are interdependent (section 1.5) and give a brief overview of the next chapters (section 1.6).

1.1 Performance monitoring

Most studies on performance monitoring have used speeded response tasks during which subjects have to make fast choices between two alternative responses (two-alternative forced choice task). In the Flanker's task for example, a row of five arrows is displayed. Subjects are required to press a left button if the central arrow points towards the left and to press a right arrow if it points towards the right in a limited amount of time. In most trials, the four flanking arrows point in the same direction. In a limited number of trials (typically 10-30%), the central arrow points towards the opposite direction and subjects tend to press the wrong button. Such trials are referred to as incongruent or conflicting. Subjects tend to correct their mistake even in the absence of sensory feedback (Rabbitt, 1966). Depending on the task parameters, errors can lead to post-error adjustments such as a slowing of the response time in the next trial (Danielmeier and Ullsperger, 2011). These behavioral results imply that some brain function is devoted to monitor our actions, hereby detecting errors and adapting subsequent behavior accordingly.

Neural correlates of performance monitoring were found in the anterior cingulate cortex (ACC). The firing rate of neurons in ACC increases after errors (Niki and Watanabe, 1979) and is related to subsequent adaptive changes (Shima and Tanji, 1998; Williams et al., 2004). Some neurons responding to errors also signaled reward omission while a different set of neurons encoded unexpected reinforcement (Ito et al., 2003). These findings led to the theory that the ACC monitors the consequence of actions and subsequent adaptive control mechanisms. Electrophysiological correlates of performance monitoring were found at the scalp level using electroencephalography (EEG). When averaging signals time-locked to erroneous button presses an event-related potential (ERP) consisting in a negative deflection –the error-related negativity (ERN), was found over the frontal midline of the scalp (Falkenstein et al., 1991; Gehring et al., 1993). This negativity is followed by a positivity which is referred to as the Pe. Interestingly, when subjects observe an external agent committing an error, an ERP of similar shape and scalp topography can be observed (van Schie et al., 2004). The later ERPs can be reliably decoded at the single-trial level by machine learning algorithms (Ferrez and Millán, 2005; Chavarriaga et al., 2010) and were used in the field of brain-machine interfaces (BMI) to guide a robotic hand to a specific target by trial-and-error (Iturrate et al., 2015).

Early evidence suggested that the neural substrate of the ERN lied in the ACC (Dehaene et al., 1994). Later studies confirmed this hypothesis using combined EEG-fMRI (Debener et al., 2005). The lateral prefrontal cortex (LPFC) was also found to be involved in the cortical network underlying the ERN (Edwards et al., 2012). Its role could be to provide top-down support to processes involved in the task, a process referred to as cognitive control (MacDonald, 2000; Kerns et al., 2004). Lesion studies also support the role of the LFPC for error monitoring, as patients with LPFC damage were found to correct less their errors, and showed an ERP of similar amplitudes after error and correct responses (Gehring and Knight, 2000). This suggests that although the LPFC is not the generator of the ERN, it is closely linked to the error monitoring circuitry.

Furthermore, various recent studies using invasive recordings in different brain structures have found early correlates of error processing preceding ACC activity, in particular the supplementary motor area (SMA) (Bonini et al., 2014), the internal globus pallidus (Ruiz et al., 2014) or the anterior insula (Bastin et al., 2017).

Next, we review the three main theoretical accounts of performance monitoring: the mismatch theory, the response conflict theory and the reinforcement learning theory.

The mismatch theory

The latency of the ERN around 60 ms after response onset is considered too early to rely on sensory feedback only (Rodriguez-Fornells et al., 2002). Moreover, a similar deflection but with reduced amplitude is observed after correct responses (Vidal et al., 2000), suggesting that the neural processing underlying the ERN is not only responsible for signaling errors but could instead index the comparison process leading to error detection (Falkenstein et al., 2000; Vidal et al., 2000; Coles et al., 2001; Rodriguez-Fornells et al., 2002). The ERN would then index an early comparison between an efferent copy of the motor response (Shadmehr and Mussa-Ivaldi, 1994; Wolpert et al., 1995; Desmurget and Grafton, 2000) and (instantaneous) state of evidence (Resulaj et al., 2009; Van Den Berg et al., 2016). This mismatch theory was supported by the fact that a deafferented patient had normal ERNs (Allain et al., 2014).

The response conflict theory

In parallel, some researchers observed that the ACC was also active during correct response under conflicting stimuli (Carter et al., 1998; Botvinick et al., 1999) leading to the influential theory of response conflict theory (Botvinick et al., 2001). This theory posits that the ACC monitors the occurrence of conflicting response signals; conflicting stimuli lead to the co-activation of competing response signals. When a strong prepotent but erroneous response signal is not overridden in time by a slower correct signal an error occurs. The response conflict theory has been both supported (Danielmeier et al., 2009) and refuted (Burle et al., 2008) using computational models.

The reinforcement learning theory

A third account of performance monitoring named reinforcement learning theory is based on studies showing modulations of the mesoencephalic dopaminergic system by reward (Schultz and Dickinson, 2000). This theory proposes that the ERN is generated by a negative reinforcement signal emerging from dopaminergic projections between the basal ganglia and the ACC (Holroyd and Coles, 2002). The reinforcement learning theory received support from computational models (Frank et al., 2005), but was also criticized on the basis that slow unmyelinated dopaminergic connections to the ACC are too slow to modulate the ERN (Ullsperger et al., 2014). The theory remains nevertheless valid even if fast electrophysiological correlates of performance monitoring do not directly depend on dopaminergic circuit.

Nowadays, new theories have striven to integrate the multiple functions of the ACC (Kolling et al., 2016) in broader theories which encompass error, conflict and reinforcement learning. The ACC could thus predict error likelihood rather than error per se (Brown and Braver, 2005) or more generally action likelihood, whether good or bad (Alexander and Brown, 2011), refined recently (Brown and Alexander, 2017). Shenhav et al. have also proposed that the function of the ACC is to allocate control based on the resulting expected value of control (Shenhav et al., 2013).

1.2 Decision making and confidence judgment

In this section, we cover findings on metacognitive abilities, describing how subjects can accurately report their confidence (confidence judgment; type 2 task) about their performance in past actions (type 1 task). Models of confidence judgments have been linked to theories of decision making such as signal detection theory (SDT; Macmillan and Creelman 2004) or evidence accumulation (Gold and Shadlen, 2007). Studies have shown that the strength of neural activity preceding the action is related to confidence (Kiani and Shadlen, 2009; Gherman and Philiastides, 2015) and confidence is altered by microstimulation of neurons encoding sensory evidence (Kiani et al., 2014b).

Measuring metacognition is a difficult task due to the influence of confidence bias, the general tendency to respond with high or low confidence. Indeed, subjects with a propensity to answer with high confidence do not necessarily have better metacognitive abilities (i.e., overconfidence implies poor error detection). A less biased measure of metacognitive performance is to compute threshold decoders of the correctness of the type 1 response based on the confidence ratings. True positive and false positive rates can be computed for each threshold level and plotted in a two-dimensional plane as a receiver operating characteristic (ROC) curve (Galvin et al., 2003). The performance of the decoder can be measured as the area under the curve (AUC). One criticism of the AUC is that it is influenced by type 1 performance. Intuitively, it appears easier to make confidence

judgments on an easy type 1 task than on a difficult one. One approach to extract pure measures of metacognitive (type 2) performance is to keep type 1 performance constant by adjusting task difficulty with adaptive staircase procedures (Levitt 1971). Another approach is to normalize type 2 performance by type 1 performance. This implies the use of similar metrics for the two types of performance, as recently proposed by Maniscalco and Lau (Maniscalco and Lau, 2012, 2014).

Different brain regions seem to be involved in metacognitive evaluation of actions. In a seminal study, Fleming et al. found that metacognitive ability during a visual task depended on to the amount of grey matter in the frontal pole, but also to a lesser extent, in the DLPFC and ACC (Fleming et al., 2010). A follow-up fMRI study showed that BOLD activation in the right rostral prefrontal cortex was higher during metacognitive judgments and correlated with confidence (Fleming et al., 2012). Of note, these two studies relied on the above-mentioned staircase procedures to control for type 1 performance. These findings suggest that metacognitive introspection does not solely depend on the strength of perceptual signal represented in posterior brain regions (Lau and Maniscalco, 2010), but also non-perceptual brain regions. This was further supported by the observation that transcranial magnetic stimulation (TMS) over the prefrontal cortex impaired metacognitive efficiency but not perceptual discrimination performance (Rounis et al., 2010) but see (Bor et al., 2017). There is a debate about whether metacognitive abilities are domain-general or domain-specific. Some studies found that metacognitive abilities correlated between different sensory domains (Faivre et al., 2017) or between perceptual and memory task (McCurdy et al., 2013) while others did not (Morales et al., 2017). Although the later study did not find a consistency in metacognitive abilities across domains, confidence-related activity was observed in the ACC and pre-SMA in both tasks.

1.3 Linking performance monitoring, decision making and confidence judgments

Recently, computational models of decision making and confidence judgment have been extended to explain changes of mind. Drift diffusion models assume that sensory evidence is accumulated from noisy observations until it reaches some criterion that can be adjusted based on task demands in speed versus accuracy (Ratcliff et al., 2016). The strength of the resulting accumulated evidence can then be used, along with the elapsed time (Kiani et al., 2014a) to derive a confidence measure (Figure 1-1A). In one study, subjects were shown random dots moving stimuli and had to quickly move a cursor to one of the two zones indicating their choice. Changes of cursor trajectories indicated that subjects occasionally changed their mind even though a first decision was made and no additional visual information was provided after the movement onset (Resulaj et al., 2009). These findings showed that evidence accumulation continues even after an initial decision and can explain subsequent changes of mind, implying some type of performance monitoring. A follow-up study showed that changes in confidence can be accounted by similar mechanisms of post-decision evidence accumulation (Van Den Berg et al. 2016; Figure 1-1B).

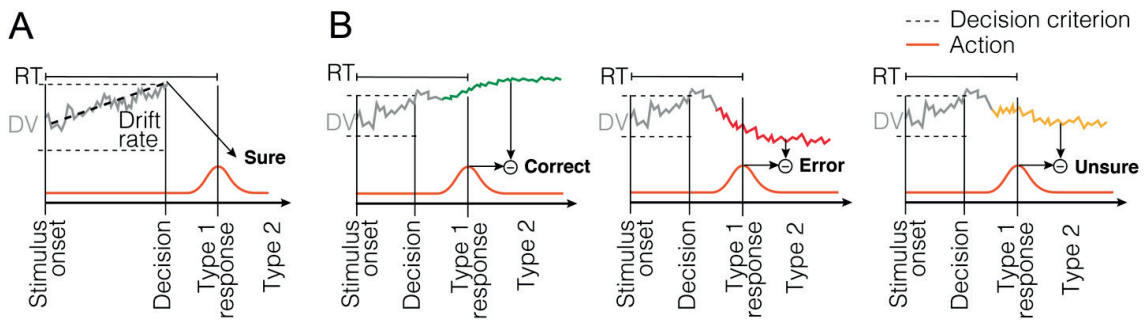

Figure 1-1. Drift-diffusion models for decision making and confidence judgments. *(A) Drift diffusion models assume that the decision variable is sampled from noisy evidence and accumulated with a certain drift rate (black dashed lines) that depends on signal strength until it reaches a decision criterion (horizontal grey dashed line). Early models assumed that the level of evidence is then used (amongst other variables, see text) to derive confidence. (B) When speed is emphasized over accuracy (i.e. subjects are under time pressure to respond), decision thresholds (dashed lines) are lower and there can be changes-of-mind due to evidence accumulating after the response. Depending on the decision variable (DV) after the response, subjects can be i) certain to have responded correctly if the DV is similar to the DV when the decision was made (left), ii) certain to have made an error if the DV is very different from the DV when the decision was made (center) or iii) uncertain when the DV has not converged to one or another level (right).*

There is an ongoing debate about the nature of the additional information used to derive confidence. Lau and Maniscalco found that hierarchical models for which type 1 decision variables are used for later second-stage confidence judgments explained data better than parallel architectures (Maniscalco and Lau, 2016). Fleming and Daw developed a second order Bayesian model assuming that confidence is derived from signals from the type 1 task as well as some additional signal that can be correlated with the first (Fleming and Daw, 2017). The later model also integrates the possibility that past actions inform confidence judgments, a hypothesis experimentally supported by the fact that metacognitive performance is lower when no action precedes confidence ratings (Kvam et al., 2015) as well as when confidence is rated before an action compared to when it is rated after (Siedlecka et al., 2016). In accordance with the later, evidence from the motor action was shown to inform metacognitive confidence judgments; subjects were less accurate in their confidence judgments when TMS was applied on the premotor cortex both before and after the action (Fleming et al., 2015).

Electrophysiological studies have also started to depart from the traditional flanker tasks and use perceptually more difficult stimuli followed by confidence ratings. Early work from Scheffers and Coles suggested that the amplitude of the ERN was reduced when errors were rated as uncertain (Scheffers and Coles, 2000). Later work using multivariate pattern classification showed that only the Pe and not the ERN could discriminate reported errors from correct responses (Steinhauser and Yeung, 2010). Follow-up work supported the idea that the ERN is a fast binary evaluation of the error while the Pe indexes confidence (Boldt and Yeung, 2015). Wokke et al. showed a positive relation between frontal theta oscillations and metacognitive performance, which was not explained by task performance (Wokke et al., 2017). Data from another study suggested that post-response frontal midline theta oscillatory power in the medial prefrontal cortex informed the confidence judgments (Murphy et al., 2015). These findings suggest that performance monitoring and confidence judgments share common neurophysiological processes.

1.4 Performance monitoring during reaching movements

In this section, we depart from the traditional two-choices discrimination tasks reviewed in the last section to study performance monitoring during reaching tasks which are arguably at midway (in terms of complexity of analysis) between discrete button presses and sustained, continuous movements. Indeed, they have a discrete onset and offset but then unfold in a continuous way. Reaching movements are remarkably precise considering the delay in sensory feedback loops. To achieve such accuracy, it is widely accepted that the brain uses an internal predictor of the sensory consequences of its movements. Firstly, the prediction of the outcome of the

movement can be used for immediate movement correction before sensory feedback is available. Secondly, the delayed sensory feedback can be compared to the prediction and the resulting error can be used to adjust motor parameters (Wolpert and Ghahramani, 2000; Shadmehr et al., 2010). Although the concept of internal models is widely accepted and has received experimental support (Goodale et al., 1986; Wolpert et al., 1995), the exact way that this control system is implemented in the brain is still under debate (Karniel, 2011).

The typical experimental paradigms to study online corrections of movements consist in perturbing the position of the arm of the subject using mechanical forces. Alternatively, visual perturbation can be applied to a virtual target and/or a virtual cursor representing subjects' hand (end-effector). Both virtual target and cursor can be manipulated during the movement and, in both cases, subject make fast corrections (Saunders and Knill, 2004), even when instructed not to (Pisella et al., 2000). This implies the existence of an automatic brain process monitoring the position of the target and cursor and correcting for deviations. Interestingly, while the efficiency of online corrections to target jumps is modulated by attention, the efficiency of online corrections to cursor jumps is independent from visual attention, suggesting that target and cursor information follow different neural pathways (Reichenbach et al., 2014). Moreover, while subjects correct for target and cursor jumps in less than 150 ms, when both the target and the cursor position are altered, it is only after 200 ms that subjects start integrating the difference between target and cursor into their correction (Franklin et al., 2016). This finding suggests that the computation of a difference vector takes more time than comparing cursor or target position to their expected position.

Interestingly, recent accounts of motor planning have proposed that the brain combines noisy sensory input with prior information from the task to estimate a posterior probability of the limb's state using Bayesian decision theory (Körding and Wolpert, 2004, 2006) which has led to the proposition that "motor control is decision making" (Wolpert and Landy, 2012). Another study has shown that when probing the motor system by perturbing the arm during decision formation under perceptual uncertainty, the strength of the reflex gain depended on the strength of the stimuli and the viewing time (Selen et al., 2012). If motor control uses the same evidence accumulation mechanisms as during decision making, could it be that it also relies on some measure of confidence?

Among its numerous functions, the posterior parietal cortex (PPC) seems to be crucial for online correction of ongoing movements. Indeed, lesions of the PPC, whether due to stroke (Pisella et al., 2000; Mutha et al., 2014) or experimentally induced by brain stimulation (Desmurget et al., 1999; Della-Maggiore et al., 2004) strongly impair the ability to produce fast corrections of the moving limb. Moreover, neurons in the PPC encode both target position (Buneo et al., 2002) and a forward state estimation that could neither be explained by an efferent copy of the motor command, nor by sensory reafference (Mulliken et al., 2008). When online corrections had to be made after a target jump, PPC neurons either predicted or followed the resulting change in limb kinematics (Archambault et al., 2009).

Remarkably, neurons in the dorsal premotor cortex (PMd) responded earlier after target displacement than PPC neurons, but only signaled the change of plan while parietal neurons encoded hand trajectories more faithfully (Archambault et al., 2011). This suggests that frontal cortices could encode higher-level corrective actions. The PPC takes care of integrating visual feedback with the output of the internal models computed in the cerebellum (Imamizu et al., 2000). The involvement of the cerebellum in predicting the state of the end-effector was showed by instructing subjects to make slow lateral movements and then at the sound of a beep, reach towards a visual target situated in front. When disrupting the cerebellum with TMS, subjects missed the target by a distance that was consistent with a delayed end-effector state estimate of 130 ms (Miall et al., 2007), consistent with behavioral models (Saunders and Knill, 2004).

Few electrophysiological correlates of errors during reaching movements have been reported at the scalp-level. Vocat and colleagues (2011) showed that errors during pointing movements elicit an early event-related potential (ERP) over the medial frontal cortex (MFC), whose amplitude is related to the magnitude of the error (Vocat et al., 2011). Using a robotic arm and unpredictable changes in force-fields, Torrecillos and colleagues (2014) also showed an error-modulated ERP over the MFC (Torrecillos et al., 2014). Source localization of these ERP indicated neural generators in the ACC and pre-SMA. Additionally, recent evidence indicate that post-movement beta rebound over the motor cortices could be a correlate of recalibration of the motor system based on the magnitude of the error committed during the preceding movement (Tan et al., 2014a, 2014b; Torrecillos et al., 2015).

1.5 Performance monitoring during continuous visually-guided movements

Two-alternative force choice tasks allow studying the performance monitoring system during perceptual decisions. On the other hand, reaching movements are arguably most representative of precise upper-limb movements most relevant in daily life. However, for both paradigms, performance monitoring and correction typically happens only once per action. How does the performance monitoring system operate when it has to constantly monitor its motor output and correct for drifts such as while driving a car? In the following section, we review the mechanisms of performance monitoring during continuous movements under visual guidance.

A prominent theory of motor control and learning posits that movements are composed of a set of fundamental building blocks that can be dynamically combined to build movements (Flash and Hochner, 2005; Giszter, 2015). These so-called "motor primitives" can either consist of stereotypical cohererent muscles activations termed synergies (d'Avella et al., 2003), or be kinematically defined (Mussa-Ivaldi and Bizzi, 2000). These kinematic primitives are particularly visible for reaching movement in stroke patients (Krebs et al., 1999; Rohrer et al., 2002, 2004) and infants (Berthier, 1996), progressively blending into the more stereotypical bell-shaped movements during the course of (re-)learning. In healthy adults, these motor primitive are especially manifest during (sustained) visuo-motor tracking of a target with the upper limb: the kinematics of the upper limb then reveal a succession of bell-shaped speed pulses, henceforth referred to as sub-movements (Craik, 1947) which seem to disappear when visual feedback from the upper limb is not provided (Miall et al. 1993; McAuley et al. 1999; but see Doeringer and Hogan 1998 for contradicting results).

Behavioral studies have shown that the magnitude of these sub-movements corresponds to deviations from the desired position, indicating their error-related or corrective nature (Miall et al., 1986; Selen et al., 2006). Such intermittencies in motor control are difficult to explain using the framework of a continuous performance monitoring system, raising the yet unresolved question of whether the motor system continuously or intermittently computes a control signal (Karniel, 2011; van de Kamp et al., 2013). In an intermittent control system, motor commands are sporadically generated, followed by an open-loop period during which the consequences of the previous motor command is observed, allowing time for the next motor command to be computed. Such models are able to explain behavioral data (Sakaguchi et al., 2015). Moreover, in a step-tracking experiments in which the tracked target could jump twice with varying time intervals between jumps, Van de Kamp et al. showed that the response time to the second jump was higher and decreased with the time between the two jumps, suggesting some refractory period in the corrective mechanism estimated between 150 ms and 250 ms (van de Kamp et al., 2013). In another study, the authors manipulated the frequency at which feedback was provided and noted improvements in tracking performance until 6.4 Hz after which performance plateaued (Slifkin et al., 2000).

Few attempts have been made to find the neural substrate of sub-movements or performance monitoring in continuous movements. Limanowski et al. showed that tracking error led to increased BOLD activation in the PPC, SMA and cerebellum. Moreover, BOLD correlates of sub-movement amplitude have been found in the basal ganglia and the medial frontal cortex (Grafton and Tunik, 2011). Furthermore, correlates of sub-movements have been found in human scalp manetoencephalography (MEG) in the form of low frequency cortical oscillations coupled to rhythmic motor output (Gross et al., 2002; Jerbi et al., 2007). At the spinal cord level, these low frequencies oscillate in anti-phase with their cortical counterparts, possibly reducing tremor (Williams et al., 2010). Their functional role remains however unclear. Additionally, a recent study found that local field potentials phase-locked to sub-movements showed similar oscillatory activity during sleep and sedation, raising the question of whether sub-movements are due to factors such as dynamics of sensorimotor feedback loops or rather spontaneous oscillations of local neuronal populations (Hall et al., 2014a).

1.6 Contribution of the thesis

In **Chapter 2**, we study the neural substrate of performance monitoring and confidence judgments during a difficult perceptual decision making task under time pressure, after which subjects were asked to rate their confidence about the previous response. The EEG contained correlates of these confidence ratings that we could decode earlier in the active compared to the observation condition. The scalp regions that were informative for decoding confidence were above the medial frontal cortex during the active condition and above the sensorimotor cortices during the observation condition. In the fMRI data, we found that the supplementary motor area (SMA) was activated when subjects believed they had committed or observed errors. Importantly, the SMA was also activated when subjects were uncertain about their responses or the observed responses. On the other hand, the anterior cingulate cortex (ACC) was only activated for committed errors. The left insula and right posterior parietal cortex (PPC) were also activated when subjects believed they committed or observed an error. Finally, we also found differences in metacognitive performance: subjects were more accurate when rating their confidence about their own actions than when rating their confidence about actions they had observed. This difference in metacognitive performance between the active and the observation condition was increased for subjects showing more activation of a frontal network comprising the pre-SMA and the inferior frontal gyrus (IFG).

In **Chapter 3**, we asked whether similar EEG correlates of performance monitoring could be found during continuous movements with no strict experimental segmentation of motor actions and visual feedback. Using a visuo-motor tracking task in which subjects followed a moving target with the mouse cursor, we found an event-related potential (ERP) time-locked to periodically occurring pulses in hand kinematics (sub-movements). We then compared the amplitude of the ERP with the deviation of the cursor with respect to the target. We found that when the cursor was lagging behind the target and sub-movements were larger, the amplitude of the ERP was larger. In fact, the amplitude of the ERP increased proportionally to the amount of deviation occurring 110 ms before the sub-movement. This modulation of the amplitude of the ERP by cursor deviation was observed even when selecting a subset of sub-movements showing similar kinematics and could therefore not be solely due to differences in hand kinematics. Finally, a comparable ERP time-locked to sub-movements but of reduced amplitude was found when subjects were spontaneously drawing trajectories on the screen.

In **Chapter 4,** we analyzed data recorded during a visuo-motor tracking task from the medial frontal cortex of four patients implanted with electrocorticographical strips (ECoG) or intracranial electrodes for surgical resection of epileptic tissues. We found that theta oscillations in the SMA and ACC were coupled to sub-movements. Importantly, we also found that high-gamma activity in these brain structures was coupled to theta oscillations, sub-movements or both.

In **Chapter 5,** we compared the desynchronization of mu cortical oscillations during the visuo-motor task of the previous chapters and an assistance condition in which the position of the mouse cursor was experimentally manipulated to reduce the cursor deviation by 80%. Subjects were thus tricked to believe that they performed better than they actually did and showed smoother sub-movements (i.e. less corrections). We found that in this assistance condition, the power of mu oscillations in the right hemisphere (ipsilateral to the tracking hand) was higher, indexing reduced cortical activity. Moreover, during normal tracking, we observed a transient modulation of mu power by the amplitude of the sub-movements that was not present during the assistance condition.

Chapter 2 Performance monitoring during decision making and observation under uncertainty

2.1 Introduction

Performance monitoring has been mainly studied in simple decision tasks under time pressure leading to possibly erroneous actions. In these tasks, neural correlates of performance monitoring were found by contrasting brain activity after correct and erroneous actions. However, erroneous actions activate different adaptation mechanisms such as a slowing of the response or an improvement in accuracy during the next trial (Danielmeier et al., 2011). The neural mechanisms leading to the response and the possible adaptations following errors can thus confound the results. This is less the case when errors from an external agent are observed without any possible interference on the current or next decisions. Moreover, performance monitoring is usually considered as a binary process, flagging responses as either correct or erroneous. On the other hand, studies on confidence judgments use more difficult perceptual discrimination tasks without time pressure. Subjects are probed for their confidence on a scale ranging from uncertain to certain, thus assuming that they are never confident about making errors.

In the study covered in this chapter, subjects performed a difficult perceptual discrimination task under time pressure (type 1 task). The task consisted in displaying 100 dots unequally distributed in two boxes for 60 ms. To investigate the neural substrate of performance monitoring independently from the response and possible adaptations following errors, we designed an experimental paradigm in which subjects were asked to either make a decision about which side contained most dots and indicate it with a button press (*active* condition), or to observe the computer answering the task by displaying a virtual hand on one of the two stimuli (*observation* condition). The stimuli, response times and performance of the computer at the type 1 task were a permutation the trials recorded during the active condition, and were thus identical. Perceptual processing was stopped by showing a mask after the button press or the onset of the virtual hand. In both conditions, subjects were asked to rate their confidence on type 1 performance using a continuous scale ranging from certainty that the response was correct to certainty that the response was erroneous. This scale allowed us to assess confidence and performance monitoring altogether, and to quantify the effect (or absence) of motor actions on the subjects' metacognitive accuracy, defined as their ability to correctly rate actions under uncertainty (type 2 task). Additional details of the experiment can be found in Figure 2-1.

Using simultaneous EEG and fMRI, we aimed at answering three research questions. i) What are the common and distinct brain regions involved in detecting active vs. observed errors? ii) How do neural correlates of confidence judgments unfold over time for active vs. observed error unfold over time? iii) Are confidence judgments different when subjects are the agents of the type 1 actions (active condition)? Our study design and hypotheses were pre-registered on the Open Science Framework[1].

[1] (http://osf.io). A copy of the preregistration is provided in the appendix at the end of the thesis.

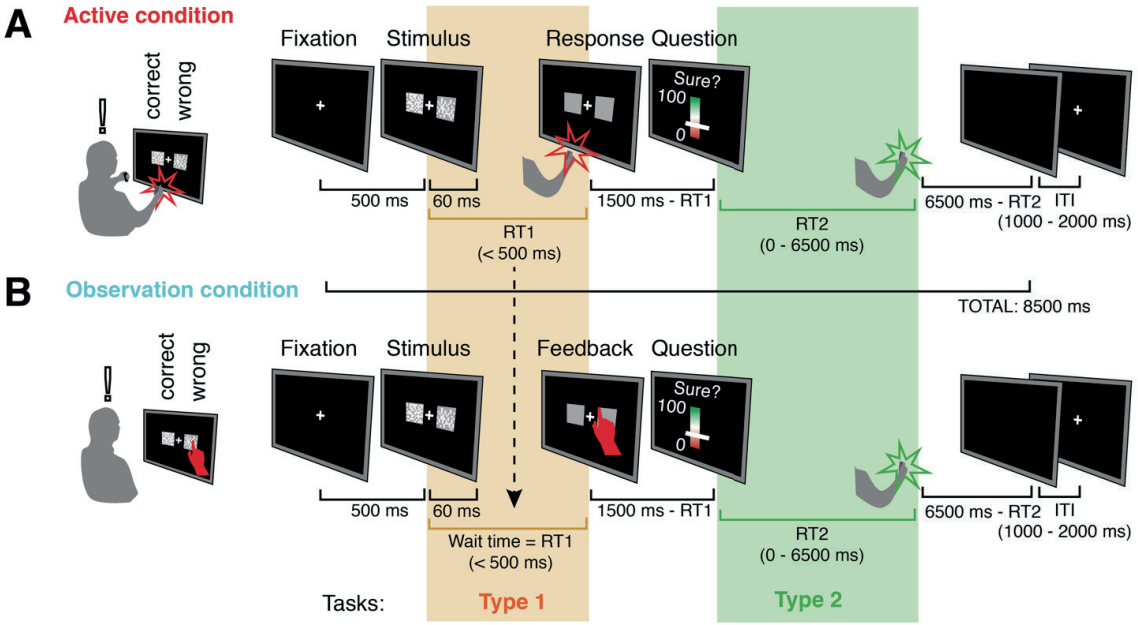

Figure 2-1. Task design. *A) In the active condition, subject responded to the type 1 task with either the left or the right button. A trial started with 500 ms of fixation cross followed by a brief presentation of the stimulus (60 ms). The response time (RT) of the subjects was defined as the time needed from the stimulus onset to the response. This type 1 task lasted 2000 ms. After, the subjects were asked to press the left button when a cursor moving up and down a scale between 0% and 100% reached their level of confidence. The subjects had 6500 ms to answer to this type 2 task. B) The observation condition was identical, except that the subjects did not answer but observed the computer answering (a virtual hand was shown on the screen). The stimuli and RTs were sampled from the previous 12 active trials.*

Firstly, we anticipated the existence of both commonalities and specificities regarding the brain regions activated during errors detection in both conditions. We expected commonalities because the perceptual processing was identical in both the active and the observation condition. On the other hand, we expected specificities because error detection differed between conditions. More specifically, in the active condition, perceptual processing led to a type 1 decision and a resulting action that could then be compared to the current stage of evidence accumulation to detect errors (Resulaj et al., 2009) and give rise to a certain level of confidence (Pleskac et al., 2010; Van Den Berg et al., 2016). In the monitoring condition, subjects were provided with the type 1 response but the decision was taken by the computer (based on their previous performance). Based on recent electrophysiological and neuroimaging studies (Bonini et al., 2014; Iannaccone et al., 2015), we predicted that the common substrate would lie within the anterior cingulate cortex (ACC) while the supplementary motor areas (SMA) would be more activated during the active task. Secondly, we wanted to investigate how the neural correlates of confidence evolve over time in both conditions. For each condition, we expected to see electrophysiological correlates of confidence time-locked to the response. However, such correlates should occur later in the observation condition due to the delays of visual sensory feedback. Finally, we predicted that the action performed by the subjects during the type 1 task in the active condition would inform the metacognitive judgments and lead to better type 2 performance compared to the observation condition. Our prediction was based on recent models suggesting that first, perceptual processing continues after type 1 responses to inform confidence judgments (Pleskac et al., 2010) and secondly, that the type 1 response interferes with the confidence judgment process (Kvam et al., 2015; Van Den Berg et al., 2016; Fleming and Daw, 2017), leading to better type 2 accuracy. Our prediction was supported by the result of a pilot behavioral study.

2.2 Results

Behavior

We first looked at type 1 behavior during the active condition. The error rate of the subjects (type 1 performance) was kept constant with a staircase procedure that lowered the perceptual difficulty after an error and raised it after two consecutive correct responses (Levitt, 1971). This procedure led subjects to converge to a 71.5±2.9% (std. dev) type 1 performance. Two subjects did not converge with type 1 performance of 59% and 51%. These subjects were performing close to random with aberrantly low task difficulty and were excluded from further analysis. The perceptual difficulty (difference in number of dots between sides, henceforth referred to as the delta) was 26.5±7.9 points on average and type 1 response time (RT1) was 0.386±0.019 s.

We looked at the distributions of confidence ratings (type 2 behavior) for both conditions. We binned the confidence in 5 bins corresponding to error certain ($0.0 \leq conf < 0.2$), error uncertain ($0.2 \leq conf < 0.4$), uncertain ($0.4 \leq conf < 0.6$), correct uncertain ($0.6 \leq conf < 0.8$), correct certain ($0.8 \leq conf \leq 1.0$). Confidence ratings were well distributed over the five bins for both conditions (Figure 2-2A), showing that subjects used the full confidence rating scale. Confidence ratings were similar across conditions (paired t-test; $|t(21)|<2.6$; $p>0.16$, Bonferroni corrected) although there was a trend towards a higher number of correct uncertain responses ($p=0.08$, corrected). We separated distributions for correct and error to show whether: (i) the probability of a type 1 response being correct increased with increasing confidence (Figure 2-2B); and (ii) the probability of erroneous type 1 response decreased with increasing confidence (Figure 2-2C). Among correct type 1 responses, there were significantly more confidence ratings for correct uncertain in the active condition ($t(21)=2.8$; $p=0.049$, Bonferroni corrected). No significant difference was observed for erroneous type 1 responses ($|t(21)|>1.8$; $p>0.45$, Bonferroni corrected).

On average, subjects also showed significant post-error slowing of RT1 after perceiving an error (Figure 2-2C; +2.5±3.0% for high error certainty, +1.7±1.7 % for low error certainty; $t(21)>3.9$; $p<0.01$, Bonferroni corrected). Intriguingly, there was a small but significant speeding up of RT1 after low correctness certainty (-0.8±1.2%; $t(21)=-4.71$; $p<0.01$, Bonferroni corrected).

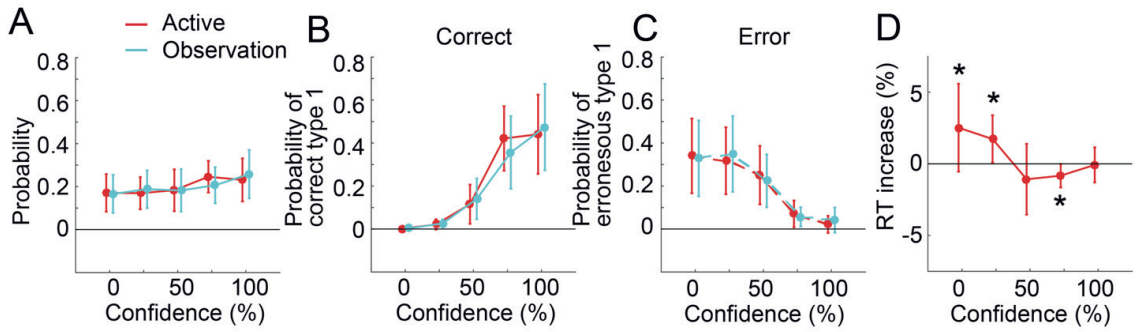

Figure 2-2. Distribution of confidence ratings. *(A) The probability of any trial being rated with a certain confidence level for active (red trace) and observation (cyan trace). Whiskers indicate standard deviation. (B) The probability of any correct trial being rated with a certain confidence level for active (red trace) and observation (cyan trace). Whiskers indicate standard deviation. (C) The probability of any correct trial being rated with a certain confidence level for active (red trace) and observation (cyan trace). Whiskers indicate standard deviation. (D) The percentage of increase or decrease in the RT1 of the next trial based on a certain confidence level. Whiskers indicate standard deviation. Only depicted for the active condition since there is no response during the observation condition. Stars indicate significant deviations from zero (p<0.05, Bonferroni corrected).*

Electrophysiological correlates of performance monitoring

To observe how performance monitoring and confidence evolve over time, we computed event-related potentials (ERP) time-locked to the type 1 response (i.e. the button press in the active condition or the onset of the virtual hand in the observation condition). For details on the pre-processing of the EEG signal, please refer to materials and methods section at the end of the chapter. First, for each condition, we constructed three ERPs based on a binning of the confidence ratings into three levels: certain-error (0-0.33); uncertain (0.34-0.66) and certain-correct (0.67-1). In the active condition, the ERPs resembled the typical error-related negativity (ERN) over the frontal midline for all bins (FCz electrode; Figure 2-3A), maximal around 40 ms after response onset, followed by a positivity around 120 ms after response onset (Pe). To assess statistical significance, we modeled the ERP every 10 ms using confidence, response time and task difficulty (delta) as covariate (mixed models). There was a significant effect of confidence between 70 and 130 ms after response onset ($F>14.2$; $p<0.05$, Bonferroni corrected). A small effect of task difficulty was found ($p=0.01$, uncorrected) at similar latency but did not survive a multiple comparisons correction. In the observation condition, confidence-related differences between the certain-error and certain-correct occurred later, around 300 ms after the onset of the virtual hand. Low ratings (confidence in error) led to a negativity over the frontal midline (FCz electrode; Figure 2-3B). The effect of confidence was significant from 280 to 300 ms (mixed models; $F>14.0$; $p<0.05$, Bonferroni corrected). Again, a small effect of task difficulty was found ($p=0.03$, uncorrected) at similar latency but did not survive a multiple comparisons correction. We also conducted a more conventional ERP analysis, dissociating erroneous from correct responses (i.e. not based on subjective confidence ratings; Figure 2-8 in supplementary material). The ERP differences between erroneous and correct trials were very similar to the ERP differences between certain-error and certain-correct.

To understand when differences in the ERP explain confidence, we constructed decoders of confidence using a 100 ms sliding window (c.f. materials and methods). We found that in the active condition, decoders rapidly started to perform better than chance level ($p<0.05$, Bonferroni corrected) as early as 50 ms after the response onset (Figure 2-3C), thus immediately after the negativity. In the observation condition, the decoders only started to perform higher than chance level after 325 ms (Figure 2-3D), thus after the negativity and slightly before the following positivity. We projected the weights of the contribution of each electrode on a topographic scalp representation. Interestingly, while confidence was mostly explained by frontal midline electrodes in the active condition, electrodes over the sensorimotor cortices carried most information in the observation condition (Figure 2-3C,D).

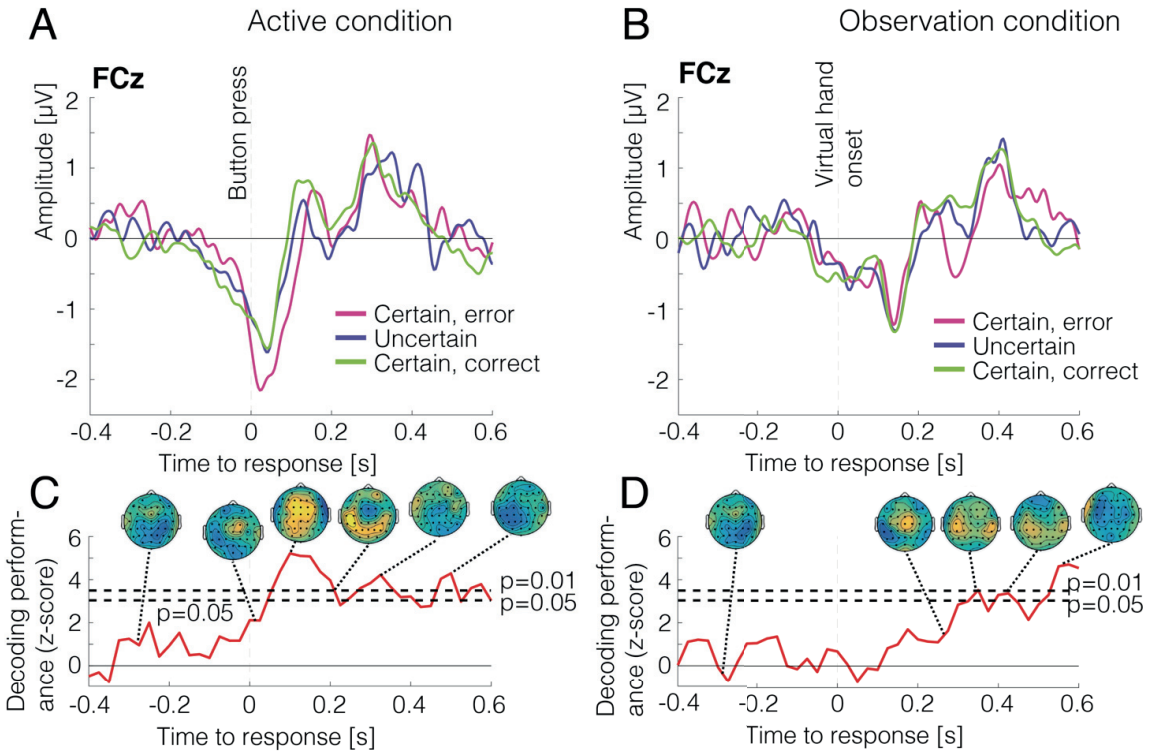

Figure 2-3. ERP for both conditions. *(A) ERP (FCz electrode) for the active condition and three bins of confidence: certain-error; uncertain and certain-correct. (B) ERP (FCz electrode) for the observation condition and three levels of confidence. (C, D) Confidence decoding performance (z-score; red curve) from the EEG data for the active condition (C) and observation condition (D). The weights of the decoder for each electrode are shown topographically above at selected times. The vertical dashed line indicates the response onset. The two horizontal dashed lines represent the threshold of better-than-chance performance at p<0.05 and p<0.01 respectively (Bonferroni corrected).*

Hemodynamic correlates of performance monitoring

Next, we set out to find the hemodynamic correlates of confidence ratings. For this, we constructed a general linear model (GLM) modelling the hemodynamic response to the stimulus onset of each condition with separate regressors (active and observation). We then added parametrically modulated regressors for confidence ratings, perceptual difficulty (delta, i.e. difference in dots) and type 1 response times (RT1) to each of the initial regressors. A second-level analysis on the confidence ratings regressors revealed the brain regions whose blood-oxygen dependent (BOLD) activation covaried with confidence ratings after regressing out the variance explained by the task itself as well as parameters of no-interest.

For the active condition, we found significant clusters of BOLD activity inversely related with confidence (i.e. more activated for perceived error) in the bilateral SMA, ACC and middle frontal gyri (MFG) as well as in the left inferior frontal gyrus (IFG), insula and posterior parietal cortex (Figure 2-4A; $p<0.05$, using cluster-extent family-wise error (FWE) correction with a voxel-height threshold of $p<0.001$). For the observation condition, significant clusters were limited to the left SMA and insula. A conjunction analysis between activations of the active and observation conditions showed that the commonly activated brain regions were the left SMA, insula and inferior parietal cortex (Figure 2-4B). Finally, significant clusters of BOLD activity covarying positively with confidence (i.e. more activated for confident responses) were found bilaterally in the cuneus and middle occipital

cortex for both conditions but with no statistically significant overlap. During the observation condition, the right supramarginal cortex, superior temporal, the bilateral insula, amygdala and medial orbitofrontal cortex were also related to high confidence ratings (Figure 2-4C).

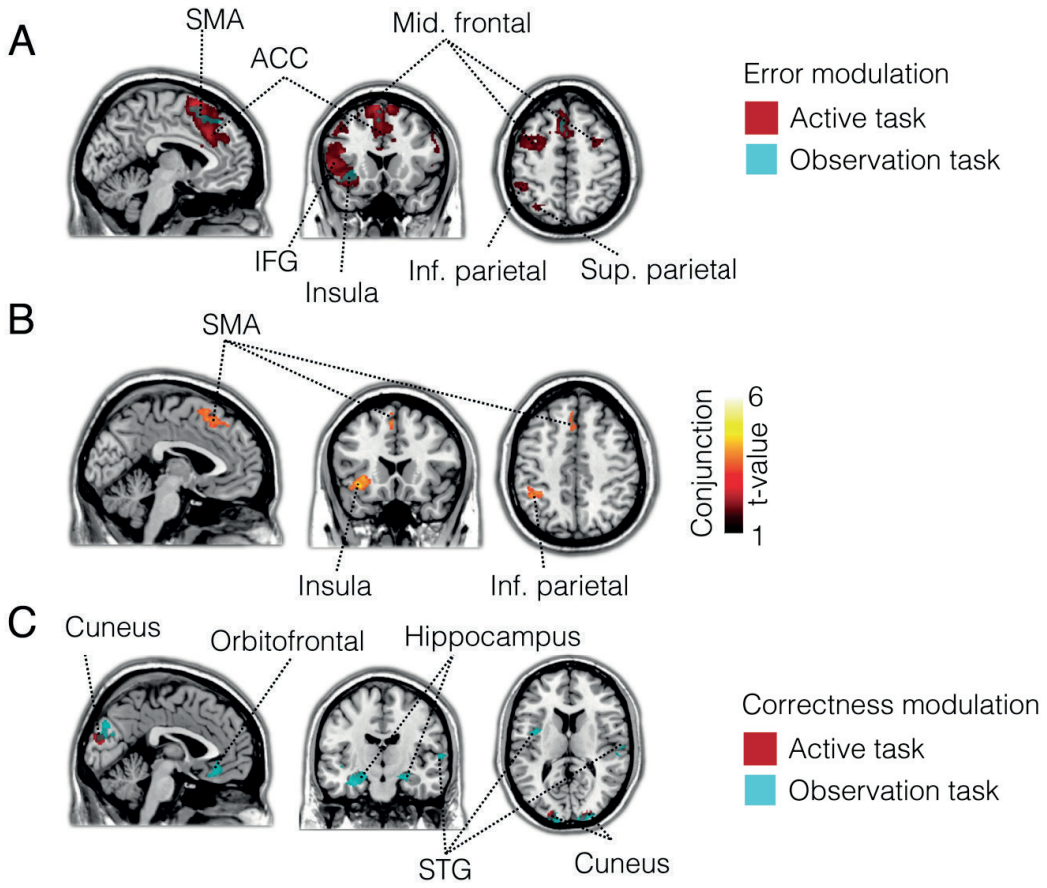

Figure 2-4. Brain regions modulated by confidence ratings. *(A) Brain regions modulated by low confidence ratings (error certainty) for the active (red) and observation (cyan) conditions. (B) Brain regions conjunctively modulated by low confidence ratings in both conditions. (C) Brain regions modulated by high confidence ratings (correct certainty). See Table 2-1 for a list of activated brain regions.*

This analysis showed which regions were activated for confidence in error or confidence in correctness. To find which regions are activated specifically for uncertain responses, we used an absolute measure of confidence: 1-|conf – 0.5|. This measure was one when the subjects were uncertain (confidence=0.5) and lower with increasing certainty of error or correct. Significant activations correlating positively with uncertainty were found in the SMA and IFG in both conditions (conjunction analysis; Figure 2-5A). Additionally, in the observation condition only, the left insula, supramarginal cortex and sensorimotor regions such as the precentral and postcentral cortices were also activated (Figure 2-5B).

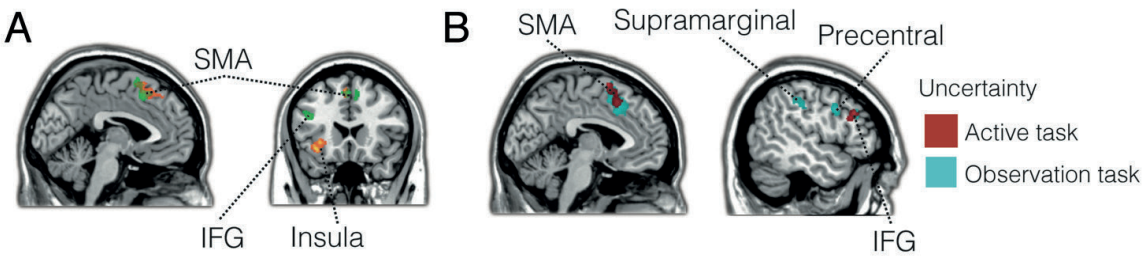

Figure 2-5. Brain regions activated by uncertain responses. *(A) Conjunction analysis (green clusters) of brain regions activated by uncertainty in both conditions. Orange clusters represent regions activated by error in both tasks. (B) Regions activated for the active task are shown in red and for the observation condition (cyan). See Table 2-2 for a list of activated brain regions.*

Behavioral differences in metacognitive performance between active and observation conditions

After finding a common neural substrate of performance monitoring in both conditions using confidence ratings, we asked whether the motor action in the active condition could have an effect on metacognitive accuracy (i.e. whether the confidence ratings of subjects were more accurate in predicting type 1 performance in the active condition). We assessed how well type 1 performance (error or correct) could be explained by confidence ratings using signal detection theory (SDT; Macmillan and Creelman 2004). We compared the hit rate to the false alarm rate of simple decoders predicting type 1 performance by thresholding confidence ratings. Different thresholds led to different ratios of hit rate and false alarm rate that was plotted on a two-dimensional axis (receiver operating characteristic (ROC) curve; Figure 2-6A). Metacognitive accuracy was quantified by computing the area under the curve (AUC) of the ROC curve for each condition. All subjects showed high metacognitive accuracy (94.7±4.2% for the active task and 92.7±6.8% for the monitoring task; Figure 2-6B). There was a trend towards lower type 2 performances during the observation condition compared to the active condition (paired t-test; $t(21)=1.92$, $p=0.069$). Subjects with high type 2 accuracy in the active condition tended to show high type 2 accuracy in the observation condition ($R^2=0.45$, $p=0.007$, Bonferroni corrected). Importantly, type 2 performance was independent from task 1 performance, mean delta and mean type 1 response time, although there was a trend of type 2 performance correlating with mean delta for the active condition ($R^2=0.20$, $p=0.035$, uncorrected; Figure 2-6C).

Finally, we probed whether type 2 performance was influenced by the type 1 response time (RT1). For this, we binned the trials into early and late responses/feedback based on the median type 1 reaction time (RT1; Figure 2-3D; 0.38±0.03 s). Type 1 performance increased ($t(21)=-7.77$, $p<0.001$) dramatically for late RTs (mean: 81.2±7.2%) compared to early RTs (mean: 64.4±5.0%). There was also an effect of RT on metacognition ($F(1,19)=6.73$, $p=0.018$, repeated measures ANOVA), no effect of task ($F(1,19)=2.20$, $p=0.16$) and an interaction between RT and task ($F(1,19)=5.19$, $p=0.034$). Post-hoc tests (Bonferroni corrected) revealed a significant decrease in metacognitive abilities with increasing RT for the active condition ($t(19)=3.01$, $p=0.027$) but not for the observation condition ($t(19)=-0.12$, $p=1$). More importantly, subjects showed better metacognitive efficiency only for early RTs ($t(19)=3.72$, $p=0.0058$) but not for late RTs ($t(19)= 0.65$, $p=1$).

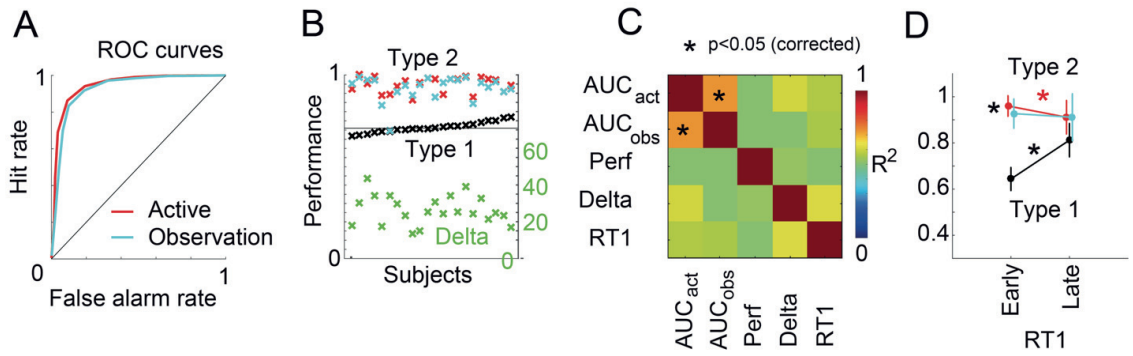

Figure 2-6. Modelling metacognitive differences. *(A) Receiver operating characteristic (ROC) curves representing the hit rate versus the false alarm rate as a function of a threshold applied on the confidence ratings to decode correct responses. The red curve represents the average ROC across subjects during the active condition. The cyan curve represents the average ROC across subjects during the monitoring condition. (B) Metacognitive accuracy was estimated by computing the area under the ROC curves (AUC) from panel A. There was a trend towards higher AUC during the active condition (red crosses) compared to the observation condition (cyan). The type 1 performance converged to 71.5±2.9% (black crosses, ordered) while the perceptual difficulty (delta) varied across subjects (green crosses). (C) The between-subject relations between behavioral variables measured in R^2. AUC_{act} is the AUC for the active condition, AUC_{mon} is the AUC for the observation condition, Perf is the type 1 performance, Delta is the mean perceptual difficulty of the type 1 task in number of points difference (scale on the right). RT1 is the response times of the type 1 task. (D) Type 1 task performance (black line) and metacognitive performances for the active (red line) and observation (cyan line) tasks as a function of early or late RT1. Whiskers indicate standard deviation and stars indicate significant differences (p<0.05, Bonferroni corrected).*

Between-subject correlation with differences in metacognitive performance

Next, we asked whether the differences in metacognitive accuracy between conditions could be explained by differences in BOLD activation between conditions. We built a new GLM with only two regressors for the active and observation condition but no parametric regressors. We performed a second-level analysis on the t-contrast between the active and observation conditions and added the following covariates: i) AUC difference between tasks, ii) mean type 1 performance, iii) mean task difficulty (delta) and iv) post-error slowing. We found that in the bilateral inferior frontal gyri (IFG), middle orbitofrontal cortices, the pre-SMA and the insula, the differential BOLD activity between the active and observation conditions was negatively related with the metacognitive performance difference between the active and observation conditions (Figure 2-7A). In other words, subjects with better metacognitive accuracy in the active than in the observation condition were prone to show either less activation in those regions during the active condition or more activation during the observation condition.

We then conducted a conjunction analysis to find regions that explained the difference in metacognitive accuracy and were either more activated in the active condition or more activated in the observation condition. We found that the among the previously found regions, the left pre-SMA and IFG were more activated during the observation task (Figure 2-7B). We did not find an effect of mean type 1 performance or mean task difficulty. The right middle frontal gyrus however correlated positively with the amount of post-error slowing (p=0.011, cluster size=277, peak t-value=7.53 at MNI coordinates: 39, 38, 29 mm).

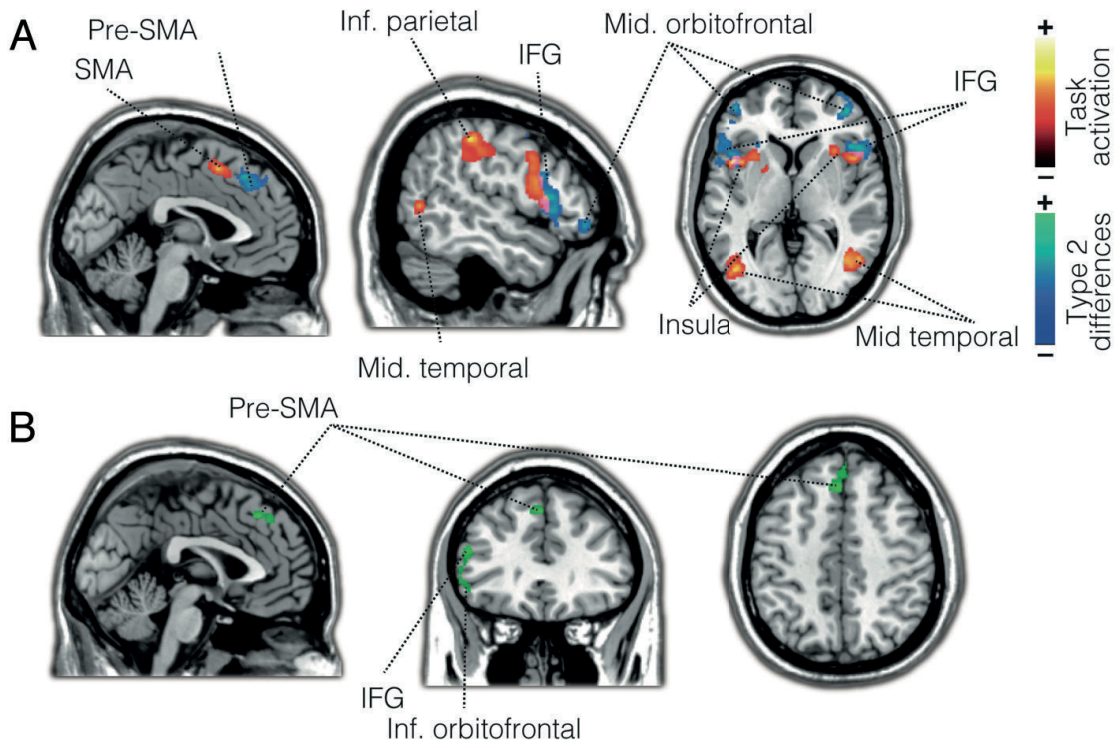

Figure 2-7. Between-subject covariates of metacognitive performance differences. *(A) Clusters of activation covarying with the metacognitive performance differences between the active and observation conditions (blue-green scale). We also show regions activated by both conditions (conjunction analsis; c.f. materials and methods) (B) Clusters with higher activation during the observation condition and negatively correlated with the metacognitive performance differences between conditions. See Table 4-3 and 4-4 for a list of activated brain regions.*

2.3 Discussion

In this study, we compared performance monitoring based on confidence judgments between an active condition during which subjects made errors and an observation condition during which subjects observed errors made by the computer in response to identical visual stimuli. We found electrophysiological correlates of confidence in both conditions. During the active condition, EEG over the midline of the scalp predicted confidence as early as 50 ms after the response. During the observation condition, this prediction was delayed by around 270 ms and the signal carrying these correlates was topographically distributed over the sensorimotor regions. We found hemodynamical correlates of performance monitoring that were activated for both conditions in the SMA, left insula and right PPC. These regions were thus activated independently from the motor action. There were no clear differences in confidence ratings across conditions. However, subjects were more accurate in rating their type 1 responses when they were the agents of the action. This difference in metacognitive accuracy was reduced in subjects with a higher activation of the pre-SMA and IFG during the observation condition.

Event-related potentials and the timing of confidence appraisal

As opposed to previous electrophysiological studies of performance monitoring, we found a large negativity for all levels of confidence (error/certain, uncertain and correct/certain). We found an effect of confidence right after the ERN, but this effect peaked at the Pe latency. This finding contrasts with results obtained using more classical paradigms for studying performance monitoring such as the flanker task (Falkenstein et al., 1991; Gehring et al., 1993), where the ERN encodes error. Our study differs by the definition of errors, based on confidence instead of true type 1 performance. However, when comparing ERPs after errors and correct we found similar results (data not shown). One study using a similar perceptual discrimination task with confidence ratings

found an effect of confidence on the ERN amplitude but could only decode errors at the single trial level at the Pe latency (Boldt and Yeung, 2015). It is worth noticing however, that Boldt and Yeung allowed the subjects up to 1.5 seconds to answer, three times more than in the present study. On the other hand, when pressing subjects to respond in less than 1 s, Charles et al. found that shorter stimulus onset asynchronies (i.e. less time to perceive the stimuli) led ERPs for correct responses to show similar deflections as for erroneous responses. It is probable that pressing subjects to respond in less than 500 ms and showing the stimuli for only 60 ms led to much uncertainty at the time of the response, thus explaining the large negativity for correct responses. Nonetheless, our behavioral modelling of the metacognitive accuracy showed that subjects' confidence judgments were very accurate, implying a strong relation between type 1 errors and error confidence. Confidence thus had to gradually build-up during the time between the action onset and the confidence rating scale even if perceptual processing was stopped at response onset by a mask. Consistent with this hypothessi, our single-trial decoding over time shows that EEG can explain confidence even 500 ms after response onset suggesting that confidence related parietal activity continues well after the Pe.

In the active condition, the EEG over the frontline midline of the scalp explained confidence judgments above chance level starting around 50 ms after the response onset, therefore just after the ERN and reaches its maximal decoding performance at the latency of the Pe, suggesting that the latter is a correlate of confidence (Nieuwenhuis et al., 2001; Overbeek et al., 2005; Steinhauser and Yeung, 2010; Boldt and Yeung, 2015). This latency is much earlier than the 250 ms found in the Bolt and Yeung study. Recent opinions suggest that the ERN (and similar frontal midline ERPs) represent fast alarm signals, indicating the necessity to adapt or react (Ullsperger et al., 2014), rather than error monitoring per se. It is possible that when pressing subjects to respond fast but with difficult perceptual tasks (as in our experiment), evidence has to be accumulated very quickly, thus leading to earlier correlates of confidence after the response.

The unfolding of confidence correlates was different in the observation condition. We found that the first correlates of confidence occurred around 350 ms after the observed type 1 response. This delay is likely due to the time needed for visual information to be processed while in the active condition, an efference copy is available shortly after the response. Surprisingly, frontal midline scalp regions seem to contribute before the time when decoders started performing better than chance (around 250 ms after the observed type 1 response, corresponding to the difference observed in the ERP). The information contributing to successful decoding arose from scalp areas over the sensorimotor regions.

After studying the timing of performance monitoring and confidence correlates, we investigate their neural substrate in the next section.

A common neural substrate for performance monitoring during the active and observation conditions

We hypothesized that the common substrate for performance monitoring in both the active and observation condition would lie in the ACC while the SMA would only be active during the active condition, in accordance with recent findings of dissociation between response conflict in the SMA and error detection in the ACC (Iannaccone et al., 2015). Our results showed the contrary; the common regions activated by perceived errors in both tasks were the left SMA, the left insula and the right PPC. Single cell activity in the SMA, pre-SMA and ACC was recorded during action and observation (Mukamel et al., 2010). The cells responding to both action and observation were mainly found in the SMA but no role of performance monitoring was investigated.

Our results also show activation of the SMA during uncertainty, suggesting that its role is rather to signal error likelihood than error *per se*, consistent with the idea that the SMA is more involved in monitoring conflict than errors (Bonini et al., 2014; Iannaccone et al., 2015). However, our task did not include the same type of response conflict as in flanker or Simon tasks since no obvious prepotent response needed to be inhibited. Moreover, our conjunction analysis shows that the SMA also plays a role in monitoring observed actions, in accordance with previous electrophysiological evidence (Koelewijn et al., 2008). Together, these findings suggest that the role of the SMA is to signal situations of suboptimal behavior, either in cases of errors, or uncertainty but independently from motor actions. The SMA was also shown to be a common substrate for confidence judgments in both perceptual and memory retrieval tasks (Morales et al., 2017).

Moreover, we found a dissociation between the SMA and the ACC; while the SMA was activated for errors and uncertainty in both conditions, the ACC was only activated for errors in the active condition and was globally

more activated in the active vs. observation condition. Although we cannot conclude that the ACC was not activated in the observation condition, the differential activation between the active and observation conditions is consistent with a role of the ACC for adjustments in control (Kerns et al., 2004) and/or strategy (Heilbronner and Hayden, 2016) rather than error monitoring per se. In that sense, the relative deactivation of the ACC in the observation condition is expected as subjects had no control on type 1 performance.

Finally, the left insula was also activated in both the active and the observation conditions. Recent evidence using intracranial recordings showed that errors in a go-nogo task led to a feedforward flow of information from the insula to the ACC and pre-SMA while correct response led to an inversion of this directionality (Bastin et al., 2017). Future connectivity analysis with seeds in the insula could possible disentangle its role.

Self-generated actions improve the accuracy of confidence judgments

Our results show that metacognitive monitoring (defined as type 2 performance) was better in the active compared to observation condition. This difference cannot be accounted by previous models of metacognitive confidence judgments assuming that confidence is a readout of the state of evidence accumulated, possibly continuing after the response (Pleskac et al., 2010). Indeed, the evidence accumulation was identical in the active and observation conditions. Therefore, the decision and/or the motor action in the active task must have some effect on the confidence judgments.

Previous evidence showed that subjects have similar metacognitive improvements when there is a type 1 response prior to the confidence judgments, compared to confidence judgments alone (Kvam et al., 2015). To explain this difference, the authors used a model taking into account a possible influence of type 1 decision on the state of evidence, thus departing from previous evidence readout models (Pleskac et al., 2010). In their so-called quantum[2] walk model, the evidence state is not definite and each evidence level can be assigned a probability. A decision is considered as a measurement that creates a definite state from the previously indefinite evidence states. Evidence coming after the decision continues to be gathered in an undefined state, but starting from the defined state induced by the decision.

Our study differs in the way that the confidence ratings are gathered: in the study of Kvam et al. the confidence relates to the side of the response and can therefore be considered as a second type 1 response on a continuous scale. On the contrary, we probed –at the same time as confidence, the appraisal of errors versus correct. Thus, in both conditions, the sign of the confidence value (error versus correct) can only be defined after the action (whether self-generated or observed). Consequently, an interaction between the action and the evidence state has to occur *somehow* for subjects to rate their confidence. Crucially however, in the observation task, the action is not congruent with a decision taken by the subject. Therefore, in the observation task, the action does not arise from a measurement of the state of evidence and following the model from Kvam et al., it should not create a definite state of evidence (Kvam et al., 2015). In accordance with this hypothesis, in the active task, type 1 decision fix the evidence to a definite state. Further evidence is then accumulated in an undefined state, but starting from the state of the type 1 response which is favorable since type 1 performance is above 50%. In the observation condition however, the evidence is never defined in a favorable state until the confidence rating decision, since no type 1 decision is made.

An alternative model was proposed by Van den Berg et al. using a two choice perceptual decision task with two levels of confidence. The authors showed that changes of mind when rating confidence level could be explained by an adaptation of the boundaries of the evidence accumulation process leading to confidence after the initial decision (Van Den Berg et al., 2016). Our data does not allow us to make inferences about changes of confidence during a trial. However, we can speculate that initially low confidence at the time of the type 1 response raises the bound for high confidence after the type 1 decision is made. This is supported by the results of the Van den Berg et al. study. Using a two choice perceptual decision task with two levels of confidence, the authors showed that changes in confidence level following uncertain type 1 responses could be explained by a raise of the boundaries of the evidence accumulation process leading to confidence after the initial decision (Van Den Berg et al., 2016). Such adaptive boundaries could have a beneficial effect on type 2 performance by leading

[2] Note that the quantumness of the model is only in the way decision fix evidence and the authors of this study do not imply that the brain performs quantum computations.

subjects to make less extreme confidence judgments. Our behavioral data shows that subjects made more type 2 ratings of medium confidence for correct responses in the active condition (Figure 2-2B). This effect of more cautious confidence judgments after a type 1 response was also observed by Kvam et al. (Kvam et al., 2015).

We found a correlation between BOLD activation and differences in type 2 accuracy between conditions. Two brain regions (the left pre-SMA and the IFG) were more activated in the observation task with activation explaining worse metacognitive performance during the observation task compared to the active condition. Interestingly, these two brain regions are part of a network responsible for motor inhibition (Aron et al., 2003; Swann et al., 2009; Picazio et al., 2014; Fiori et al., 2016). The activation of this network during the observation task could thus be explained by the inhibition of the motor response. A speculative but nonetheless attractive hypothesis is that one compensatory strategy of some subjects during the observation condition could be to use the motor system to predict a response (Schubotz, 2007) and then compare it to the visual feedback of the virtual hand. Those subjects with higher activation of the inhibitory network (likely to prevent an inadvertent motor response) would benefit less from this strategy. This would explain the contribution of sensorimotor areas of the scalp in predicting confidence in our EEG decoding analysis. A previous EEG study found sensorimotor contribution to error detection (van Schie et al., 2004). Moreover a TMS study showed that disrupting signals from the motor cortex impaired metacognitive judgments (Fleming et al., 2015). Future work using fMRI-informed EEG (Hauser et al., 2015) could possibly help understanding the timing of the activation of sensorimotor regions and provide further experimental support to this hypothesis.

2.4 Materials and methods

Subjects and task

Twenty-two healthy subjects (9 women) with normal or corrected-to-normal eyesight and no reported neurological problems performed a perceptual decision task in a MRI scanner. Electroencephalographic data was concurrently recorded from 63 scalp electrodes.

Each trial started with a fixation cross displayed for 500 ms. Then a total of 100 dots were distributed unequally among the two boxes situated on each side of the fixation cross and flashed for 60 ms. Subjects then had to make rapid decisions about which box contained most dots. To dissociate between self-generated and observed errors we divided the task in two conditions. During the motor task, subjects had to respond in less than 500 ms, by pressing a button on the side where they perceived most dots. Slow responses (>500 ms) were discouraged by playing a loud and annoying alarm sound. During the observation condition, a virtual hand appeared on one side of the screen which could correspond to either a correct or incorrect response. After each response (button press or virtual hand onset), perceptual processing was stopped by showing a mask composed of all dots (100 in each box). After 1.5 s following the stimulus onset, subjects had to input how confident they were, either about their own response (during the motor task), or about the response they saw on the screen (during the observation condition). For this, a vertical scale was shown, ranging from 0 for certainty that the previous response was erroneous to 1.0 for certainty that the previous response was correct. The middle of the scale (0.5) meant that the subject was unsure about the previous response. A cursor moved back and forth along the scale at slow speed during 6.5 seconds. The subjects had to press the left button when the cursor was at the level of the scale corresponding to their confidence. The subjects were instructed to use the whole length of the scale. The cursor would always pass through each position at least twice so that subjects had one more chance were they to miss the first pass of the cursor.

Each experimental run was divided into four blocks of 12 trials of one condition, alternating between blocks and with a 10 s rest period between each block. The inter-trial interval (ITI) and rest durations were optimized a-priori to maximize design efficiency (Friston et al., 1999). The experiment comprised six experimental runs, totalizing 144 trials per condition (active and observation). During the active condition, the task difficulty was adjusted by an automatic one-up two-down staircase procedure to make the type 1 performance rate converge to 71% (Levitt, 1971). Every time subjects made an error, the perceptual difficulty of the task was decreased by one (by increasing the difference in the number of dots on each side). Every time subjects made two consecutive correct responses, the perceptual difficulty was increased by one. The perceptual difficulty was pre-tuned to individual perceptual abilities by performing 96 trials of the active condition without confidence ratings prior to entering the scanner.

EEG data acquisition and preprocessing

EEG data were recorded at 5000 Hz using a 63 channel BrainAmp DC-amplifier from BrainProducts GmbH (Munich, Germany) synchronized to the scanner's internal clock. MR-gradient artifacts were removed using sliding window average subtraction (Allen et al., 2000). We used the TP10 electrode on the right mastoid to detect heartbeats in a semi-automatic procedure and applied ballistocardiogram artifact (BCG) removal. We then applied zero-phase (two-pass) bandpass filtering between 1 and 30 Hz, re-referenced to a common average and applied independent component analysis (ICA (Makeig et al., 1999)) to remove residual BCG and ocular artifacts. Single-trial epochs were defined using a one second time interval of [-0.4, 0.6 s] around the response onset (i.e. the button press for the active condition or the appearance of the virtual hand for the observation condition). Statistics were conducted using mixed models with fixed- and random-effects and degrees of freedom were estimated using Satterthwaite's correction.

EEG decoding models

To assess whether the ERP found in this study contained confidence information, we used single-trial regression to predict the confidence from the EEG. We used a 100 ms sliding window between -0.4 and 0.6 seconds after the action. The EEG signal was averaged across the time window for each electrode. Since there were few trials (144/conditions) compared to the 64 electrodes, we used ridge regression (L2 regularization). For each subject, condition and time point, we split the data in two equal sized partitions. We used the first partition to fit 15 regression models to the confidence ratings with different regularization factors. Next, we used a model showing maximal performance on the training data (in terms of correlation) to regress the unseen data from the second partition and computed the performance of the model (correlation). We then switched the partitions and repeated the same procedure. We performed 10 different splits, leading to 20 partitions and corresponding performance (correlation). To assess if our models performed better than chance, we repeated the whole procedure 200 times while shuffling the confidence ratings across trials (surrogate data). We z-scored the performance of the original models using the mean and standard deviation of the surrogate data. The resulting z-scored correlations represent how much better the models performed in standard deviations of the surrogate data.

fMRI data acquisition and processing

fMRI was recorded in a 3T Prisma Siemens scanner with a 32-channel coil. We used an EPI sequence (TR=1280 ms, TE=31 ms, FA: 64°) with 4x multiband acceleration. We acquired 64 slices of 2 x 2 x 2 mm voxels without gap (FOV: 215 mm) with slice orientation tilted 25° backward relative to the AC-PC line so as to include the cerebellum. Structural T1-weighted images were acquired using a MPRAGE sequence (TR=2300 ms, TE: 2.32 ms, FA: 8°) with 0.9 x 0.9 x 0.9 mm voxels (FOV: 240 mm).

The functional scans were realigned, resliced and normalizated to MNI space using the flow fields obtained by diffeomorphic anatomical registration through exponential linear algebra (DARTEL). Finally, the normalized scans were smoothed using a Gaussian kernel of 5 mm full-width at half maximum (FWHM). The pre-processing was done using SPM12. We then first modelled the BOLD signal using a general linear model (GLM1) with two separate regressors (stick functions at stimulus onset) for the active and observation condition as well as their spatial and temporal derivatives. Bad trials with i) RTs above 500 ms (thus provoking the alarm sound), ii) without type 1 or type 2 responses or iii) with a button press during the observation condition were modelled by two separate regressors (one for active and one for observation) and their spatial and temporal derivatives. We added six realignments parameters as regressors of no interest. This GLM1 allowed us to conduct a second-level analysis with the contrast between the regressors for the active and observation conditions. Mean behavioral variables were added for each subject as covariates (see results). Additionally, GLM1 allowed us to isolate the task-activated brain regions for both task (Figure 2-7).

Secondly, to find the brain regions covarying with confidence ratings, constructed a second GLM (GLM2) by parametrically modulating the two trial regressors from GLM1 with i) confidence, ii) RT and iii) delta. The variance of the task was explained by the two regressors and a second-level analysis was conducted on the parametric regressor for confidence. A third GLM for uncertainty (GLM3) was constructed in a similar way but changing confidence with absolute confidence, computed as the absolute value of the confidence minus 0.5. All group-level results are reported at a significance-level of $p<0.05$ using cluster-extent family-wise error (FWE) correc-

tion with a voxel-height threshold of p<0.001. We used the anatomical automatic labelling atlas for brain parcellation (Tzourio-Mazoyer et al., 2002).

2.5 Supplementary material

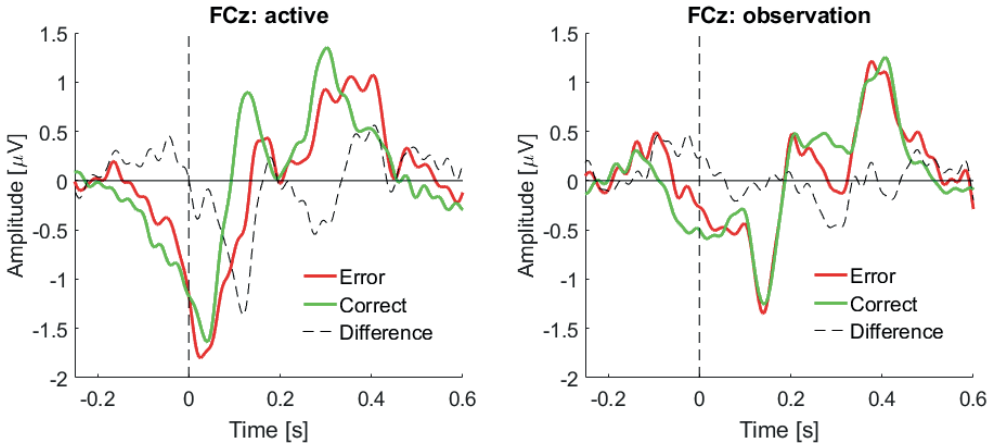

Figure 2-8. ERP analysis dissociating error (red) from correct (green) responses for the active condition (left) and the observation condition (right). Dashed black lines show the difference trace (error – correct).

Table 2-1. fMRI activation related to confidence ratings

	p(FWE)	Size	t(peak)	p(peak)	MNI			Label
Conj.	0.008	366	4.24	0.914	-6	9	60	Supp_Motor_Area_L, Frontal_Sup_Medial_L
	0.019	308	4.57	0.653	-36	21	-11	Insula_L, Frontal_Inf_Orb_2_L
	0.033	273	4.15	0.951	-38	-44	45	Parietal_Inf_L
Act-	<0.001	14067	9.27	<0.001	-6	14	65	(*)
	<0.001	2952	5.95	0.024	-60	-51	33	Parietal_Inf_L
	<0.001	846	5.21	0.172	-53	-39	-3	Temporal_Mid_L
	0.002	458	4.52	0.701	56	20	32	Frontal_Inf_Tri_R, Frontal_Inf_Oper_R
	0.003	434	4.81	0.429	35	0	56	Frontal_Mid_2_R, Frontal_Sup_2_R
	0.009	358	5.79	0.037	-23	50	27	Frontal_Sup_2_L, Frontal_Mid_2_L
Mon-	0.007	381	4.21	0.914	-6	9	60	Supp_Motor_Area_L, Frontal_Sup_Medial_L
	0.015	325	4.57	0.653	-36	21	-11	Insula_L, Frontal_Inf_Orb_2_L
	0.024	294	4.15	0.951	-38	-44	45	Parietal_Inf_L
Act+	<0.001	591	4.71	0.522	0	-87	18	Cingulate_Ant_L, Recturs_L, Frontal_Med_Orb_L
	0.013	336	5.63	0.058	-23	-8	-12	Occipital_Mid_L
Mon+	<0.001	2013	5.90	0.027	-5	-83	32	Cuneus_R, Cuneus_L
	<0.001	1781	5.95	0.024	-26	-5	-15	Hippocampus_L, Temporal_Sup_L
	<0.001	642	4.64	0.587	-3	32	-11	Frontal_Med_Orb_R
	0.007	379	4.82	0.421	63	-15	8	Temporal_Sup_R, SupraMarginal_R, Rolandic_Oper_R
	0.010	352	5.39	0.110	-21	-99	9	Occipital_Mid_L, Occipital_Sup_L
	0.010	351	6.05	0.018	15	-99	11	Occipital_Sup_R, Cuneus_R
	0.018	312	5.05	0.258	27	-5	-27	Hippocampus_R

Table 2-2. fMRI activation related to absolute confidence ratings.

	p(FWE)	Size	t(peak)	p(peak)	MNI			Label
Conj.	<0.001	648	4.19	0.561	-8	11	60	Supp_Motor_Area_L
	0.044	232	4.99	0.319	-50	26	30	Frontal_Inf_Tri_L
Act.	<0.001	836	5.05	0.248	-5	9	68	Supp_Motor_Area_L
	0.003	389	5.58	0.074	-50	26	30	Frontal_Inf_Tri_L
Mon.	<0.001	2642	5.58	0.074	-2	21	44	Supp_Motor_Area_L, Supp_Motor_Area_R
	<0.001	1239	5.31	0.148	62	-15	30	Postcentral_R, SupraMarginal_R
	<0.001	695	5.22	0.185	-59	-23	36	Supramarginal_L, Postcentral_L, Parietal_Inf_L
	<0.001	552	5.47	0.098	56	11	26	Frontal_Inf_Oper_R
	0.012	310	4.99	0.319	-50	26	30	Frontal_Inf_Tri_L
	0.023	269	4.20	0.951	-44	11	-6	Insula_L
	0.036	243	5.68	0.056	-47	6	33	Precentral_L

Table 2-3. fMRI activation for metacognitive differences between conditions.

	p(FWE)	Size	t(peak)	p(peak)	MNI			Label
Any	<0.001	2409	7.89	0.069	-47	17	2	Frontal_Inf_Oper_R, Frontal_Mid_2_L
	<0.001	1598	8.39	0.037	47	24	-5	Frontal_Inf_Tri_R, Frontal_Inf_Oper_R
	<0.001	1091	7.51	0.110	8	35	48	Frontal_Sup_Medial_L, Frontal_Sup_Medial_R
	<0.001	763	9.88	0.006	50	47	-6	Frontal_Mid_2_R, Frontal_Inf_Orb_2_R
	0.017	254	8.68	0.026	26	15	47	Frontal_Sup_2_R
	0.027	230	6.10	0.552	-24	27	57	Frontal_Mid_2_L, Frontal_Sup_2_L
	0.042	207	5.54	0.834	41	14	41	Frontal_Mid_2_R, Frontal_Sup_2_L
Conj. Monitor	0.007	302	6.19	0.505	-40	30	20	Frontal_Inf_Tri_L, Frontal_Inf_Orb_2_L
	0.034	218	6.62	0.319	-2	30	47	Frontal_Sup_Medial_L

Table 2-4. Task-related activations.

These regions are activated by both conditions (conjunction analysis)

	p(FWE)	Size	t(peak)	p(peak)	MNI			Label
Conj.	< 0.001	3830	9.42	<0.001	-17	-66	56	Parietal_Inf_L, Parietal_Sup_L
	< 0.001	3318	9.25	<0.001	20	-62	59	Parietal_Sup_R
	< 0.001	1273	8.20	<0.001	-27	-5	56	Precentral_L, Frontal_Sup_2_L
	< 0.001	1553	6.35	0.008	44	14	5	Frontal_Inf_Oper_R
	< 0.001	1120	6.35	0.008	27	-5	51	Frontal_Sup_2_R, Precentral_R, Frontal_Mid_2_R
	< 0.001	925	6.69	0.003	-6	18	48	Supp_Motor_Area_L, Supp_Motor_Area_R
	< 0.001	844	7.49	<0.001	51	-63	5	Temporal_Mid_R
	< 0.001	782	7.24	0.001	-45	11	3	Insula_L, Frontal_Inf_Oper_L
	< 0.001	668	6.06	0.018	32	-54	-29	Cerebellum_6_R
	< 0.001	615	6.80	0.002	-42	-69	3	Occipital_Mid_L, Temporal_Mid_L

	0.001	558	6.56	0.004	-54	5	39	Precentral_L

Chapter 3 Correlates of performance monitoring coupled to sub-movements

Most of the material from this chapter was taken form an accepted manuscript: *Pereira M, Sobolewski A, Millán JdR. Action monitoring cortical activity coupled with submovements, eNeuro. 2017.* The analysis were entirely conducted by the author.

3.1 Introduction

The last chapter investigated the neural substrate and electrophysiological correlates of a performance monitoring system stripped from correlates of motor and post-error adjustments in a perceptual decision task. However, much of human behavior and resulting visual feedback is a seemingly continuous and not easily parsed operation (Cisek and Kalaska, 2010). In this chapter, we study performance monitoring in behaviors that demand constant monitoring of motor errors and in which erroneous and corrective actions are closely linked in a closed sensorimotor loop of error detection and correction based on continuous visual feedback.

In order to have access to an objective measure of "error", we used a visuo-motor tracking paradigm in which the instantaneous distance between the cursor and the tracked target can be quantified. During such tasks, the kinematics and electromyographical (EMG) activity of the upper limb reveal a succession of bell-shaped pulses or "sub-movements", with periodicities between 2 and 10 Hz, depending on the muscles involved (Vallbo and Wessberg, 1993; Jerbi et al., 2007; Williams et al., 2010). Behavioral studies have shown that the magnitude of these sub-movements corresponds to deviations from the desired position, indicating their error-related or corrective nature (Miall et al., 1986; Selen et al., 2006). However, although some studies have found electrophysiological correlates of perturbations during reaching movements (Archambault et al., 2009; Torrecillos et al., 2014; Dipietro et al., 2015), to the best of our knowledge, no brain correlate of error processing has been linked to periodic endogenous sub-movements so far. Moreover, none of the above studies dissociated error processing from differences in kinematics.

In this study, 23 healthy participants used a mouse cursor to follow a moving target on the computer screen (tracking condition). The trajectory followed by the target was visible and was drawn by the subjects themselves in a previous condition (spontaneous condition; Figure 3-7). Additionally, after half of the tracking trials, a replay of the trial was shown to the subjects as a control condition (viewing condition): subjects watched (without moving) the target and the mouse cursor moving on the screen. We recorded high-density electroencephalography (EEG) and thereby report an event-related potential (ERP) time-locked to the sub-movements. Finally, we compared the amplitude of these ERPs with the deviation of the cursor relative to the target, while controlling for motor confounds. We found that the ERP was modulated by cursor deviation, 110 ms before the sub-movement, irrespectively of hand kinematics.

3.2 Results

Subjects failed to keep the mouse cursor inside the target

We quantified instantaneous task performance as the cursor's position projected onto the tangent to the target's direction (Figure 3-1A). Our measure allowed discriminating between deviations consisting in the cursor falling behind the target (negative values) and overtaking it (positive values). The cursor was behind the target 35±6 % (mean±standard error of the mean (s.e.m.) across subjects) of the time and ran ahead 25±5 % of the time; the remaining 40±5 % of the time, the cursor was inside the target. Figure 3-1B shows the distribution of

cursor deviations parallel to the target direction (solid line) and perpendicular to the target direction (dashed line). The mean distance between the cursor and the trajectory (7.4±0.18 px) was much lower than the average Euclidian distance to the target center (20.6±0.5 px) suggesting that subjects were good at following the trajectory but failed to keep up with the target position along the trajectory. On average, subjects spent 0.322±0.010 s outside the target's area before successfully correcting the deviation (Figure 3-1C).

Hand kinematics are composed of periodic sub-movements

To represent sub-movements, we used hand acceleration, computed from hand positions recorded during the task. Consistent with earlier studies (Vallbo and Wessberg, 1993), these kinematics were composed of successive sub-movements, which were not due to the curvature of the trajectories (e.g. Figure 3-1H,I). Sub-movements were defined as peaks in the hand acceleration to which we aligned all subsequent analyses. The resulting averaged profile of sub-movement showed a triphasic waveform which was similar between the tracking and the spontaneous condition (Figure 3-1D). For both conditions, the peak of the acceleration showed an exponentially decreasing distribution (Figure 3-1E). The median time interval between two sub-movements was 0.200±0.002 s for tracking and 0.195±0.002 for spontaneous tracing, corresponding to a frequency of 5.0 Hz and 5.1 Hz respectively (Figure 3-1F).

To verify the periodicity of sub-movements, we normalized the distribution of the time intervals between two consecutive sub-movements by the theoretical distribution expected from a random (Poisson) process with identical rate. This measure thus quantifies how much more probable is a time interval between two consecutive sub-movements compared to a random process. A consistent peak was found for the tracking condition (2.55 times more probable than a random process; maximum at 0.200±0.007 s; Figure 3-1G). On the other hand, the same analysis applied to the times when the cursor leaves the target area showed a lower and more smeared peak (1.84 times more probable than a random process; maximum at 0.72±0.035 s). Finally, Figure 3-1H shows an example of five seconds of tracking with cursor and target positions marked every 0.5 s along with the corresponding deviation and kinematics metrics (Figure 3-1I).

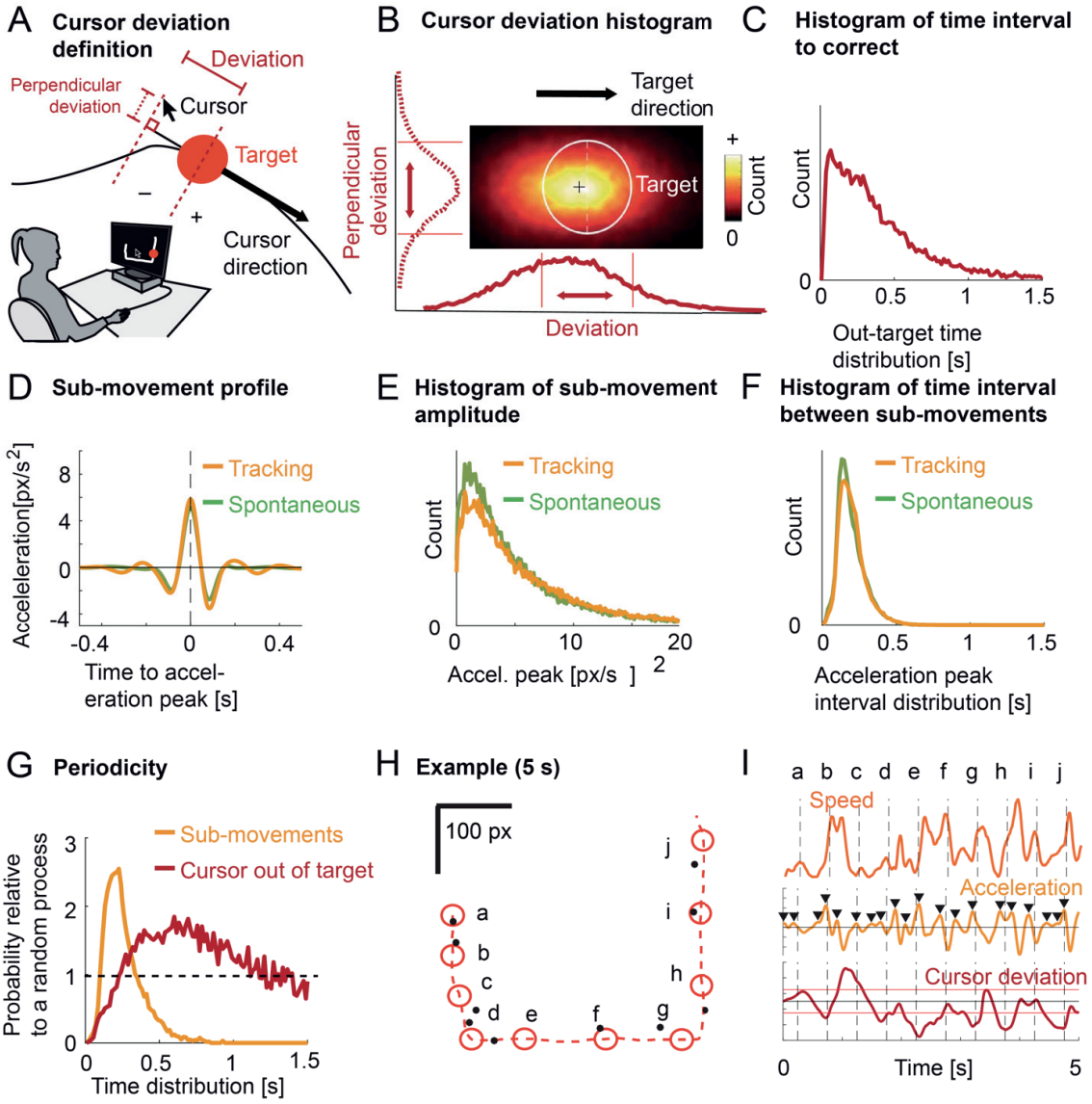

Figure 3-1. Cursor deviation and hand kinematics (sub-movements). *(A) Experimental setup and definition of cursor deviation. Subjects used a mouse cursor (a typical arrow) to track a target (red circle) moving on a computer screen along a visible trajectory. Cursor deviation was defined as the cursor's position relative to the position of the target along the tangent to the target's direction. Perpendicular deviation was defined as the deviation relative to the tangent. (B) Distribution of cursor deviations around the target (white circle), averaged across subjects. The lower curve corresponds to the distribution of the cursor deviation used in the rest of the manuscript. The left (dashed) curve corresponds to the perpendicular deviation. Red vertical lines indicate target borders. (C) Distribution of the time needed to correct cursor deviations: from the time the cursor left the target area to the time it went back in, averaged across subjects. (D) Average hand acceleration profile, time-locked to sub-movements for tracking (yellow trace) and for spontaneous tracing (green trace), averaged across subjects. (E) Distribution of the magnitude of hand acceleration peaks for tracking (yellow trace) and spontaneous tracing (green trace), averaged across subjects. (F) Distribution of time intervals between sub-movements for tracking (yellow trace) and spontaneous tracing (green trace), averaged across subjects. (G) Probability of time intervals relative to a random (Poisson) process for two types of events: sub-movements (yellow trace) and cursor leaving the target area (red trace). (H) An example of five seconds of tracking. The target is depicted by red circles shown every 500 ms (a-j). The dashed red trace shows the trajectory of the target, moving from a to*

j. The corresponding cursor positions are depicted by black dots. (I) Hand speed (orange trace), hand acceleration (yellow trace) and cursor deviation (dark red trace) for the five seconds depicted in panel H. Peaks selected by the peak selecting algorithm are depicted by black triangles. Horizontal red lines show target borders. Vertical dashed lines correspond to target positions in H.

Existence of an ERP locked to sub-movements

We investigated the existence of electrophysiological activity locked to sub-movements. By averaging one second epochs of EEG centered around sub-movements, we found a significant ERP (Figure 3-2A left; FCz; $p<0.01$a, $t(22)<-5.19$). The ERP mainly consisted of a negative peak (trough), 0.038±0.003 s after sub-movement onset. For the spontaneous condition, a smaller yet significant (Figure 3-2B left; FCz; $p<0.01$b, $t(22)<-5.20$) negative ERP wave was found, reaching its trough 0.070±0.003 s after the acceleration peak (Figure 3-8 for ERPs of individual subjects).

Exact low-resolution brain tomography (eLORETA) was used to locate the sources of the ERP (Pascual-marqui, 2007). For tracking, the trough of the ERP had its strongest source in the medial frontal gyrus, Brodmann area 6 (MNI: X=-5, Y=-5, Z=55, corresponding to the left supplementary motor area (SMA) using the automatic anatomical labeling atlas (Tzourio-Mazoyer et al., 2002); Figure 3-2A, right). In the spontaneous condition, the sources of the ERP were strongest in the left precentral gyrus, Brodmann area 4 (MNI: X=-30, Y=-20, Z=65; Figure 3-2B, right). This region also showed activation in the tracking condition.

To control for the influence of pure visual input on the ERPs, we also repeated the ERP analysis using data from the viewing condition during which subjects were simply watching their performance recorded in the preceding tracking task (identical visual stimulation). The analysis was thus aligned to peaks in cursor acceleration. No ERP was found for the visual condition (Figure 3-2B left; FCz; $p>0.087$c, $t(22)>-2.49$). These results, in addition to our EOG correction and the absence of discernable differences due to target-direction (Figure 3-9) allow us to assert that neither the pure visual input without the behavioral context, nor EOG artefacts, were the origin of the electrophysiological phenomenon described herein.

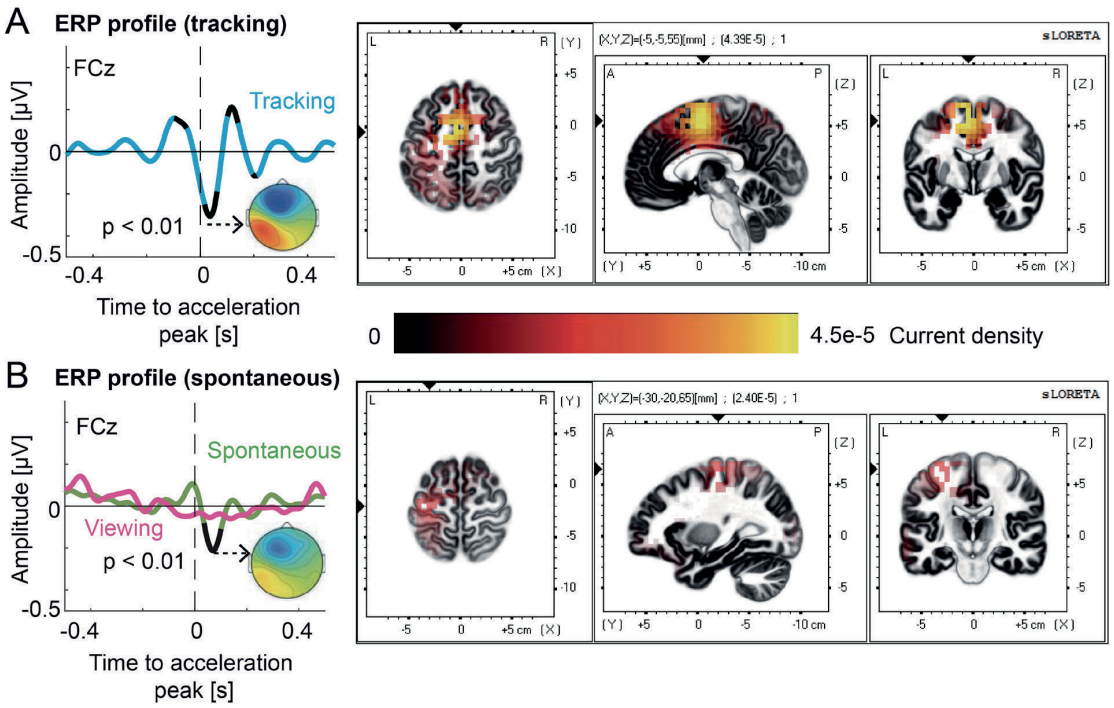

Figure 3-2. ERP time-locked to sub-movements. *(A) The ERP time-locked to sub-movements for the tracking (cyan trace) conditions, averaged across subjects. The ERP showed a significant trough localized in the medial frontal gyrus (right inset). Significant portions of the ERP are shown in black (p<0.01, Bonferroni corrected).(B) The ERP time-locked to hand acceleration for the spontaneous (green trace) and viewing (magenta trace) conditions, averaged across subjects. During the spontaneous condition, the ERP showed a significant trough (black segment, p<0.01, Bonferroni corrected), localized in the left (contralateral) precentral gyrus.*

Latency of the influence of cursor deviation

Following the goal of our study, we sought to investigate the relationship of the ERP to behavioral performance, i.e. cursor deviation. However, we did not know a priori the latency with respect to the sub-movement at which the cursor deviation would, hypothetically, modulate the amplitude of the ERP (Figure 3-3A). We thus constructed a two-dimensional map of single-trial amplitudes depending on the cursor deviation and the latency at which it occurred with respect to the sub-movement.

The resulting map showed that the largest troughs (negative amplitude, i.e. large ERP trough; blue color) were observed for cursor deviations behind the target, occurring 0.11 s before the sub-movement (Figure 3-3B). This latency was further confirmed by analyzing which latency around the sub-movements led to the largest standard deviation of the ERP amplitudes across cursor deviations. The largest ERP modulation occurred at a latency of 0.11±0.04 s before the sub-movements' acceleration peaks (Figure 3-3C). Informed by the results of this exploratory analysis, we sought to verify them, controlling for the possible influence of varying hand kinematics.

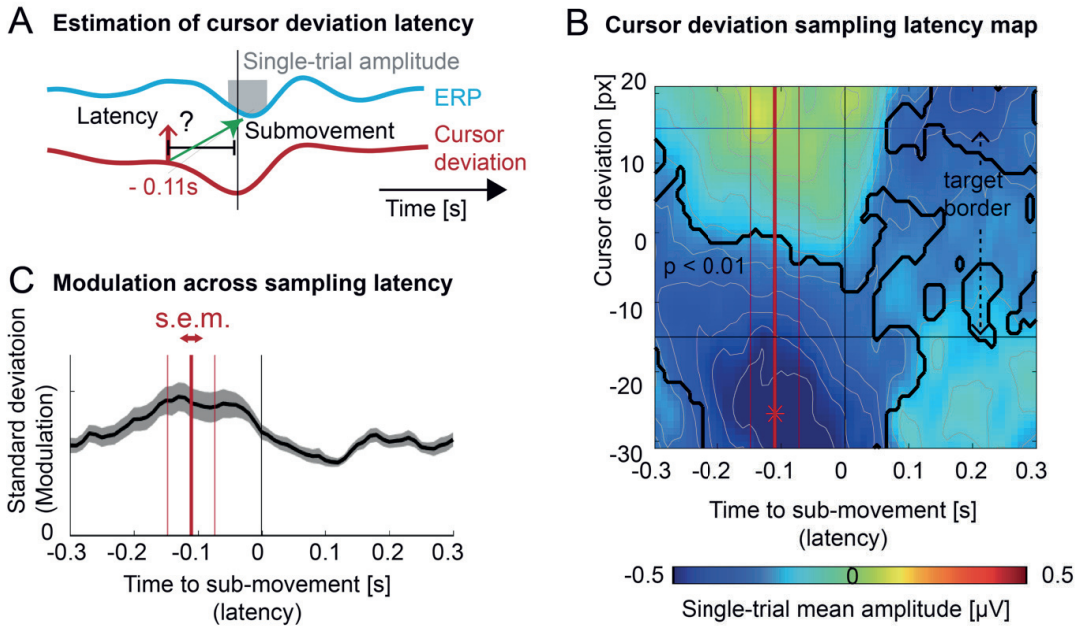

Figure 3-3. Latency of the sampling of cursor deviation *(A) Average profile of the ERP (cyan trace) and cursor deviation (red trace), time-locked to hand acceleration peaks. The upward pointing arrow depicts one potential sampling latency of the cursor deviation, possibly influencing the amplitude of ERP (grey box) (B) Averaged single-epoch mean amplitude (FCz electrode) as a function of the cursor deviation (vertical axis) and the sampling latency of the cursor deviation relative to the sub-movement (horizontal axis). The largest trough (depicted by a red asterisk) was observed for the cursor markedly lagging behind the target (negative cursor deviation) before the acceleration peak. The black trace shows portions of the map corresponding to ERP amplitudes significantly different from zero across subjects (p<0.01, Bonferroni corrected). The horizontal black lines represent the target borders. (C) The standard deviation of the ERP amplitudes across cursor deviation. The maximum value, averaged across subjects (thick red vertical bar) of the minimum single-trial amplitude was estimated to be 0.11 s before the sub-movement. The two thin red vertical bars represent the standard error of the mean (s.e.m.) of this estimation.*

Modulation of the ERP by cursor deviation

To verify that hand kinematics are not the main factor of ERP modulation, we divided the EEG epochs of the tracking condition into bins according to the cursor deviation 0.11 s before the acceleration peak. For each bin, we selected a subset (N=100) of epochs for which we could find an equal number of epochs in the spontaneous condition that showed maximal similarity in terms of hand kinematics (Figure 3-10). For the tracking condition, different bins showed different cursor deviation (Figure 3-4A), corresponding to different sub-movement kinematics (Figure 3-4B). These selected sub-movements showed increasing acceleration as the cursor lagged behind the target but similarly low acceleration when the cursor was in front of the target center (Figure 3-4B, inset).

For the tracking condition, the ERP was larger for cursor deviations behind the target. The ERP in the spontaneous condition, which did not correspond to any cursor deviation but had identical kinematics showed a much reduced modulation (Figure 3-4C). We quantified these ERP amplitudes by computing the mean of the ERP for every subject in a 0.1 s window centered around the ERP trough's latency (Clayson et al., 2013). A repeated measures ANOVA on the so-computed ERP amplitudes revealed a significant effect of cursor deviation ($F(6,132)=16.42$, $p<0.001$d), but not of task (tracking versus spontaneous; $F(1,22)=2.79$, $p=0.11$e). However, there was a significant interaction between task and cursor deviation ($F(6,132)=11.86$, $p<0.001$). Post-hoc tests showed that the amplitude of the ERP was significantly correlated to the cursor deviation (Figure 3-4D; $r2=0.97$, $p<0.001$f, $F(1,6)=141.05$), strongest above the frontal midline (Figure 3-4D, inset). For the spontaneous condition, the correlation was much weaker ($r2=0.63$, $p=0.034$g, $F(1,6) = 8.32$). There were also significant

differences in ERP amplitudes between the tracking and the spontaneous condition (p<0.01h, Bonferroni corrected).

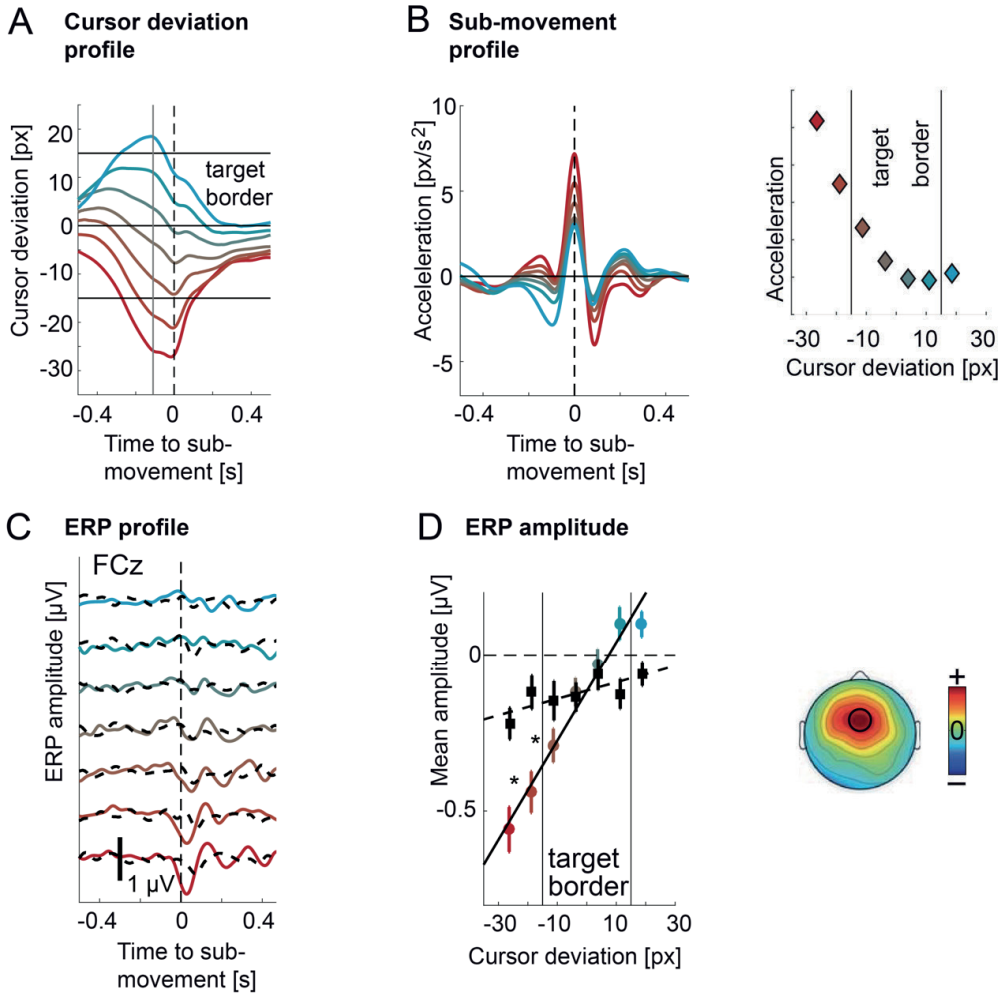

Figure 3-4. Modulation of the ERP by cursor deviation. *(A) Colored traces correspond to different average cursor deviation time courses leading to ERPs in panel C for the tracking condition. Red traces correspond to deviations occurring behind the target and cyan traces correspond to deviations occurring ahead of the target. The same coding scheme was used throughout the Figure. The vertical grey line corresponds to the sampling of the error at 0.11 s before the sub-movement, leading to the modulation of the ERP. Horizontal black lines indicate the target's center and borders. (B) Average hand sub-movement kinematics (acceleration) corresponding to cursor deviations in panel A and ERPs in panel C for the tracking condition. Increasing lagging of the cursor behind the target led to increasing sub-movement kinematics (in order to catch up with the target). The panel on the upper-right shows the relation between cursor deviation and sub-movement peak acceleration. The results of the matching procedure can be found in Figure 4-1 with colored traces showing kinematic profiles of sub-movements from the tracking condition and dashed black traces corresponding to matched sub-movements from the spontaneous condition. Panels are ordered from left to right in order of increasing cursor deviation. (C) ERP (FCz) for different cursor deviations (and sub-movement kinematics) showed increasing amplitudes for increasing lag of the cursor behind the target (negative values). (D) Amplitude of the ERP troughs (FCz) from panel C against cursor deviation at 0.11 s pre-sub-movement. The colored dots correspond to ERP amplitudes from the tracking condition and were correlated with cursor deviation (r^2 = 0.97, p < 0.001). The black squares correspond to ERP amplitudes from the spontaneous condition and also linearly increased (r^2 = 0.63, p = 0.034). The amplitudes were computed by averaging the ERP in time over a 0.1 s window centered on the ERP trough. More negative values correspond to larger troughs. Whiskers denote s.e.m. across subjects. The aster-*

isks show significant differences between the tracking and the spontaneous condition (p<0.05, Bonferroni corrected). Vertical black lines indicate the target's border. For the tracking condition, the slope of this linear fit was strongest over the frontal midline (see inset).

Modulation by cursor deviation is independent from hand kinematics

Since binning the cursor deviation led to differences in hand kinematics, we sought to repeat the analysis controlling for this confound (low frequencies in EEG are known to carry correlates of motor behavior (Waldert et al., 2008)). Therefore, we divided the EEG epochs into the same bins according to the cursor position 0.11 s before the acceleration peak. However, we used only a subset of epochs (N=80) that showed the most similar acceleration profiles across bins. Using this method, we were able to keep hand acceleration profiles similar (Figure 3-5B) across different deviations (Figure 3-5A). The ERP were still larger for cursor deviations behind the target (Figure 3-5C), with amplitudes significantly correlated to cursor deviation (Figure 3-5D; r2=0.95, p<0.001i, F(1,6)=97.54).

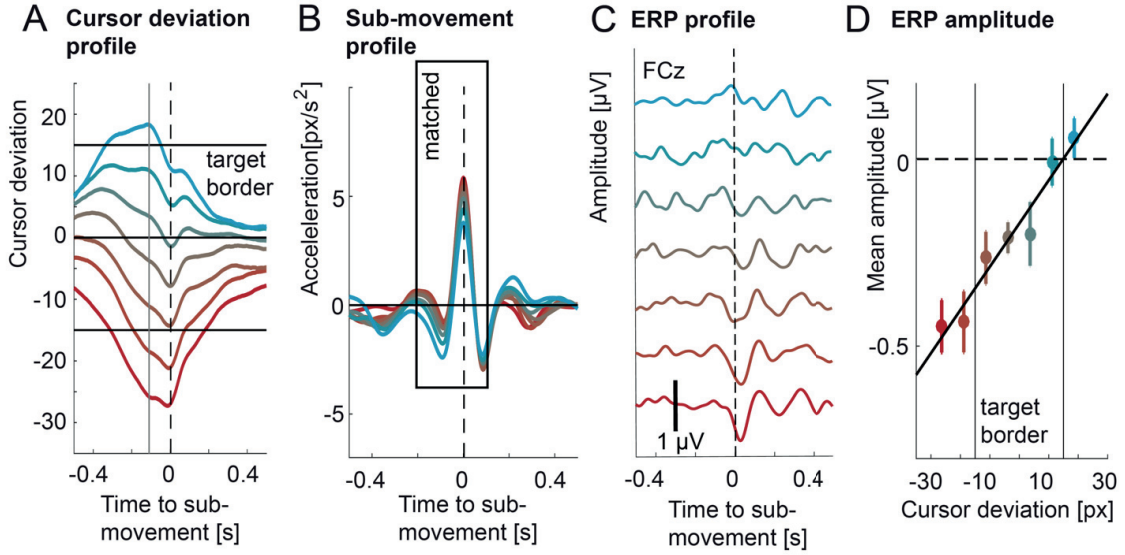

Figure 3-5. Modulation of the ERP by cursor deviation while controlling for kinematics. *(A) Colored traces represent average cursor deviation time courses leading to ERPs in panel C. Red traces correspond to deviations occurring behind the target and cyan traces correspond to deviations occurring ahead of the target. The same coding scheme was used throughout the Figure. The vertical grey line corresponds to the sampling of the error at 0.11 s before the sub-movement leading to the modulation of the ERP. Horizontal black lines indicate the target's center and borders. (B) Matched average sub-movement kinematics (acceleration) corresponding to cursor deviations in panel A and ERPs in panel C. (C) Average ERPs (FCz) for different cursor deviations during the tracking task (colored traces) for matched hand kinematics. The size of the ERP increased with increasing lag of the cursor behind the target (negative values). (D) Amplitude of the ERP troughs (FCz) from panel C correlating to cursor deviation at 0.11 s pre-sub-movement (r^2 = 0.95, p < 0.001). The amplitudes were computed by averaging the ERP in time over a 0.1 s window centered on the ERP's trough. Negative values correspond to larger troughs. Whiskers denote S.E.M. across subjects. Vertical black lines indicate the target's border. The peak-to-peak ERP amplitudes for the control experiment with constant target speed are in Figure 3-11A. Vertical black lines indicate target borders. Kinematics (top) and cursor deviation profiles corresponding to the ERP amplitudes are in Figure 3-11B.*

Control analyses

Since our task comprised many inter-dependent variables such as differences in target speed (target acceleration), cursor deviation and hand kinematics, we performed two control analyses to verify that the ERP was (i) truly coupled to hand-kinematics and not to target acceleration or cursor deviation and (ii) truly related to cursor deviation and not to unexpected differences in target speed.

Firstly, to verify that the coupling between the EEG and the kinematics was not due to indirect couplings with any visual event, we assessed phase-locking for four different types of events using z-scored phase-locked values (zPLV) and phase histograms.No significant modulation was found for target acceleration peaks (Figure 3-6A; zPLV=0.09±0.21, p=0.67j, t(22)=0.43) nor when the cursor crossed the target borders from inside to outside the target (Figure 3-6B; zPLV=0.42±0.36, p=0.25k, t(22)=1.17). We found significant modulations for peaks in the Euclidian distance between the cursor and the target (Figure 6C; zPLV=1.50±0.33, p<0.001l, t(22)=4.60) and sub-movements (Figure 3-6D; zPLV=5.26±0.64, p<0.001m, t(22)=8.18). The phase-locking for sub-movements was significantly stronger than for peaks in the Euclidian distance (p<0.001n, t(22)=6.86, paired t-test). We thus confirm that, although peaks in the Euclidian distance between the cursor and the target modulate the phase of the EEG and could therefore lead to an ERP (Hill and Raab, 2005), the behavioral event leading to the strongest phase modulation were the sub-movements, in accordance with our analysis.

Secondly, since during tracking, the target speed corresponded to a smoothed copy of the hand kinematics from the spontaneous task, we controlled that our results corresponded to an action monitoring process of subjects' own errors and not solely of unexpected target speed differences. We thus replicated the results from Figure 3-11 in a control task during which 16 subjects tracked a target moving at constant speed along pre-defined trajectories (N=20). Amplitudes were still significantly correlated to cursor deviation (Figure 3-11A; r2=0.976, p=0.012o, F(1,6)=82.46)

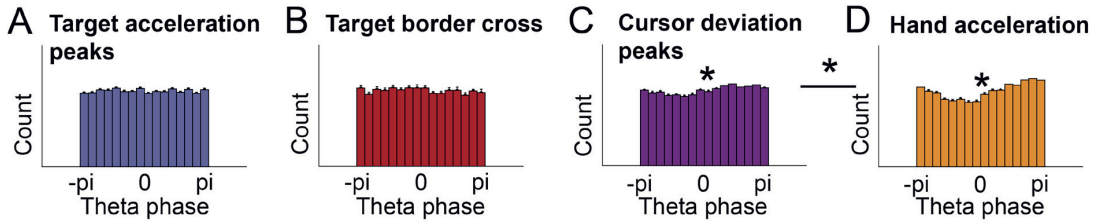

Figure 3-6. EEG phase-locking for different behavioral events. *(A) No significant phase modulation was found for target acceleration peaks (zPLV=0.09±0.21, p=0.67, t(22)=0.43, one-sample t-test). Each histogram bar corresponds to the count of corresponding EEG phases at target acceleration peaks. (B) No significant phase modulation was found when the cursor left the target area (zPLV=0.42±0.36, p=0.25, t(22)=1.17). (C) A weak but significant phase modulation was found for peaks in the Euclidian distance between cursor and target (zPLV=1.50±0.33, p=0.00014, t(22)=4.60). (D) The largest (significant) phase modulation was found for sub-movements (peaks in hand acceleration; zPLV=5.26±0.64, p<0.001, t(22)=8.18). This modulation was significantly stronger than for peaks in the Euclidian distance between the cursor and the target (panel C) (p<0.001, t(22)=6.86, paired t-test).*

3.3 Discussion

This study reports an ERP source-localized in the SMA and encoding behavioral deviations during continuous, visually-guided movements. The ERP was coupled to sub-movements defined by hand acceleration – a correlate of agonist/antagonist muscular activity (Vallbo and Wessberg, 1993). Phase-locking between the EEG and the sub-movements was much stronger compared to phase-locking with visual events such as target accelerations, the cursor leaving the target area or peaks in the Euclidian distance between target and cursor (Hill and Raab, 2005)-

Relation to cursor deviation

The amplitude of the ERP was positively correlated with the deviation of the cursor, 0.11 s before the sub-movement, thus 0.15 s before the ERP's through. The more the cursor deviated behind the target, the larger the ERP and the acceleration of the sub-movements. When the cursor was in front of the target however, no discernible ERP was observed and sub-movement accelerations were similar. These results imply that the brain mechanism underlying the ERP does not encode an absolute value of the error such as the Euclidian distance but the amount of correction needed to catch up with the target. This modulation was also present, albeit much weaker when selecting similar sub-movements from the spontaneous task. This suggests that the cortical process underlying the ERP could be a hard wired component of visually-guided movement loops, though not serv-

ing a functional purpose in artificial lab scenarios such as aimless (spontaneous) movements.

However, the modulation of the ERP by cursor deviation was still present in the tracking condition when selecting identical kinematics but different cursor deviations, excluding the possibility that the modulation due to cursor deviation is solely driven by differences in kinematics.

No significant ERP was found in the viewing condition, during which deviations were only observed with no motor output. The ERP is thus not generated by the visual content of the task stripped of its behavioral context. This does not eliminate the possible existence of an evaluative process in the brain such as in (van Schie et al., 2004), but not aligned to the same events (i.e. peaks in cursor acceleration).

Relation to previous studies of action monitoring

The morphology and topography of the ERP shows clear similarities with ERP correlates of error found in discrete cognitive paradigms. The error-related negativity (ERN) is generated by the subjects' own erroneous responses in speeded choice-response tasks, which do not require external sensory input to appraise the accuracy of the choice (Falkenstein et al., 1991; Gehring et al., 1993). The ERN peaks around 0.06 s after the motor response, a timing considered too early to rely on sensory feedback (Rodriguez-Fornells et al., 2002). The ERP in this study also peaks shortly after movement but its amplitude correlates with the cursor deviation. This suggests that it relies on visual feedback, alike the FRN which is observed when errors are detected based on sensory feedback (Miltner et al., 1997).

Our analysis showed that this feedback is sampled 0.11 s before the sub-movement, inline with behavioral models suggesting that 0.115 s are enough to generate a corrective motor plan based on experimentally displaced cursor positions (Saunders and Knill, 2004).

Since the ERP occurs 0.038 s after the peak, this 0.11 s feedback sampling occurs around 0.15 s before the trough of the ERP, thus faster than the latency of the FRN (0.25 – 0.30 s after feedback onset). Interestingly, the continuous unfolding of the present task could allow for a better prediction of the feedback, thus allowing the brain to respond faster. Without motor output, error-related brain correlates do not scale to the magnitude of the error (Hajcak et al., 2006). However, similar scaling of the ERP amplitude by deviation/error can be seen when errors are motor-related (Vocat et al., 2011; Torrecillos et al., 2014).

These previous studies however, did not control for differences in hand kinematics. Moreover, there is a fundamental difference between behavior requiring one discrete response, or pointing hand movement, and continuous motor behavior, during which performance has to be constantly monitored. Our study can be seen as generalizing previous error-related ERP findings to the later case, demonstrating that equivalent electrophysiological phenomena do actually operate in scenarios where feedback and behavior are not strictly experimentally segmented.

Cortical network involved

For the tracking condition, the SMA was identified as the strongest source of the ERP. Previous studies have shown that the SMA is active during visually guided movements (Picard and Strick, 2003) and it's activation is related to both sub-movement amplitude (Grafton and Tunik, 2011) and tracking error (Limanowski et al., 2017). Although the role of action monitoring was previously attributed to the anterior cingulate cortex (Ridderinkhof et al., 2004), a recent study showed that the activity of local field potentials in the SMA actually preceded activity in the anterior cingulate cortex when inhibiting a pre-potent response (Bonini et al., 2014). This suggests that – consistent with our results – the SMA is involved in the recalculation of motor plans based on action monitoring. Interestingly, the precentral gyrus (were the motor cortex lies) was also part of the sources of the ERP and was found to be the strongest source of the ERP during the spontaneous condition. This suggest that the cortical network coupled to sub-movements is broader than the SMA, as was found in previous studies (Gross et al., 2002; Jerbi et al., 2007). Sources in the SMA were found only during tracking and not during spontaneous tracing, further supporting its involvement in action monitoring.

Relation to low frequency cortical oscillations

Our results show that an ERP is generated in synchrony with sub-movements. Considering the periodicity of the sub-movements, the ERPs should thus overlap with a periodicity of 5 Hz, therefore oscillating in the theta frequency band. Hence, it remains unknown whether the electrophysiological activity in this study corresponds to a

succession of ERPs occurring at 5 Hz or oscillatory activity per se coupled to hand kinematics, as proposed in previous studies (Jerbi et al., 2007; Williams et al., 2010; Hall et al., 2014a). Theta (5 Hz) oscillations are believed to support a number of cognitive operations (Cavanagh and Frank, 2014) such as memory encoding (Sederberg et al., 2003), error (Luu et al., 2004), response conflict (Cohen et al., 2008) or differences in decision confidence/threshold (Herz et al., 2016). Theta oscillations have also been linked to errors during tracking tasks (Huang et al., 2008; Cohen, 2016). Furthermore, modulations of attention have been found in the theta range in behavior (Fiebelkorn et al., 2013), electroencephalography (Busch and VanRullen, 2010) and magnetoencephalography (Landau et al., 2015), leading to the hypothesis that theta represents the brain's periodic attentional sampling mechanism (Fries, 2015; VanRullen, 2016). Theta periodicity found in active sensing behaviors (Schroeder et al., 2010) such as sniffing and whisking (Colgin, 2013) add support to this hypothesis. Our results can therefore also be interpreted within the framework of an oscillatory attentional process, periodically up-regulating cortical excitability to sample visual feedback at an optimal timing after the sub-movement. The network of low-frequency cortical oscillations coupled to hand kinematics (Jerbi et al., 2007) would thus serve to synchronize the periodic evaluation of cursor deviation to the motor output. It could be speculated that the periodicity of this brain mechanism could thus be scaled to match its capacity limit and explain the functional role of sub-movements in the framework of intermittent motor control (Craik, 1947; Neilson et al., 1988; Karniel, 2011). Interestingly, when varying the frequency of the display of visual feedback during a force tracking task, behavioral performance increased with increasing frequency of intermittent visual feedback up to 6.4 Hz and then reached an asymptote (Slifkin et al., 2000), supporting an optimal sampling of the visual feedback at theta frequency. Computational models have also approximated a capacity limit to be between around 0.25 s (van de Kamp et al., 2013), corresponding to a theta rhythm. This hypothesis however, needs further experimental support.

3.4 Materials and methods

Subjects

Twenty-three right-handed healthy subjects (7 women) participated in the study. Subjects were aged between 20 and 30 years, with normal or corrected-to-normal vision. They had no reported neurological or psychiatric problems. The study was approved by the local university ethics committee and all participants gave written informed consent.

Experimental protocol

Subjects performed 20 times the following sequence of tasks. First, participants were instructed to move the computer mouse at a constant speed for 20 seconds to create a spontaneous curvilinear trajectory ("spontaneous" condition). This trajectory was spatially restricted to an area of the (24'') computer screen subtending a 20° horizontal and 13° vertical visual angle, corresponding to 840 by 525 pixels. The unfolding trajectory was not drawn on the screen: only a cursor was visible to the subjects. Subjects were compelled to keep a steady pace by having to repeat trials exceeding speed limits. Their pace was automatically monitored by our software. Additionally, apparent speed of the mouse cursor was kept under 250 px/s by a smoothing algorithm, applied in real-time during the spontaneous condition.

Spontaneous trials were followed by a visuomotor tracking task ("tracking" condition): the previously generated trajectory was shown on the screen and a target (a red circle of 15 pixels radius) moved along it replicating the movement recorded during the preceding spontaneous trial (after the real-time smoothing). The rationale behind showing the trajectory was to study motor errors rather than surprising changes in target position. The participants were instructed to track the target with a standard computer mouse driving a typical cursor (an arrow), keeping it as close to the target's center as possible. At the end of each trial a score ranging from 0 to 100 was displayed as an incentive to perform well. The score was based on a linear transformation of the mean distance between the cursor and the target center. Subjects used their right hand to operate the computer mouse in both conditions. Finally, after half of the tracking trials, a replay of the preceding trial was shown to the subjects as a control condition ("viewing" condition): subjects watched (without moving) the target and the mouse cursor move on the screen as recorded during the preceding tracking condition. This additional control was used in only half of the trials in order to reduce the duration of the experiment.

Behavioral measures

As opposed to discrete action monitoring paradigms, our tracking experiment allowed for continuous behavioral variables to be measured. We recorded mouse cursor and target positions at 50 Hz (the refresh rate of the monitor) and interpolated these data offline (using piecewise cubic interpolation) to match the 256 Hz sampling rate of the preprocessed EEG. Two measures were derived from these positional data.

Firstly, we quantified the subjects' instantaneous performance using the distance between the target center and the mouse cursor, projected onto a line tangential to the trajectory of the target (Figure 3-1A). This cursor deviation measure was then smoothed using a quadratic Savitzky-Golay filter with a 0.106 s window (Savitzky and Golay, 1964). The absolute value of this cursor deviation measure explained most of the variance of the more intuitive Euclidian distance between cursor and target center (R^2=0.84±0.01 on average). However, we assumed that the brain uses a more functional deviation measure that can be directly translated into the amount of correction needed.

Secondly, to decompose the subjects' hand kinematics into sub-movements in order to align our ERP analysis, we computed the acceleration of the hand (or cursor). We first computed hand velocity by differentiating consecutive hand positions with a quadratic Savitzky-Golay filter and rectifying to obtain the hand speed profile. We differentiated the speed profiles using a quadratic Savitzky-Golay derivative filter to obtain the hand acceleration profile. We set the window length of the smoothing filter to 0.106 seconds as we found this was an optimal balance between efficiently removing high frequency spurious peaks while keeping the spectral structure (Figure 3-12). Sub-movements were defined as peaks in the hand acceleration profiles, i.e. samples higher than their neighbors and higher than zero. Since hand acceleration is closely related to EMG (Vallbo and Wessberg, 1993), we assumed that these peaks were the best available markers of sub-movements.

Electrophysiological recording and pre-processing

Scalp electroencephalographic (EEG) activity was recorded from 64 active electrodes in an extended 10-20 layout using a Biosemi ActiveTwo system (Amsterdam, the Netherlands) and digitized at 2048 Hz. Data were down-sampled off-line to 256 Hz, re-referenced to a common average reference and band-pass filtered (Butterworth; zero-phase two-pass) between 1 and 15 Hz (3dB cutoff). To verify that the filtering did not induce any distortion, we replicated the findings without filtering but using only de-trending of each one second epoch and obtained similar results. Electroocular artifact were removed (see Artifact rejection section). EEG data were then segmented into one-second epochs, each centered around one acceleration peak. ERP were obtained by averaging epochs and averaging the resulting waveform across subjects. Mean amplitudes were computed by taking the mean of the ERP in a 0.1 s time interval centered around the latency of the ERP trough. This method is considered to be robust against noise (Clayson et al., 2013) and was used for both single-trial measurements (Figure 3-3) and ERP amplitude measurement of individual subjects (Figures 3-4 and 3-5).

Artifact rejection

Although smooth pursuit of the target is the natural ocular behavior during visuomotor tracking at low speed (Miall et al., 1993), we took great care in excluding any possible effect of eye movement artefacts on the results. Firstly, the instructions to the subjects to keep the speed of the mouse cursor low during the spontaneous condition and the real-time speed smoothing helped prevent possible saccadic eye movements. Secondly, EOG data were recorded with three sensors, placed above the nasion and below the outer canthi of the participants' eyes. Horizontal EOG was defined as the difference between signal from the outer canthi sensors and vertical EOG (vEOG) activity as the difference between the nasion and the mean of the outer canthi signals. All parts of the signal containing EEG, vEOG or hEOG amplitudes larger than 50μV were discarded from further analyses. Furthermore, to ensure that no small EOG component (such as saccades) could influence our results, we regressed out hEOG and vEOG signals (bandpass filtered with the same filter as for the EEG) from the remaining EEG signals.

Single-epoch amplitude map

To explore the ERP's relationship to task performance (Figure 3-3), we computed the amplitude of the EEG

single-epochs (FCz electrode) and binned these amplitudes according to the cursor deviation. Since this cursor deviation could be measured at various latencies with respect to the acceleration peak, we could not know a priori at which latency the brain samples end-effector deviation. Therefore, for every sampling times (0.01 s bins, range: [-0.3, 0.3] s around the acceleration peak; dimension 1), we binned single-trial ERP amplitudes according to cursor deviations from -60 to +60 px into 1 pixel [px] wide bins (dimension 2). The resulting two-dimensional deviation-latency map of single-epoch amplitudes was smoothed along the spatial dimension using a Gaussian kernel (2.5 px standard deviation). However, not all the subjects had the same cursor deviation distribution so we restricted the displayed area of the so-obtained map in a way that all points in the map corresponded to a minimum of 40 single-trial measurements for every subject.

If no relationship existed between single-trial amplitudes and the cursor deviation, we expected the map to be flat, not showing any systematic pattern. On the contrary, if the ERP was modulated by cursor deviation occurring before the sub-movement onset (acceleration peak), we expected to see larger amplitude differences in the left part of the map. If the ERP was modulated by cursor deviation occurring after the sub-movement, the map should reflect this with larger amplitude differences in the right part.

Matching kinematics

To obtain sets of epochs with similar kinematics between either experimental conditions (Figure 3-4) or cursor deviation bins (Figure 3-5), we constructed a matrix of pairwise mean-square errors (MSE) between epochs of each condition and iteratively selected (without replacement) pairs with the smallest MSE until a threshold number of paired epochs was achieved (or all epochs from one condition were included).

Phase-locking to behavioral events

To confirm that our ERP was coupled to sub-movements and not to any visual event (Figure 3-6), we assessed phase-locking for four different types of events. Phase-locking is preferable over comparing ERP amplitudes since it dissociates phase from amplitude contributions. Since the ERP has a low frequency support (around 5 Hz), any event underlying the ERP should be associated with a significant phase modulation at this frequency range. The phase was computed by bandpass filtering (Butterworth two-pass zero-phase) between 3 and 7 Hz (3dB cutoff), correcting for EOG (see Artefact rejection section) and applying a Hilbert transform. Phase-locked values (PLV) were extracted at each behavioral event. To control for different number of events and non-genuine phase-locking, the PLV was normalized (z-score) using the mean and standard deviation of 1000 surrogate PLV computed by randomly shifting the behavioral data with respect to the EEG. It was then possible to assess whether these z-scored PLV (zPLV) were consistently different from zero across subjects with a one sample t-tests.

Table 3-1. Statistical table.

	Data structure	Type of test	Power
a	ERP (257 time points; within subject)	One sample T-test	1*
b	ERP (257 time points; within subject)	One sample T-test	1*
c	ERP (257 time points; within subject)	One sample T-test	0.73*
d	ERPs amplitude (2 conditions; within subject)	Repeated measures ANOVA	0.70
e	ERPs amplitude (7 levels; within subject)	Repeated measures ANOVA	0.16
f	Mean amplitude of ERPs (7 levels; average across subjects)	F-test	1
g	Mean amplitude of ERPs (7 levels; average across subjects)	F-test	0.41
h	Mean amplitude of ERPs (7 levels; within subject)	Paired T-test	0.96*
i	Mean amplitude of ERPs (7 levels; average across subjects)	F-test	1
j	Mean zPLV (within subject)	One sample T-test	0.07
k	Mean zPLV (within subject)	One sample T-test	0.07
l	Mean zPLV (within subject)	One sample T-test	0.95
m	Mean zPLV (within subject)	One sample T-test	1
n	Mean zPLV (within subject)	Paired T-test	1
o	Mean amplitude of ERPs (7 levels; average across subjects)	F-test	1†

* Bonferroni corrected †p = 0.05 instead of p=0.01

Statistics

Due to the exploratory nature of the study, the alpha level was set to 0.01, except for the control experiment that was hypothesis driven for which the alpha level was set to 0.05. Bonferroni corrections were applied when necessary. Post-hoc achieved power was computed with the G*Power software (Faul et al., 2007) and reported in Table 3-1. In the case of multiple comparisons, the power of the test returning the minimum p-value is reported with the alpha level adjusted (divided by the number of multiple comparisons). For the two-way repeated measures ANOVA, we estimated the power of each of the two main effects independently, using two one-way repeated measures ANOVA.

3.5 Supplementary material

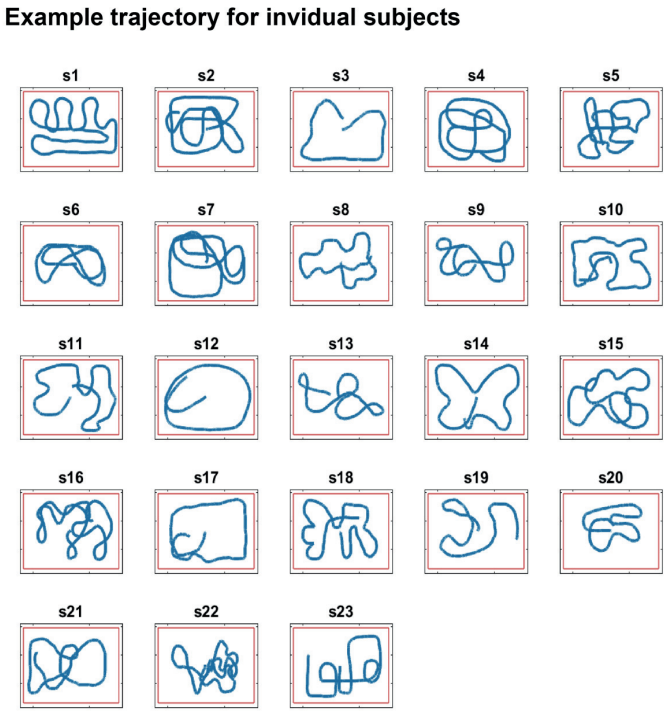

Figure 3-7. Example trajectory for individual subjects. *We show the 10th trajectory drawn by each individual subject. The red rectangle shows the area subtending a 20° x 13° vertical visual angle in which the trajectories were constrained.*

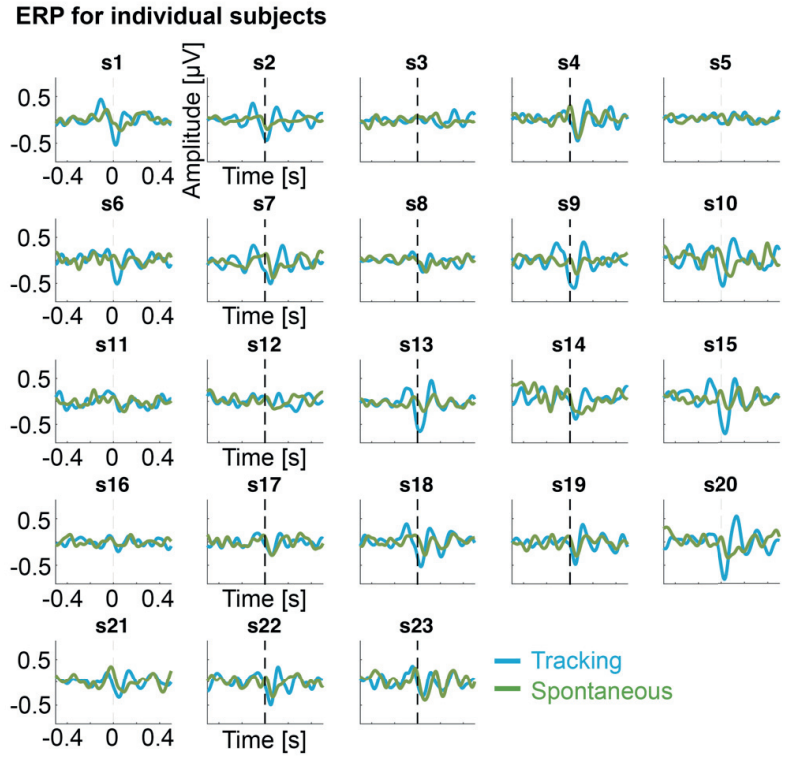

Figure 3-8. ERP for individual subjects. *We show the ERP for the tracking (cyan trace) and spontaneous (green trace) for each individual subjects.*

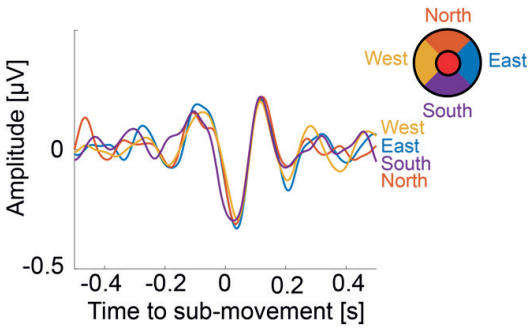

Figure 3-9. ERP for different target directions. *To show that the ERP is not influenced by eye movements artifacts, we binned epochs according to the direction of the target (orange for upwards; violet for downwards; yellow for leftwards; blue for rightwards). No discernible differences were observed.*

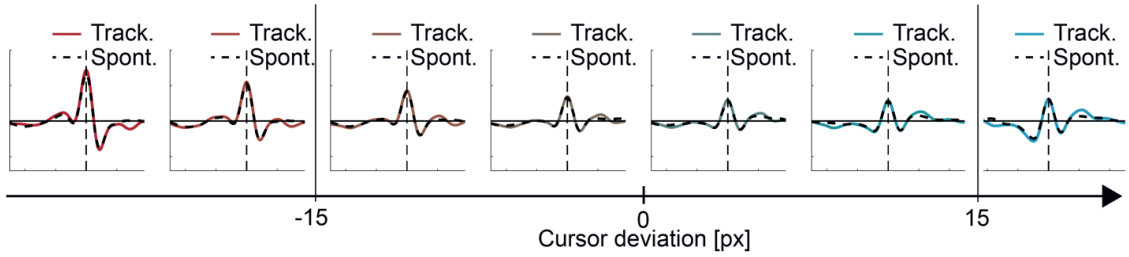

Figure 3-10. Matching between sub-movements from both conditions. *Sub-movement profiles corresponding to different cursor deviation binnings for the tracking condition (red for deviations behind the target; blue for deviations in front of the target) with corresponding sub-movement profiles from the spontaneous condition (dashed black traces).*

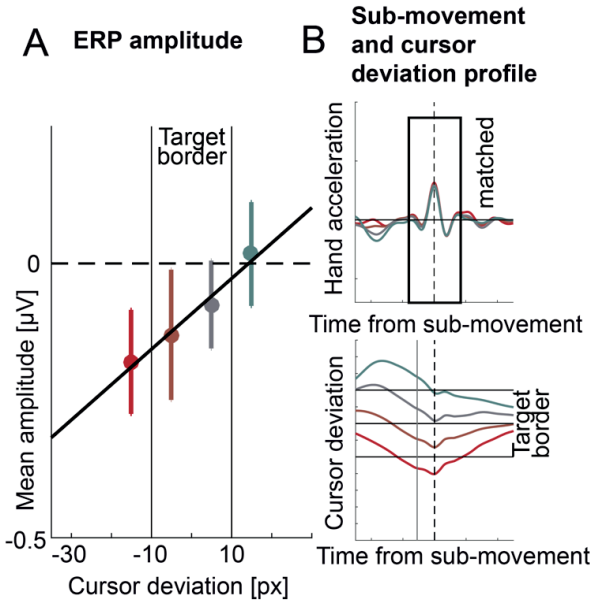

Figure 3-11. Control experiment with constant target speed. *Since target speed was not constant, we verified that this could not confound our results. Sixteen subjects from the main experiment participated in a second experiment during which they had to follow a target moving at constant speed along visible, pre-defined trajectories. Since the task was easier due to predictability of the target, we reduced the size of the target from a radius of 15 px to a radius of 10 px and used only 4 bins for cursor deviation. (A) The amplitude of the ERP for four error bins. Hand acceleration profiles were matched to be similar across bins. Red dots correspond to deviations occurring behind the target center and cyan dots correspond to deviations occurring ahead of the target center. The same coding scheme was used throughout the Figure. (B) The sub-movement (matched hand acceleration; upper panel) and cursor deviation profiles (lower panel).*

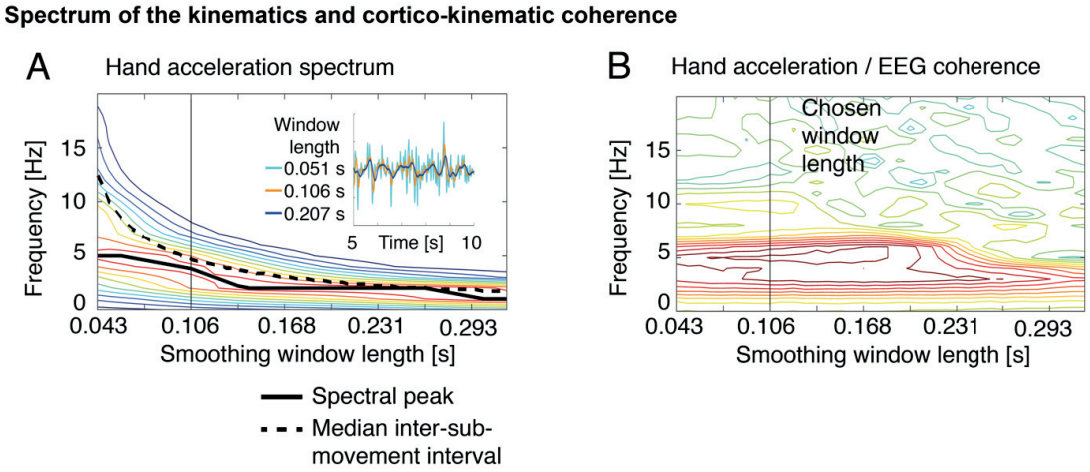

Figure 3-12. Spectrum of the kinematics and cortico-kinematics coherence. *When computing the hand acceleration by derivation and smoothing hand positions with a Savitzky-Golay filter, we faced the problem of finding the right smoothing parameter (i.e. the window length of the filter). (A) We computed the spectrum of hand acceleration for different window length between 0.043 and 0.317 s. We found a consistent spectral peak around 5 Hz for small windows (black trace), while for larger windows this spectral peak was lower in frequency. Additionally, the median time (dashed black trace) between sub-movements decreased with increasing window length. We thus chose the smoothing window to be small enough to have a spectral peak around 5 Hz but large enough to have a median window length close to the spectral peak. The vertical black line indicates the chosen window size. In the inset, we show the effect of smoothing on the acceleration signal. Small windows (0.051 s) led to spurious peaks from higher-frequencies (cyan trace), while smoothing with a large window (0.207 s) led to artificially low frequencies (blue trace). The smoothing used throughout this chapter is shown in orange (0.106 s window). (B) The presence of an ERP aligned to each acceleration peak implies some coupling between the hand acceleration and the EEG. We thus verified that this coupling was present independently from the window length. For this, we computed the coherence between the EEG and the hand acceleration for different window lengths. We normalized (z-score) the coherence by the coherence obtained from 200 surrogate signals consisting in randomly shifted hand acceleration signals. We found high coherence at 5 Hz, confirming that the spectral peak found in the acceleration profile was not an artifact of the pre-processing.*

Chapter 4 Cortical dynamics coupled to hand kinematics in the medial frontal cortex

4.1 Introduction

In the previous chapter, we showed how event-related potentials (ERP) time-locked to periodic sub-movements encoded cursor deviations. Based on the 5 Hz periodicity of sub-movements, we discussed whether it was the sub-movements triggering the ERP (the *ERP hypothesis*) or whether the ERP could represent individual cycles of a theta oscillation [4-6 Hz] time-locked to sub-movements (the *oscillatory hypothesis*). To dissociate between these two hypotheses and further investigate the electrophysiology of performance monitoring during continuous, visually-guided movements, we asked whether high gamma (HG) activity –a reliable correlate of spiking activity (Belitski et al., 2008) would couple to hand kinematics (thus supporting the ERP hypothesis) or theta oscillations (thus supporting the oscillatory hypothesis).

For this, we analyzed intracranial recordings from the medial frontal cortex (MFC) of four epileptic patients performing the same visuo-motor tracking task as in the previous chapter. Patients had to track a target along a pre-defined trajectory. Target speed was adjusted by the experimenter to achieve reasonable performance and not induce frustration. Hand kinematics were composed of sub-movements, which allowed us to probe the existence of couplings between local field potentials (LFP) in the MFC and hand kinematics. We found that hand kinematics were coupled with low frequency cortical oscillations, both in the supplementary motor area (SMA) and in the anterior cingulate cortex (ACC). Furthermore, we found that depending on the electrodes, HG activity could be either coupled with theta oscillations or with hand kinematics, suggesting the existence of two distinct neuronal networks.

4.2 Results

Behavior

All four patients were able to follow the trajectory of the target (Figure 4-1A). We assessed performance at keeping up with the target by constructing histograms of the cursor deviation. The first two patients (P1 and P2) had a tendency to lag behind the target center (Figure 4-1B) while the two last patients (P3 and P4) did not. It should be noticed that performance for each patient should be interpreted with respect to the speed of the target that was set by the experimenter. The duration of one trajectory was fixed to 10 s, so slower target speed led to shorter trajectories. Figure 4-1A shows that although patients P1 and P3 spent more time outside the target, they also had to track a target moving faster (i.e. trajectories covering a larger distance). Figure 4-1C shows the histogram of the time needed between the moment the cursor left the target area to the moment the it reentered the target area. These behavioral results show that patients were capable of performing the task correctly. Finally, as in the previous chapter, hand kinematics were composed of sub-movements with different average acceleration profile between patients (Figure 4-1B).

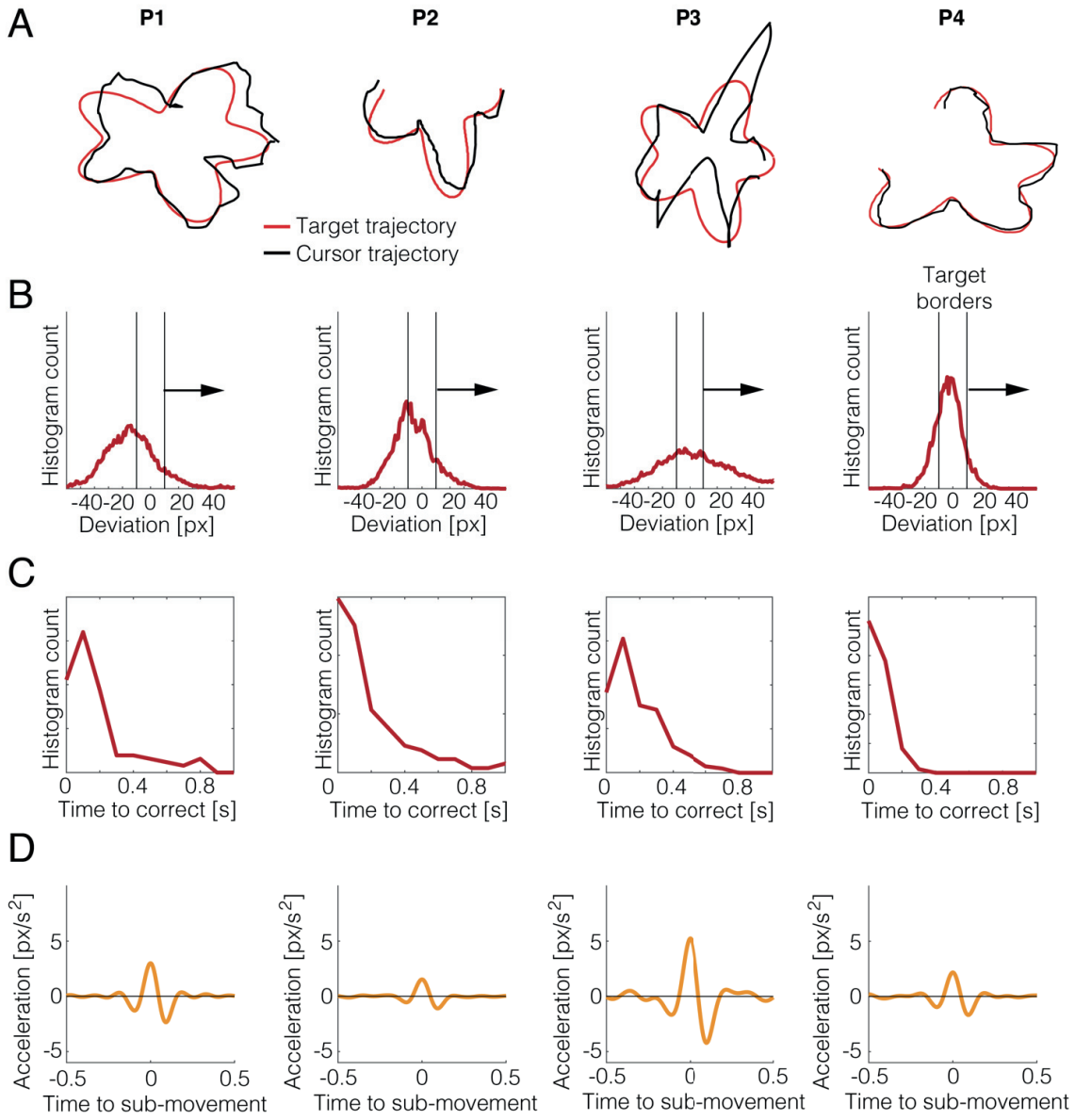

Figure 4-1. Behaviour of the four patients. *(A) an example trajectory of the target (red trace) with the trajectory followed by the patient's mouse (black trace). Note that these plots do not reflect cursor deviation with respect tot the target but the ability of subjects to follow the trajectory of the target. (B) Histograms of cursor deviation. Negative values correspond to the cursor lagging behind the target. Black vertical lines represent the target radius. (C) Histogram of the time needed between the moment the cursor leaves the target area to the moment it reentered the target area. (D) Kinematic profiles of sub-movements representing the average hand acceleration, time-locked to the acceleration peaks.*

Anatomical localization and selection of electrodes

We selected a subset of electrode contacts within an anatomical region-of-interest in the MFC comprising the supplementary motor area (SMA) and the anterior cingulate cortex (ACC). One patient (P1) was implanted with a 12 electrodes interhemispheric ECoG strip on the medial wall of the right hemisphere which we considered to be entirely within the SMA. We thus kept all the electrodes from this strip. The other three subjects (P2-P4) were stereotactically implanted with 10-contacts depths electrodes. The anatomical location of these contacts was decided in agreement with two neurologists. Their decisions were supported by the electrode localization in post-surgery CT-scans, coregistred with pre-surgery MRI anatomical scans as well as automatic cortical parcellation (Freesurfer) of these anatomical scans. We selected only contacts that were within the grey matter of the anterior cingulate cortex (ACC). All signals were verified by a neurologist and those showing epileptic activity were discarded from further analyses. These procedures led us to a total of 6 to 12 signals per subject situated in the MFC –either in the SMA (P1), or in the ACC for the other patients (c.f. Table 4-1 for details). Data pre-processing is explained in detail in the materials and methods section at the end of this chapter.

Table 4-1. Patient information. *Handedness, gender, age and lesion type, if any (RH: right hemisphere). Also included are the number of contacts in the MFC used in this study, the number of resulting electrodes after common average referencing or bipolar derivation and the number of 10s trajectories tracked.*

	Hand	Gender	Age	Lesion	Contacts (MFC)	Electrodes used[3]	# Trials
P1	Right	Male	54	RH	12 ECoG contacts in right SMA	12	20
P2	Right	Male	24	None	8 depths contacts in right ACC	6	25
P3	Left	Female	55	None	4 depths contacts in left ACC 4 depths contacts in right ACC	6	30
P4	Right	Male	23	None	7 depths contacts in left ACC 5 depths contacts in right ACC	8	20

Kinematics-LFP phase coupling

We analyzed whether sub-movements would be coupled with theta frequency oscillations in the LFP. Firstly, we filtered both the hand acceleration and the LFP signal into frequencies between 2 and 14 Hz by steps of 1 Hz. For each pair of frequencies, we computed the phase-locking value (Lachaux et al., 1999) between the filtered hand acceleration and the filtered LFP signal and normalized (z-score) using surrogate data to remove non-genuine couplings. This led to a two-dimensional representation of phase coupling (*comodulogram*) as a function of the frequency of the hand acceleration and the frequency of the LFPs. This procedure was repeated for every electrode in the MFC. From the previous study, we expected to see couplings in the theta frequency range [4 – 6 Hz]. We thus assessed significance only in the theta frequency.

We report the number of electrodes showing statistically significant phase coupling between low frequency LFPs and hand kinematics in the theta frequency range ($p<0.05$, non-parametric test). Thirty-eight percent of electrodes showed phase coupling in the contralateral hemisphere and 38% in the ipsilateral hemisphere. All four subjects had at least one electrode showing phase coupling (Table 4-2). Figure 4-2 shows phase coupling from one representative electrode for each subject. Contrary to the results obtained with EEG (see Chapter 3), phase coupling does not only occur in the theta range but also at mu frequencies (Figure 4-2, P1) or at delta frequencies (Figure 4-2, P3).

[3] After applying common average referencing or bipolar derivation

Table 4-2. Number of electrodes showing phase coupling with hand acceleration.

	Phase-locking (contralateral)	Phase-locking (ipsilateral)
P1	No contacts	4/12 (33%)
P2	No contacts	4/6 (67%)
P3	0/3 (33%)	1/3 (33%)
P4	3/5 (60%)	0/3 (0%)
TOTAL	**3/8 (38%)**	**9/24 (38%)**

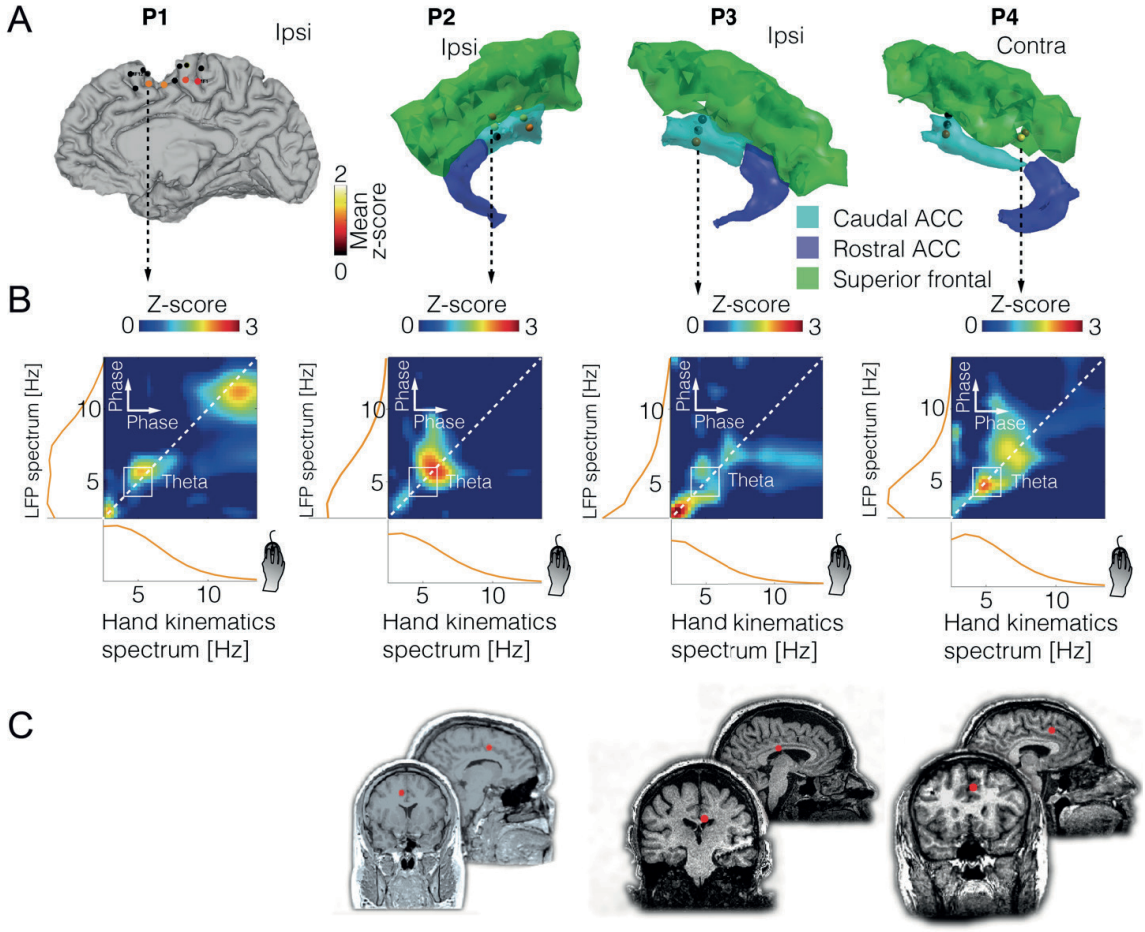

Figure 4-2. Phase-phase couplings in the medial frontal cortex of each patient. *(A) Mean coupling in the theta frequency range [4-6 Hz] for every electrode in the medial frontal cortex of one hemisphere. Electrodes with strong coupling are depicted with a white/yellow circle. Electrodes with lesser couplings are in red. Electrodes with non-significant couplings are black. The cyan highlighted regions correspond to the Freesurfer parcellation for the caudal ACC, the blue regions correspond to the rostral ACC and the green region corresponds to the superior frontal cortex. (B) Phase coupling comodulogram (z-scored) between the hand acceleration (x-axis) and the LFP phase (y-axis) for one representative electrode per subject. The PLV image was upsampled four times for display purposes but statistics were conducted on the original PLVs. The white box represent the area used for statistical significance testing ([4-6 Hz]). The inset on the left shows the spectrum of the LFP and inset at the bottom, the spectrum of the hand acceleration. (C) Electrode locations (red disks).*

LFP-LFP phase-amplitude coupling

We studied the phase-amplitude coupling of the LFPs, and more particularly the existence of PAC between HG frequencies (80 – 160 Hz; a correlate of spiking activity) and theta oscillations (Canolty et al., 2006). We thus firstly computed theta-LFP comodulograms showing the strength of the coupling between high frequency amplitudes and low frequency phases. The resulting comodulograms were normalized (z-score) using surrogate data to remove non-genuine couplings and statistical significance was evaluated ($p<0.05$, uncorrected). We found that 23 out of the 32 electrodes (72%) showed phase-amplitude coupling between theta and HG. All patients had at least two electrodes showing phase-amplitude coupling (Table 4-3, left column).

Table 4-3. Number of showing phase-amplitude coupling.

Subject	PAC with theta oscillations	PAC with hand kinematics	PAC with both
S1	10/12 (83%)	7/12 (58%)	6/12 (50%)
S2	4/6 (67%)	2/6 (33%)	1/6 (17%)
S3	2/6 (33%)	1/6 (17%)	0/6
S4	7/8 (88%)	2/8 (25%)	0/8
TOTAL	**23/32 (72%)**	**12/32 (38%)**	**7/32 (22%)**

Kinematics-LFP phase-amplitude coupling

Next, we asked whether similar phase-amplitude couplings could be found between high frequency amplitudes of the LFP and the phase of the hand kinematics. We applied the same procedure but replacing the low frequency LFP (modulating) signal by the hand acceleration signal. We found 12 out of 32 electrodes (38%) with phase-amplitude coupling between the phase of the hand acceleration within the theta range and HG amplitude. All subjects had at least one electrode showing such a coupling (Table 4-3, center column). Interestingly, no phase-amplitude coupling between HG and hand acceleration was found in the contralateral hemisphere[4]. Finally, there were 7 out of 32 electrodes (22%) showing coupling between HG and both theta oscillations and hand kinematics. Out of these 7 electrodes, 6 corresponded to the patient with SMA coverage and only one other subject showed couplings of both signals in the ACC (Table 4-3, right column).

Figure 4-3 shows two electrodes for two different patients showing either only phase-amplitude coupling with theta oscillations (Figure 4-3A, P1) or only phase-amplitude coupling with hand acceleration (Figure 4-3B, P3). Electrode locations are shown in Figure 4-3C. It is worth mentioning that although our analysis concentrated on couplings in the theta range, some electrodes also showed phase-amplitude coupling at lower (<3 Hz) and higher (8 – 13 Hz) frequencies.

[4] Note that patients P1 and P2 had only ipsilateral coverage and patients P3 and P4 had bilateral coverage.

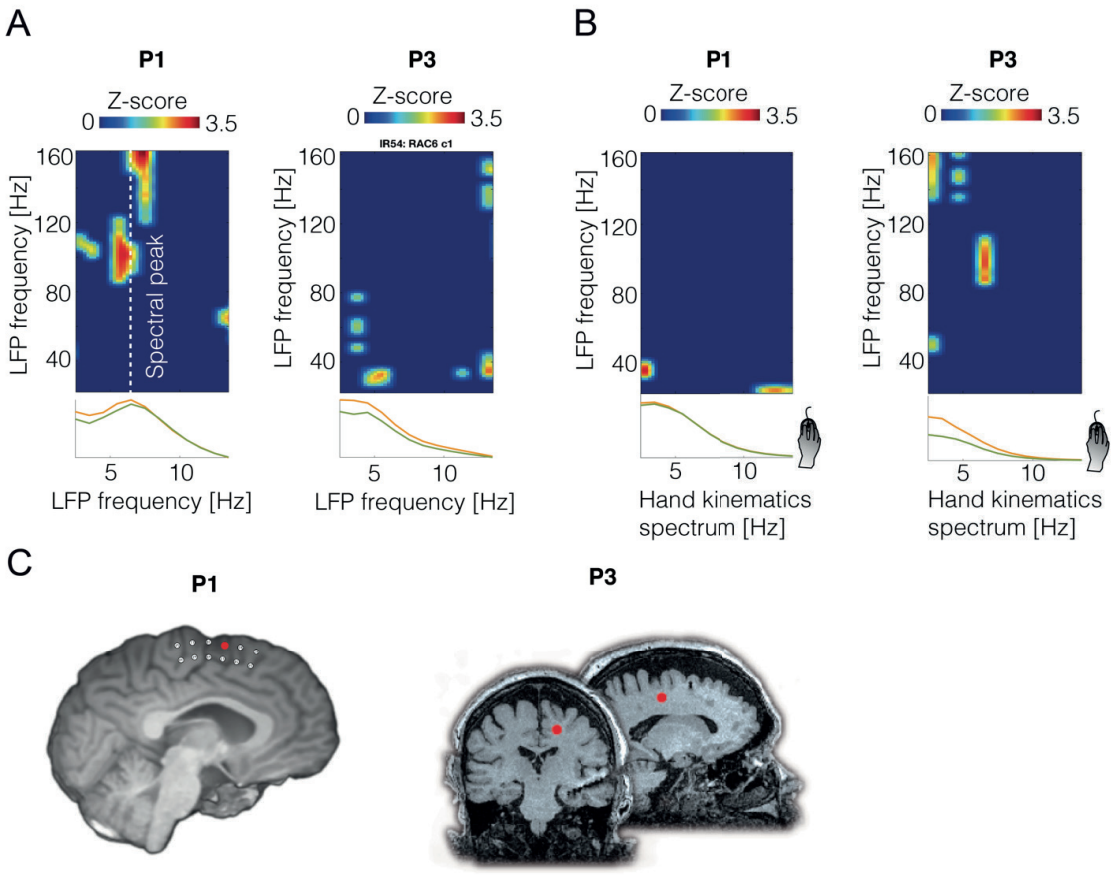

Figure 4-3. Phase-amplitude comodulogramms during tracking. *(A) Phase-amplitude comodulogramms between HG and low frequency LFPs. The comodulogramms are thresholded (p<0.05, uncorrected). The lower inset shows the spectrum of the low frequency LFPs in orange. (B) Phase-amplitude comodulogramms between HG and hand kinematics. The comodulogramms are thresholded (p<0.05, uncorrected). The lower inset shows the spectrum of the hand kinematics (acceleration) in orange. (C) The electrode localization on anatomical scan of each subject.*

High gamma correlates of cursor deviation

Lastly, we conducted an exploratory analysis to find HG activity that would be predicted by cursor deviations in the past. For this, we searched for troughs in the LFP signal filtered in the theta band. A logarithm function was applied to high frequency amplitudes to make the distributions more symmetrical. The resulting signals were highpass filtered with a cutoff frequency of 2 Hz to remove possible slow drifts in time and z-scored with respect to a baseline preceding the movement. We tested for time-frequency pairs that significantly differed from zero. We found significant increases of HG activity between 80 and 160 Hz coupled to theta troughs (Figure 4-4) and averaged these significant HG activations in time and frequency for each epoch. We then correlated the resulting values with the cursor deviations of each epoch, at different latencies with respect to the theta trough. We found two electrodes with HG activity correlating with cursor deviation better than chance level. The latency at which this correlation was strongest was consistent for both electrodes; 100 ms (P1; one sample t-test; p=0.013) and 60 ms (P3; p=0.019) (Figure 4-4). Finally, we repeated this analysis using hand acceleration instead of cursor deviation and also found significant correlations 36 ms before the theta trough for one electrode (p=0.040, uncorrected; Figure 4-4, P3).

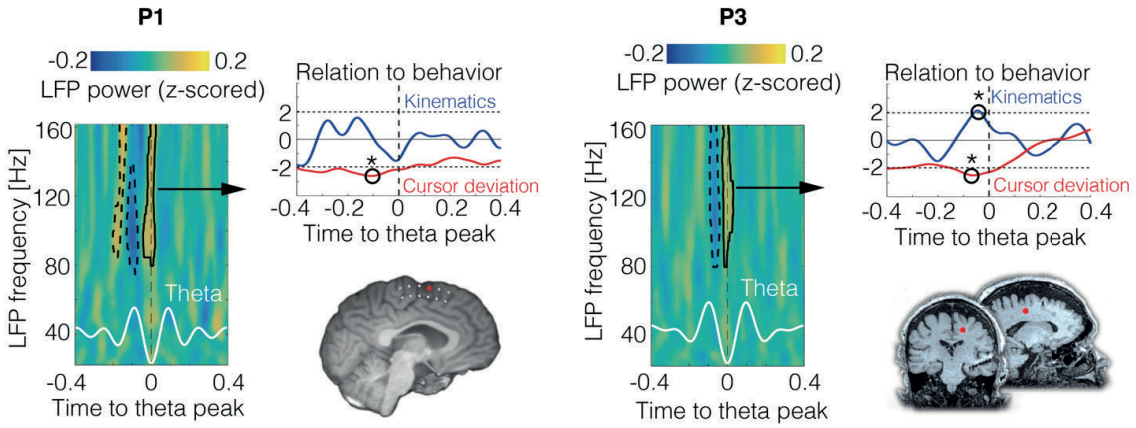

Figure 4-4. High-gamma coupled to theta oscillations and relation to cursor deviation. *Left: time-frequency plots of LFP power, time-locked to theta oscillations peaks. Black contours indicate time-frequency pairs significantly different than zero ($p<0.05$, corrected using a permutation test) that were averaged and correlated to the cursor deviation and hand acceleration signals. Dashed black contours represent other statistically significant frequency pairs ($p<0.05$, corrected) that were not used in the correlation analysis. The averaged theta cycle is depicted in white at the bottom. The high-gamma power inside the black contours was then averaged across the significant activation region and correlated to behavior at every time-point around the theta peak (Right side: "relation to behavior"). The red curve shows the relation to cursor deviation compared to random (i.e. z-scored using surrogate data). The blue curve shows the relation to hand kinematics. Dashed horizontal lines show the threshold for chance level (uncorrected for the number of time points). The latency of maximum correlation is shown with a black circle and a star. The vertical dashed line represents the theta trough.*

4.3 Discussion

In this study, we showed that the kinematics of the hand during continuous visually-guided movements are coupled to theta oscillations in local field potentials (LFPs) recorded subdurally or intracortically from the medial frontal cortex of human subjects. Furthermore, the amplitude of high gamma (HG) activity was found to couple to the phase of both the theta oscillations and the hand kinematics, depending on the electrode.

Patients were able to complete the task and the kinematics profile of their hand showed repetitive sub-movements, similar to subjects in the previous chapter. These sub-movements were coupled to low frequency LFPs in the medial wall (ACC and SMA) at the theta frequency. Similar findings have been reported using magnetoencephalography (MEG); Gross et al. found that slow finger movements generated periodic patterns of electromyographic (EMG) activity between 6 and 9 Hz that were coupled to a network of MEG activity in the motor and premotor cortices, cerebellum and thalamus (Gross et al., 2002). Hand speed was also found to couple with MEG activity in the primary motor cortex at a peak frequency of 4 Hz (Jerbi et al., 2007). This primary motor cortex activity was in turn coupled with activity in a broader network including the SMA.

The functional relevance of sub-movements and coupled oscillations is still not clear. Early works suggested that sub-movement were due to sensory delays since they are rather insensitive to hand speed (Roitman et al., 2004; Pasalar et al., 2005) or target size (Selen et al., 2006) and tend to disappear in the absence of visual feedback (Miall et al., 1986; McAuley et al., 1999), but see (Doeringer and Hogan, 1998). However, cortical dynamics of low frequency LFPs and spiking activity coupled to kinematics were similar during sleep and sedation, raising the possibility that sub-movements arise from intrinsic properties of oscillating cortical networks rather than external factors or feedback delays (Hall et al., 2014a). Another study showed that the phase difference between coupled oscillations in the motor cortex and in the spinal cord was optimally tuned to cancel out and prevent tremor (Williams et al., 2010). This study found different coupling frequencies depending on the muscles and cortical areas involved. Similarly, although we concentrated on theta frequency couplings, we also found phase-amplitude couplings occurring at different frequencies lower than 3 Hz or higher than 10 Hz. While theta coupling could

vary between subjects and electrodes and 3 Hz couplings are still plausible, 10 Hz couplings probably imply some non-linear *n:m* couplings for which for example, mu oscillations would cycle twice during one sub-movement cycle (Tass et al., 1998).

Since theta-kinematics couplings are not perfect, we could ask whether HG activity would couple more to sub-movements or to theta oscillations. HG activity is considered to be a reliable marker of spiking activity (Belitski et al., 2008; Ray and Maunsell, 2011) and its amplitude has been extensively shown to couple to lower frequency oscillations in the human neocortex (Canolty et al., 2006) and hippocampus (Maris et al., 2011). We found that depending on electrode location, HG activity could be coupled either to theta oscillations only, but also to hand kinematics only, or to both. Our findings could therefore not dissociate whether the ERP in the previous chapter was generated by the sub-movement or was a theta oscillation cycle coupled to sub-movements. Our findings however advocate for a more complex interaction between kinematics, theta oscillations and HG activity. Indeed, they could imply that performance monitoring in continuous movements relies on two distinct neuronal populations.

One neuronal population underlying HG activity would be directly coupled to sub-movements. We could speculate that the functional role of this population could be the feedforward planning of the next sub-movement, the feedback evaluation of the previous sub-movement or both. A different population of neurons could be coupled to theta oscillations with a possible role of monitoring cursor deviation, as suggested by our correlation analysis. The role of theta would be to synchronize the communication between these different neuronal populations. At the scalp level, either only theta activity is observable, or the activity from both populations could sum up to generate an ERP time-locked to sub-movements. Further analyses are needed to give support to one or the other hypothesis and explain the functional role of HG activity coupled to hand kinematics. Our exploratory analysis using correlation only showed a weak relation between HG activity and cursor deviation compared to our previous study with EEG at the scalp level. It is therefore probable that the mechanisms of performance monitoring during continuous visually-guided movements are more complex than a simple monitoring of cursor deviation. This is supported by behavioral studies suggesting different processing pathways for the monitoring of cursor and target position (Reichenbach et al., 2014) and different latencies for their integration into a difference vector (Franklin et al., 2016). Moreover, it is still unknown how the monitoring of cursor deviation is compared and integrated with motor output.

Our results demonstrate the existence of a neuronal process indexed by HG activity in the medial frontal cortex, occurring at specific phases of the sub-movements. These findings bring strong experimental support to intermittent motor control during continuous movements. Future analyses dissociating kinematics from theta couplings and studying phase connectivity with other brain regions should allow further understanding of the neural dynamics of performance monitoring during continuous movements.

4.4 Materials and methods

Patients

Four epileptic patients (age: 54, 23, 55 and 23 years) with electrodes implanted for surgical resection were recorded. One patient was implanted with subdural electrocorticographic grids and three patients were stereotactically implanted with depth electrodes recording local field potentials. The study protocol was approved by the Office for the Protection of Human Subjects of the University of California, Berkeley. All patients gave written informed consent before participating.

Experimental protocol

The experiment consisted in a 10 px radius red target moving along pre-defined trajectories at constant speed during 10 seconds. Patients were instructed to follow with the target with the computer mouse, keeping the cursor (a white dot) inside the target as much as possible. Each trial started by showing a new trajectory and the target. Patients then placed the mouse cursor on the target for one second until the target color switched from red to orange and after another second from orange to green. Then the target started moving along the trajectory at constant speed and the patients had to follow it, keeping the cursor as much as possible within the target area. Trajectories were visible all the time during tracking. A score between 0 and 100 was displayed at the end of each trajectory based on the percentage of time spent inside the target. Patients first started with a

few training trials (data not included) in order to familiarize with the experiment. The experimenter adjusted the speed of the target not to induce frustration and to obtain reasonable performance. One session consisted of 10 trajectories (trials).

Behavioral measures

Mouse and cursor position were sampled at 50 Hz (the refresh rate of the screen) and upsampled to 250 Hz offline to match the downsampled electrophysiological data. Hand speed was computed by taking the absolute value of the positional data after differentiation using a second order Savitzky-Golay derivative filter with a 110 ms window (Savitzky and Golay, 1964). Hand acceleration was then obtained differentiating hand speed a second time.

The cursor deviation from the target was obtained by projecting the cursor position on the instantaneous target direction (see Chapter 3). This allowed us to dissociate deviations behind the target (negative values) leading to an increase in hand speed from deviations ahead of the target (positive values).

Electrophysiological recording and pre-processing

Electrophysiological data was recorded at 5000 Hz using a Nihon Kohden NeuroFax amplifier, downsampled offline to 500 Hz and filtered using three notch filters at 60, 120 and 180 Hz and a bandpass filter with cutoff frequencies at 1 and 200 Hz. Electrodes containing epileptic activity or excessive artifacts were discarded from further analysis. The signal from ECoG strips were re-referenced to a common average while monopolar LFP recordings from depth electrodes were converted to a bipolar montage between adjacent electrodes. To compute time-frequency maps, we convolved the resulting signals with complex Morlet wavelets defined as:

$$1/\sqrt{\sigma\sqrt{\pi}}e^{-t\hat{}2/(2\sigma\hat{}2)}e^{2\pi jft}$$

where t is time, f is frequency and σ defines the number of cycles $N = 5$ and defined as $\sigma = N/(2\pi f)$.

Pre-operation anatomical MRI scans were coregistered to post-operation computer tomography (CT) scans. Electrodes positions were obtained in the resulting common space and corrected for displacements due to brain shift (Dykstra et al., 2012). This processing was done using the Fieldtrip toolbox (Oostenveld et al., 2011). Electrode location were then plotted on a pre-operation or post-operation MRI scan depending on availability. Final anatomical locations for each electrode were decided by a consensus between neurologists and epileptologists based on the semi-automatic electrode localization.

Phase coupling with hand acceleration

To compute phase coupling between the LFP signals and the hand kinematics, we also convolved the hand acceleration with complex Morlet wavelets. For each pair of frequencies from 2 to 14 Hz, we projected the difference between the two corresponding phase signals on the (complex) unit circle and computed the magnitude of the average across time points to get the phase-locked value (PLV). The PLVs were then averaged across trials. To control for non-genuine couplings and non-uniform phase distributions, we repeated the same procedure 200 times using surrogate data, constructed by splitting the signals into two segments at a random time point and interverting segments. We normalized PLVs to z-scores using the following procedure: the mean of the surrogate PLVs were subtracted to the original PLV and the result dividied by the standard deviation of the surrogate PLVs. Based on the results of the previous chapter we expected the phase locking to occur in the theta range. We thus summed PLVs for frequency pairs included in the theta [4-6 Hz] frequency interval and counted the percentage of (averaged) surrogate PLVs with higher value. The so-obtained p-values are reported along with the averaged normalized (z-scored) PLVs in the theta frequency range.

Phase-amplitude coupling

To compute phase-amplitude coupling, for each time and frequency point we construct a complex number consisting in the modulus of the high frequency signal and the phase of the low frequency signal (that can be either the LFP signal or the hand acceleration, convolved with a Morlet wavelet). These complex numbers were then averaged in the complex plane and the the modulus gave the PLV. PLVs were then averaged across trials and

normalized by surrogate data as for phase coupling (previous section). The resulting comodulograms were thresholded at p=0.05, uncorrected.

High-gamma activity relation with cursor deviation

Lastly, to visualize the time evolution of HG activity coupled with theta oscillations, we constructed epochs of time-frequency amplitudes which we time-locked to troughs of the LFP filtered in the theta range [4-6 Hz] (Butterworth zero-phase IIR filter). The high frequency amplitude signals were first converted to the logarithm domain to have more symmetrical distributions and then high-pass filtered to remove possible drifts across time (Butterworth zero-phase IIR filter with cut-off at 2 Hz). The resulting signals were z-scored using a 2 s baseline after the patients placed the mouse on the target to start the trial. This allowed to compensate firstly for different amplitude levels due to the 1/f spectrum and secondly to compensate for possible non-stationary sources of noise that could vary during or between the recordings.

To test for significant differences in the resulting time-frequency maps while correcting for multiple comparisons, we used the procedure in (Maris and Oostenveld, 2007), adapted for single sample t-tests. In brief, we applied a one sample t-test on every time-frequency point, thresholds the map at a significance level of p=0.05 and sums the t-values inside each cluster of significant time-frequency points. The procedure is then repeated 200 times while permuting the signs of randomly drawn trials to construct a distribution of cluster-averaged t-value under the null hypothesis. Each original cluster is considered statistically significant if the sum of t-values is within the tails of the distribution under the null hypothesis.

Finally, we averaged HG amplitudes for each time and frequency point inside the significant clusters. The resulting values were then correlated to cursor deviation and hand acceleration at every time point around the theta trough. To test whether the correlation was higher than chance, we repeated the procedure while shuffling trials to get a distribution of correlation coefficients under the null hypothesis. We then z-scored the original correlation coefficients using this distribution and set the threshold to ±1.96, corresponding to a p-value of 0.05 (two-tailed).

Chapter 5 Ipsilateral sensorimotor activity related time-locked to sub-movements during continuous movements

5.1 Introduction

In this chapter, we investigate how corrective sub-movements affect mu oscillations [8-14 Hz]. We added one condition to the original tracking condition of the visuo-motor task from the previous chapters, in which, we experimentally manipulated the need for corrective actions by displaying the cursor closer to the target center (*assistance* condition). To dissociate this condition from the previous tracking condition, we refer to the later as the *precision* condition. This made subjects believe that they were performing better than they actually were and led to sub-movements with less acceleration, thus smoother movements. After half of the trials, the precision condition was replayed to the subjects which were instructed to appraise the kinematics of the mouse cursor (*viewing* condition). By contrasting mu power between the tracking and assistance conditions we found that the activation of the ipsilateral (right) sensorimotor cortices –indexed by mu power desynchronization, was decreased in the assistance condition. Furthermore, during a transient 500 ms period immediately following sub-movements, mu power was modulated by the amplitude of the sub-movements, with larger sub-movements leading to increased mu desynchronization, thus cortical activation. Since we measure the amplitude of sub-movement by the acceleration, we refer to sub-movements with large accelerations as *brisk* sub-movement instead of fast sub-movements which would refer to the speed.

5.2 Results

Twenty-three right-handed subjects performed a visuo-motor tracking task during which they had to track a moving target with the mouse cursor (*precision* condition, Figure 5-1A, left). In a second condition, the mouse cursor was displayed closer to the target cursor, thus reducing cursor deviation by 80% (*assistance* condition, Figure 5-1A, right). Prior to recording EEG, we conducted a behavioral pilot and asked subjects to rate the perceived difficulty of each trajectory and condition from 0 (extremely easy) to 100% (extremely hard). The assistance condition led subjects to perceive the task as easier (Figure 5-1B; $p=0.008$). During the EEG experiment, hand acceleration showed a succession of sub-movements in both condition (Figure 5-1A, bottom insets). These kinematic profiles showed a distinct spectral peak at 5 Hz for both conditions (Figure 5-1C). Higher spectral power observed during the precision condition showed that sub-movements were brisker during the precision condition as compared to the assistance condition and confirmed that subjects were correcting less.

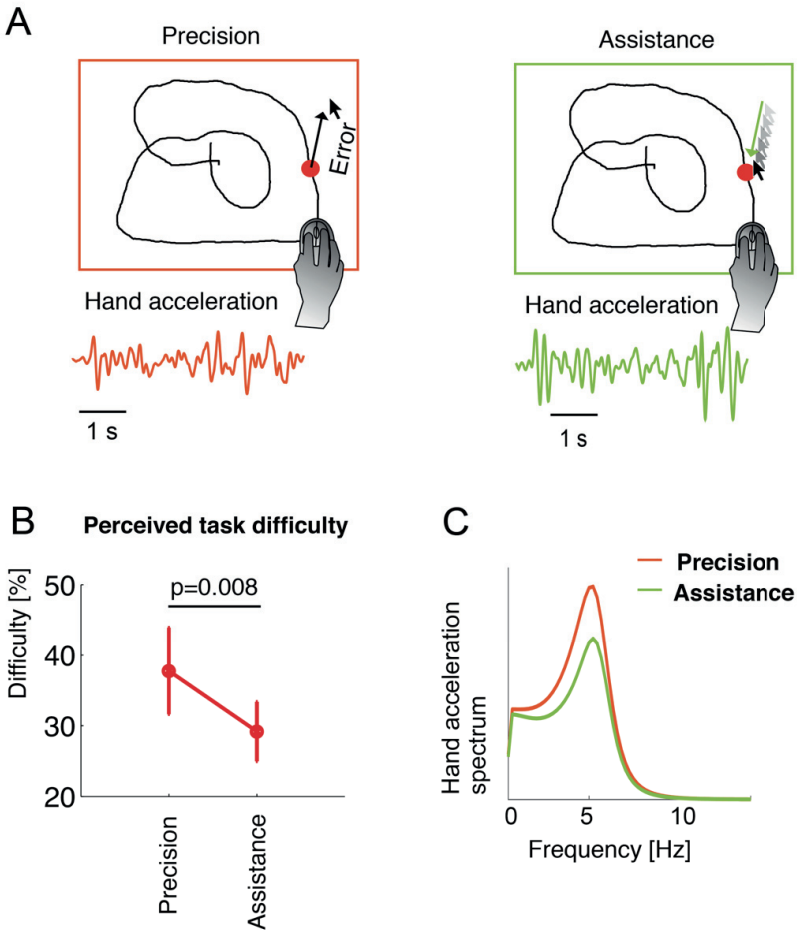

Figure 5-1. Task design and differences in spectral power between conditions. *(A) Subjects had to follow a target (red circle) moving along a visible trajectory with a computer mouse. (left). The hand kinematics (acceleration; 5 seconds) is shown at the bottom (red trace). In the "assistance" condition (right), the mouse cursor was displayed closer to the target center, reducing the distance between the cursor and the target by 80%. A trace of the hand kinematics (acceleration; 5 seconds) is shown at the bottom (green trace). (B) The average perceived task difficulty for the precision and assistance condition. Whiskers indicate standard deviation. (C) The spectrum of the hand acceleration showed a clear peak at 5 Hz for both conditions (red for precision and green for assistance). However, the magnitude of the spectrum was lower for the assistance task, confirming that submovement had lower acceleration in this condition and thus a reduction in corrective behavior.*

Average mu power differences

To investigate the spectral content of the EEG between conditions, we applied the Welch method with 1 s windows and 50% overlap. A clear spectral peak around 11 Hz was found on both hemispheres (Figure 5-2) in both conditions. Thus, we performed a repeated measures two-way ANOVA on the alpha power at this peak (i.e. at 11Hz) with *hemisphere* (left/right) and *condition* (*precision*/*assistance*), and observed a significant main effect of both *hemisphere* ($F(1,22)=26.4$, $p<0.001$) and *condition* ($F(1,22)=7.7$, $p=0.011$) and in addition a significant interaction ($F(1,22)=5.8$, $p=0.025$). Bonferroni-corrected post-hoc t-tests showed a significant difference of alpha power between precision and assistance on the ipsilateral ($t(22)=-2.75$, $p=0.023$) but not the contralateral ($t(22)=-1.62$, $p=0.47$) hemisphere. Ipsilateral and contralateral alpha power was also significantly different ($t(22) < -4.90$, $p<0.001$) tracking. This difference in μ-power between *precision* and *assistance* was topograph-

ically constrained to ipsilateral motor and (bilateral) parieto-occipital areas ($p<0.05$, cluster-based permutation test).

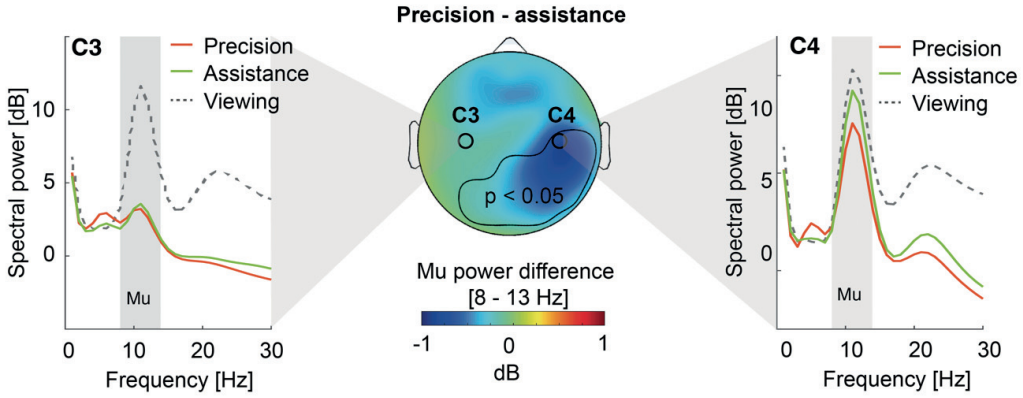

Figure 5-2. Mu power differences between conditions. *The spectral power for the C3 (contralateral; left) and C4 (ipsilateral; right) electrodes considered to be above the hand area of the sensorimotor cortices. Red traces represent the EEG spectrum for the precision condition, green traces represent the EEG spectrum for the assistance condition and the black dashed traces represent the EEG spectrum for the viewing condition. For electrode C3 (left), we could observe a stronger desynchronization during the movement conditions (precision and assistance) as compared to the viewing condition but no differences between the precision and assistance conditions. On the other hand, for electrode C4 (right), we could identify a reduced desynchronization due to movement; in addition, at this electrode location, we could observe a statistically significant difference between the precision and assistance conditions, with a stronger desynchronization during the precision condition. The difference in mu power (grey highlight on the spectra) are topographically displayed in the middle. Mu power was lower for the precision condition over the ipsilateral sensorimotor, parietal bilateral and bilateral occipital cortices ($p<0.05$, corrected for multiple comparisons).*

Mu power differences time-locked to sub-movements

Next, we investigated the temporal profiles of mu power. To extract mu power over time, we convolved the EEG with a complex Morlet wavelet with a center frequency at 11 Hz (for details on the pre-processing of EEG, please refer to the materials and methods section at the end of this chapter). We then constructed epochs of mu power, time-locked to sub-movement defined as peaks in hand acceleration. No modulations in the temporal profiles were found and ipsilateral mu power was consistently significantly lower across the epochs for the precision as compared to the assistance condition (Figure 5-3A, $p<0.05$, cluster-based permutation test). No statistically significant difference was observed over the contralateral hemisphere (Figure 5-3B). Furthermore, kinematics showed a significantly different profile between conditions; when providing assistance, hand acceleration was lower (Figure 5-3C, $p<0.05$, cluster-based permutation test) while hand speed was higher after the sub-movement (Figure 5-3D, $p<0.05$, cluster-based permutation test). This apparent paradox is explained by the fact that during the assistance condition, the assistance allowed subjects to move the cursor further away from the trajectory (data not shown) since the experimental manipulation corrected these positional errors. This led to faster but smoother movements (i.e. less acceleration).

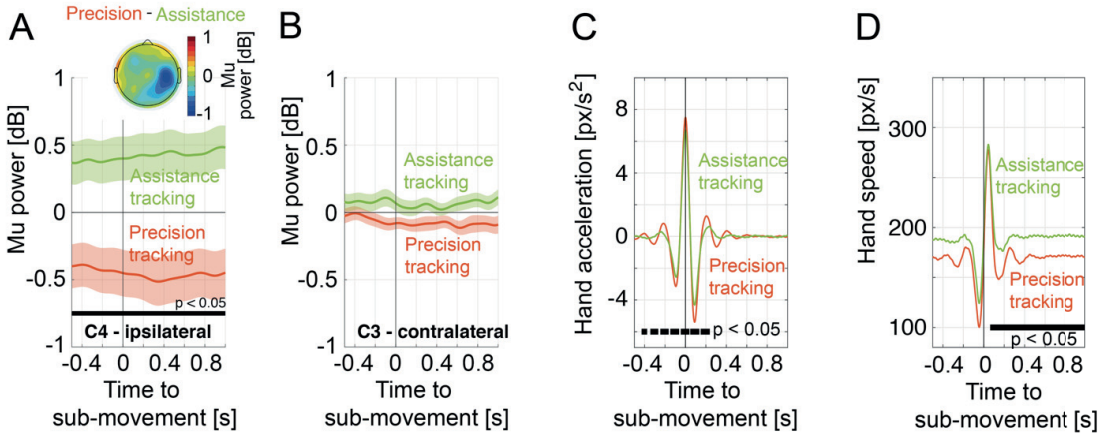

Figure 5-3. Differences in mu power and kinematics time-locked to sub-movements. *(A) We could observe a statistically significant difference in mu power (p<0.05, corrected) over the C4 electrode (ipsilateral) that did not show any modulation over the epochs. Shaded areas show the standard error of the mean. Black segments at the bottom of the plot show time points for which differences were statistically significant (p<0.05, corrected). (B) There was no difference in mu power over the C3 electrode. (C) Sub-movement profiles showed a small but significant decrease (p<0.05; black segments below) in acceleration and deceleration during the assistance condition. (D) Sub-movement profiles showed an increase in speed after the sub-movement for the assistance condition.*

Modulation by kinematics

Informed by these results, we probed whether ipsilateral activity (indexed by mu spectral power on the C4 electrode, considered to be above the sensorimotor region of the scalp) could relate to differences in hand kinematics. For each condition, we separated sub-movement-locked epochs into five based on the acceleration of the sub-movement (Figure 5-4A). Each bin contained an equal number of epochs. Increasing acceleration led to increasing peak hand speed. (Figure 5-4B).

The time courses of mu power during the precision condition showed a gradual decrease after the acceleration peak for the brisker sub-movement and a gradual increase for the smallest sub-movements (Figure 5-4C). The brisk sub-movements (i.e. the 5th bin corresponding to maximum acceleration) led to significantly different mu power compared to slowest sub-movements (1st bin) between 156 and 680 ms after the sub-movement ($p<0.05$, cluster-based permutation test).

For every time point of the epochs, we regressed mu power, averaged for every bin using the mean acceleration of each bin. We thus obtained one r^2 value per time point. We then set a threshold on these r^2 values to define clusters of time instants when hand acceleration explained 80% or more of the variance of the mu power for each bin (corresponding to a p-value of 0.045). We then tested for significance using permutation tests. We found a significant cluster starting at the time of the sub-movement and lasting 500 ms ($p<0.05$; black segments in Figure 5-4C). The regression slope of the averaged ipsilateral mu power was maximal over the ipsilateral sensorimotor cortex (Figure 5-4C, inset).

Figure 5-4D shows how the r^2 values evolve over one epoch for both conditions. For the assistance condition, the slope was lower and there was no significant difference ($p>0.05$, cluster-based permutation test). We then represented mu power as a function of hand acceleration. For the assistance condition, the brisker sub-movements did not show a qualitatively larger desynchronization (Figure 5-4D, right),

Contrarily to ipsilateral mu power, contralateral mu power was not significantly modulated by the kinematics ($p>0.05$, cluster-based permutation test). To control that our results were not influenced by eye-movements, we repeated the kinematics analysis on the electro-occulographic signals. We found no significant relation ($p>0.05$, cluster-based permutation test) for either vertical and horizontal eye movements.

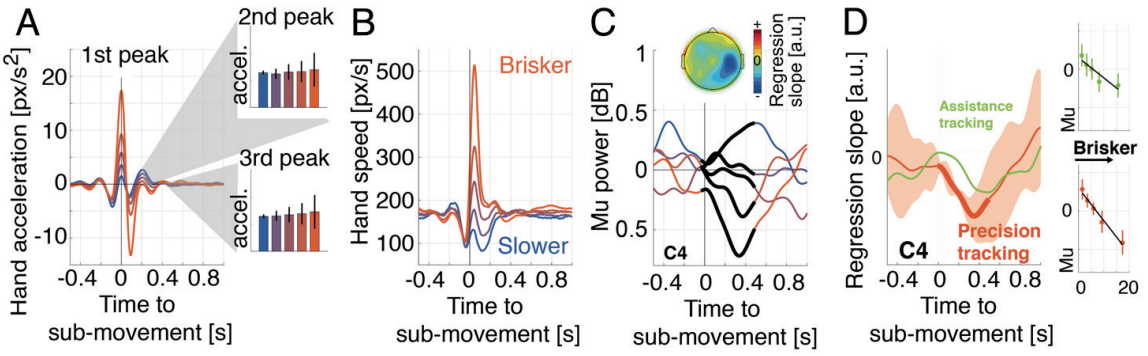

Figure 5-4. Difference in mu power after sub-movements. *(A) The acceleration profile of the binned sub-movements (5 bins with an equal number of sub-movement epochs). The larger sub-movements are in red and the smaller sub-movements are in blue. There was no difference in the amplitude of the second and third sub-movements (see insets) but more variability across subjects after large sub-movements. The whiskers indicate standard error of the mean. (B). The speed profiles of the binned sub-movements. The mu power across an epoch time-locked to sub-movements. The black segments show the time points when the correlation was significant. The topographic map (inset) shows the regression slope for each electrode. The minimum slope is over C4 electrode. (D). The time evolution of the r^2 values for each condition (precision condition in red and assistance condition in green). The shaded area is the standard error of the mean. The thicker red line shows the time interval during which the correlation was significant. The two insets on the right show the mu power as a function of the sub-movement amplitude for assistance condition (top; green) and the precision condition (bottom; red).*

5.3 Discussion

In this study, we experimentally manipulated corrective behavior during continuous movements under visual-guidance by displaying the computer mouse's cursor closer to the target (assistance). This manipulation was successful reducing the perceived difficulty of the task and reducing sub-movement acceleration. We report a decrease in the power of mu [8-14 Hz] cortical oscillations over the ipsilateral sensorimotor cortex, corresponding to higher cortical activation when high precision was needed (precision condition). By time-locking our analysis on intermittencies in motor control (sub-movements), we found differences in mu power during the 500 ms immediately following sub-movement that correlated with the briskness of the sub-movement, but only in the precision condition.

It is commonly agreed that mu oscillations index an idling cortical state and that their desynchronization corresponds to cortical activation (Pfurtscheller, 2001; Klimesch et al., 2007). Mu power decrease over the sensorimotor cortex contralateral to the moving hand has been consistently observed before and during self-paced movements (Jasper and Penfield, 1949; Pfurtscheller and Aranibar, 1979; Babiloni et al., 1999; Alegre et al., 2003). During sustained movements, contralateral mu power returns to baseline values after around five seconds (Cassim et al., 2000) and during a sequence of two sequential self-paced movements, there was hardly no changes at the onset of the second movement (Alegre et al., 2004), suggesting that contralateral mu power changes are not a direct correlate of movement kinematics during repeated or sustained movements. Similarly, we found a desynchronization of contralateral mu power for both conditions compared to the viewing condition (without movement). However, we found no differences in contralateral mu power between the tracking and precision conditions, nor for different kinematics when time-locking to sub-movements.

On the contrary, ipsilateral mu decreased during the precision condition compared to the assistance condition, replicating findings from other neuroimaging and electrophysiological studies; higher activations of ipsilateral motor areas were found for more complex (Manganotti et al., 1998; Hummel et al., 2003; Verstynen et al., 2005) or faster (Rao et al., 1996; Hayashi et al., 2008) finger tapping sequences as well as when pointing towards reduced size targets (Seidler et al., 2004; Buetefisch et al., 2014).

Crucially however, time-locking the analysis to sub-movements, we observed a decrease of mu power for brisk

sub-movement in the precision condition. These finding suggest that the overall decrease in mu power during the precision condition is due to the larger sub-movements caused by corrective behavior. Considering that all our subjects were right-handed and the ipsilateral is therefore the right hemisphere, the hypothesis is consistent with lesion studies showing that right hemisphere damage produces deficits in positional adjustments of the upper limb during movement (Haaland et al., 2004) while left hemisphere damage impairs movement direction and trajectory curvature (Mani et al., 2013). During assisted tracking, lower task difficulty led to smoother movements (lower acceleration peaks) but higher hand speed, since cursor trajectories were further away from the target's trajectory.

Differences in sub-movement acceleration affected mu power during the 500 ms following sub-movements, with lower mu power for brisk sub-movements. This contrasts with findings using self-paced finger movements that show mu power reduction already 700-1400 ms before movement onset (Pfurtscheller and Berghold, 1989; Babiloni et al., 1999). The late timing of the mu differences in our task questions the hypothesis that it could underpin the acceleration of the time-locked sub-movement itself. It could nonetheless help slowing down the hand after a rapid speed increase caused by the brisk sub-movement. Similarly, supporting evidence points towards a causal role of the ipsilateral motor cortex on motor output through inhibitory mechanisms; transcallosal inhibition indexed by TMS-induced interhemispheric inhibition and ipsilateral silent period increased during fast movements (Tazoe and Perez, 2013). Transcallosal inhibition was also shown to increase when volitional actions are inhibited (Coxon et al., 2006). Disrupting the ipsilateral cortex using repetitive transcranial magnetic stimulation (rTMS) led to an increase in timing errors (Chen et al., 1997), likely by interfering with the timing of muscle recruiting (Davare et al., 2007), but improved execution time (Kobayashi et al., 2004). On the other hand, patients with complete agenesis of the corpus callosum also showed ipsilateral activation (Reddy et al., 2000), which is incompatible with a transcallosal inhibitory mechansim. An alternative hypothesis is that the influence of the ipsilateral hemisphere on motor output is mediated by an uncrossed (or double crossed) corticospinal pathway. Ipsilateral motor cortices contain sufficient limb representations to evoke both distal and proximal motor evoked potential (MEP) of the ipsilateral limb (Wassermann et al., 1994) but their increased delay compared to contralateral MEPs suggest the presence of an indirect pathway (Ziemann et al., 1999).

Interestingly, we found that the decrease in mu power during the precision condition was maximal over the ipsilateral sensorimotor cortices but also extended to bilateral parietal areas (Figure 5-2, topographic map). This parietal activation could be due to stronger online corrections, as evidenced by brisker sub-movements during the precision condition. Moreover, several studies have related structures of the parietal lobe – in particular the posterior parietal cortex - to online movement correction (Desmurget et al., 1999; Pisella et al., 2000; Della-Maggiore et al., 2004; Archambault et al., 2009). Additionally, anatomical pathways exist between the ipsilateral parietal and motor cortices; TMS-conditioning of the ipsilateral posterior parietal cortex increases the excitability of the ipsilateral motor cortex (Koch et al., 2007). The differential activation of the ipsilateral sensorimotor cortices could thus reflect a mechanism to adjust movements based on ipsilateral (or right) parietal lobe computations.

In this study, we show that during sustained precise movements, ipsilateral activity dynamically adapts to hand kinematics at a sub-second level. Our findings suggest that the role of the ipsilateral cortex during precise continuous movements movement under visual guidance is linked to large corrective sub-movements that are less present during easier task.

5.4 Materials and methods

Subjects

We recorded 23 right-handed healthy subjects (7 women and 16 men) with normal or corrected-to-normal vision and no reported neurological disorders. The study was approved by the local ethics comity and informed written consent was obtained.

Experimental protocol

Subjects used a mouse to track a red circle (15 px radius) moving along a trajectory (*precision* condition). The trajectory was contained within an area of the computer screen subtending a 20° horizontal and 13° vertical visual angle, corresponding to a rectangle of 840 by 525 pixels. In a second condition, subjects had to track the

target on the same trajectory but the mouse cursor was displayed 80% closer to the target center, virtually improving the perceived performance and reducing the necessity for online corrections (*assistance* condition). Conditions were randomized. Both conditions lasted 20 seconds and were repeated 20 times. To compute a resting baseline with identical visual stimulation, after a subset of trajectories (50%), subjects watched a replay of the precision condition and were instructed to observe the kinematics of the cursor (*viewing* condition). As an incentive to be attentive, subjects were then asked to reproduce similar kinematics with the mouse (*repeat* condition; data not used).

Behavioral measures

Hand position (by means of a mouse) and target positions (on the screen) were sampled at 50 Hz and interpolated (offline) to match the electrophysiological recordings (after down-sampling: 256 Hz). These measures allowed us to derive two behavioral metrics, used for later analysis. First, hand speed was computed through numerical derivation of the Euclidian distance between two consecutive time samples using a quadratic Savitzky-Golay filter with a window of 120 ms. Sub-movements were defined as peaks in the hand acceleration, i.e. time samples higher than their neighbors and higher than zero. Peaks with a prominence (minimum distance between the peak and the two neighboring troughs) lower than one were discarded as noise. The remaining peaks were used as (post-hoc defined) markers for our analysis (see below).

Electrophysiological recording and pre-processing

High-density 64 channels EEG was recorded using an ActiveTwo Biosemi system (Amsterdam, the Netherlands) in an extended 10-20 system. The data were down-sampled offline from 2048 Hz to 256 Hz and re-referenced to a common average. We used 5-cycles complex Morlet wavelets for frequency decomposition. We decomposed the raw EEG signal of electrodes C3 (contralateral) and C4 (ipsilateral) into 30 different frequencies by convolving the signal with the Morlet wavelets between 1 and 30 Hz. We filtered the signal in the mu frequency band by convolving it with an 11 Hz complex Morlet wavelet. Most (95%) of the spectral power of the 11 Hz wavelet was contained between 8 and 14 Hz (Figure 5-1D, grey shading). The choice of the 11 Hz as the frequency used for our statistical test was motivated by two reasons: first, we found this frequency to show a clear peak in the spectrum of the EEG traces recorded at electrode C3 and C4, in all conditions (Figure 5-2) and, in addition, this frequency lies in the middle of the mu 8-14 Hz frequency range (Palva and Palva, 2007).

Sub-movement-locked epoching

We segmented continuous behavior based on sub-movements. For this, we time-locked epochs of behavioral and electrophysiological data around peaks in hand acceleration (sub-movements). Epochs extended 500 ms before and 1 s after the acceleration peak. To dissociate between brisk and sluggish movements, we used the magnitude of the peak in hand acceleration as a criterion to separate epochs into two (equal sized) groups (see Figure 5-3A). Epochs from each condition were normalized by dividing them by the same (one value) condition-average baseline (Cohen, 2014). Epochs from both conditions were aggregated and averaged across epochs and time. This procedure has the advantage that differences between conditions are not influenced by the baseline, but baseline mu power levels are not reflecting in the standard error of the mean.

Statistics

In order to compare waveforms recorded during the two experimental conditions ("*precision*" and "*assistance*") over time while correcting for multiple comparisons, we used non-parametric cluster-based permutation tests (Maris and Oostenveld, 2007). We used the sum of T-values in clusters of significant values across time (and possibly frequency) as a test statistics and estimated the null distribution of this statistic by repeatedly (N=10'000) randomly permuting conditions within subjects. The same method was used for topographic scalp representations, except that clusters were defined spatially instead of temporally. For the regression of mu power over time based on hand acceleration, we increased the sensitivity of the test by setting the clustering threshold to an r-square of 80%. We then applied the same non-parametric procedure using the sum of r-square as test statistic (instead of the sum of t-values).

Artefact rejection

Subjects could freely move their gaze during the experiment. Although the natural behavior during visuo-motor tracking of slow targets is to smoothly pursue the target (Miall et al., 1993), we were careful to exclude any eye movement artefact from the analysis. We thus recorded electrooculographic (EOG) data by placing one sensor over the nasion and two sensors below the outer canthi of the eyes. Horizonal EOG was defined as the difference between the two outer canthi sensors and vertical EOG as the mean of the outer canthi sensors minus the nasion sensor. Any EEG epochs containing peak-to-peak vertical or horizontal EOG exceeding a conservative 30μV threshold were discarded from further analysis.

Chapter 6 General discussion

This thesis has studied performance monitoring in yet little explored settings and combination of settings, using different neuroimaging techniques. In the first instance, we used a paradigm with discrete events and discrete responses to understand how action influences performance monitoring and its hemodynamic and electrophysiological correlates. Next, we moved beyond typical performance monitoring paradigms and set out to find similar electrophysiological processes during continuous movements under visual-guidance. We found three electrophysiological markers time-locked to periodically occurring pulses in hand kinematics (sub-movements). Firstly, an increase in theta oscillations in the SMA encoding hand deviation (i.e. error). Secondly, high-gamma activity indexing spiking activity in the SMA and ACC. And thirdly, a transient activation of the ipsilateral motor cortex after large corrections, indexed by a stronger desynchronization of mu oscillations.

We started by studying electrophysiological correlates of performance monitoring in a discrete task along with its possible neural substrate using combined EEG-fMRI. We chose a perceptual task routinely used to study confidence judgments and added a radical time pressure incentive so that subjects would commit errors and appraise them with various levels of confidence. To better dissociate the effect of motor actions from performance monitoring, we added an observation condition which was identical to the active task, except that subjects did not respond but observed the computer responding. By searching for BOLD activations common to both tasks, we found that the supplementary motor area (SMA) and not the anterior cingulate cortex (ACC) was activated after errors. Moreover, confidence judgments from the subjects allowed us to dissociate between error certainty and uncertainty. We found that the SMA was not only activated when errors were appraised but also in case of uncertain responses, whether self-committed or observed. Interestingly, we found differences in metacognitive performance: subjects were more accurate when rating their confidence about their own actions than when rating their confidence about actions they had observed. The differences in metacognitive performance between the active and the observation condition were increased for subjects with more activation of the pre-SMA and the inferior frontal gyrus (IFG) during the observation task.

Our findings suggested that the SMA plays a primary role in performance monitoring whether erroneous actions are self-committed or observed. On the other hand, there was no evidence for a role of the ACC when no motor action was involved, or when post-error adaptation mechanisms were needed. In this regard, previous studies have shown an involvement of the ACC after negative feedback observation (Ullsperger and von Cramon, 2003; Becker et al., 2014). However, the feedback in these tasks was related to the subjects' performance, thus plausibly involving post-error adjustments to improve performance on the next trials. On the other hand, thanks to the addition of an observation condition, where subjects had no control on the computer's answer, we were able to better isolate the correlates of performance monitoring as subjects had no reason to make any adjustments in case of error.

By using this paradigm combining both self-committed and observed errors as well as confidence ratings, we were able to show that motor actions have a beneficial effect on performance monitoring. Indeed, when subjects committed the action themselves, they were better at assessing their performance. Further investigation needs to be done to find out how actions influence metacognitive judgments. Following our initial analysis, we found that subjects showing more metacognitive impairment in the observation task compared to the motor task also showed a higher activation of the pre-SMA and inferior frontal gyrus. This network is known to be involved in motor inhibition (Aron et al., 2007; Picazio et al., 2014), raising the intriguing possibility that the more subjects inhibit their actions during the observation condition, the worse is their metacognitive performance. This would imply that subjects simulate motor responses also during the observation condition. This was supported by the fact that confidence was best explained by EEG over the sensorimotor cortices during the observation condition. Moreover, the causal involvement of the motor cortex in confidence judgment during active tasks has received experimental support (Fleming et al., 2015).

In the following chapters of the thesis, we asked whether the aforementioned EEG correlates of performance monitoring could also be found during continuous movements with no strict experimental segmentation of motor actions and visual feedback. To have a quantitative measure of error, we used a visuo-motor tracking task in which subjects followed a moving target with the mouse cursor. We found three markers that could index performance monitoring.

Firstly, we found an event-related potential (ERP) time-locked to periodically occurring pulses in hand kinematics (sub-movements). Strikingly, the amplitude of such ERP with the deviation of the cursor with respect to the target were linearly correlated: When the cursor was lagging behind the target and sub-movements were larger, the amplitude of the ERP increased proportionally to the amount of deviation occurring 110 ms before the sub-movement. This modulation of the amplitude of the ERP by cursor deviation was observed even when selecting similar sub-movements and could therefore not be solely due to differences in hand kinematics.

Interestingly, this ERP was in many points identical to the ERN found in the discrete task after self-committed actions. It was time-locked to the motor action –in this case the sub-movement, and its trough also occurred 40 ms after the action. The ERP encoded cursor deviation; the equivalent of error in continuous tasks. Moreover, it was observed over the frontal midline of the scalp and localized in the SMA. Although results from EEG source localization should be taken with care, a recent neuroimaging study provided further evidence that the SMA was activated by errors in a visuo-motor task (and not the ACC). One additional similarity resides in the finding that an ERP with a shape similar to the ERN but of reduced amplitude is observed after correct responses (Vidal et al., 2000), which implies that the ERN does not reflect error detection *per se* but rather a comparison process leading to error detection. We observed a similar phenomenon in continuous motor tasks: in a task during which subjects spontaneously moved the cursor across the screen without any spatial or temporal constrains, a similar ERP was observed, also time-locked to the sub-movements. This suggests that the cortical process underlying the ERP could be a hard-wired component of continuous movements under visual guidance, though not serving a functional role in the absence of error. Considering all these similarities, we argue that we uncovered a generalization of the ERN in continuous motor tasks.

Some researchers have proposed that the ERNs (Luu et al., 2004; Trujillo and Allen, 2007) and other ERPs with similar topographies (Cavanagh et al., 2012) are generated by a phase-reset of frontal theta oscillations and that these frontal theta oscillations index the need for cognitive control (Cavanagh and Frank, 2014). Since sub-movements during our continuous motor task occurred at a theta frequency, it was appealing to discuss the fact that each ERP in our study could be a cycle of theta. This hypothesis has additional support from studies showing that a broad network of low frequency oscillations couple to sub-movements during continuous tasks (Gross et al., 2002; Jerbi et al., 2007).

To support this hypothesis, we analyzed data recorded in the medial frontal cortex (ACC and SMA) of epileptic patients implanted for surgical resection of epileptic tissues. We asked whether high gamma (HG) activity –a correlates of spiking activity, would phase-lock to sub-movements or to theta oscillations. We assumed that if every sub-movement generated an ERP, then HG activity would be phase-locked to sub-movements while the ERPs were cycles of theta oscillations, we would find HG activity phase-locked to theta oscillations. We found HG activity coupled to theta oscillations, consistent with previous findings (Canolty et al., 2006; Combrisson et al., 2017). These theta oscillations themselves were also coupled to sub-movements. Importantly however, we also found that in some electrodes, HG activity was coupled to sub-movements but not to theta oscillations. These findings suggest the existence of two distinct neuronal networks in the medial frontal cortex. One network is coupled with sub-movements and should thus be involved in the planning or evaluation of these sub-movements. The other network is coupled to theta oscillations and its role could be to synchronize the integration of information from other regions. Unfortunately for our conclusions, we did not get data from both the SMA and the ACC in single subjects to compare both brain areas and thus more recordings will be needed to further shed light on the role of these two networks

Lastly, we asked what could be the corrective mechanisms triggered by the performance monitoring system. For this, we added an experimental condition in which we reduced the need for motor corrections during tracking; we displaced the mouse cursor so as to automatically reduce the cursor deviation, leading the subjects to believe that they were performing better than they actually were. We found that this experimental manipulation reduced the activity in the sensorimotor cortices ipsilateral to the tracking hand. This activity decrease corresponded to a reduced desynchronization of mu oscillations compared to rest. Moreover, during normal tracking, we observed

a transient decrease of mu power after brisk sub-movements that was not present during the assistance condition. These results suggest that the ipsilateral hemisphere is involved in the corrective sub-movements occurring in order to correct cursor deviations, possibly through transcallosal inhibitory processes.

Altogether, our findings represent a substantial advance in the understanding of the neurophysiological processes underlying action monitoring. Firstly, by choosing a typical task used to study metacognition and adding a time constrain, we contribute to bridge the two previously unrelated research branches of performance monitoring and metacognition. Secondly by generalizing –for the first time to our best knowledge, electrophysiological correlates of performance monitoring to truly continuous motor tasks, we provide a new methodological framework to link performance monitoring to the field of motor control. Lastly, by finding electrophysiological correlates of performance monitoring and of spiking activity that are time-locked to sub-movements, we provide considerable evidence supporting the debated idea that the brain uses intermittent motor control during continuous movements (Karniel, 2011). In the next sections, we discuss i) how previous findings from the field of performance monitoring and decision making could be extended to a model explaining our data from both discrete tasks and the more general case of continuous motor control, ii) how our findings fit in the framework of intermittent control and finally, iii) the implications of our findings for the design of brain-machine interfaces.

6.1 A new model for performance monitoring?

How could theories of decision making (and our findings from Chapter 2) could be extended to explain data from continuous motor tasks? A recent opinion suggests that *"motor control is decision making"* (Wolpert and Landy, 2012). It is supported by various studies showing for example that reflex gains are modulated by the state of the evidence accumulation process (Selen et al., 2012) or that changes of mind are smoothly integrated into ongoing motor plans (Resulaj et al., 2009). Consequently, we further argue that continuous visually-guided movements can also be explained in the framework of decision making.

During visually-guided movements under time-pressure such as visuo-motor tracking, delays in visual feedback imply that the scaling of the sub-movements needs to be performed fast and thus rely on very weak evidence, i.e. high uncertainty. Considering that evidence accumulation continues after the scaling of the sub-movement, the same way as in perceptual decision, evidence of the position of the cursor with respect to the target should be significantly better after the sub-movement, at the time of the ERP. We can thus speculate on the existence of a mechanism for visuo-motor tracking similar to perceptual decision making, where a decision is taken about how much to scale the upcoming sub-movement. Following the mismatch theory (Falkenstein et al., 2000; Vidal et al., 2000; Coles et al., 2001; Rodriguez-Fornells et al., 2002), after the sub-movement, the efference copy of that sub-movement is compared to the current state of evidence.

At this stage, our proposition would predict that since large sub-movements after large deviations are the correct action to undertake, we should expect a reduced ERP in such situations. Additional analyses of our data showed that this was not the case and large sub-movements after large cursor deviation led to larger ERPs than small sub-movements. One way to reconcile these findings with the mismatch theory is to propose that the ERN does not compare the current state of evidence to an efference copy, but to the state of evidence at decision time. As for the mismatch theory, this comparison would be triggered by the motor response. Such a model would still be able to explain the classical ERN in a flanker's task: for correct responses, the state of evidence is identical after the response than at decision time while for errors, the state of evidence obviously changed.

This model would also explain the data from our visuo-motor tracking task. For this, we have to consider that evidence is accumulated in favour of a corrective action, in the form of an up-scaling of the next sub-movements. Our data shows that such corrective sub-movement arises when the cursor is lagging behind the target (Figure 3-4B). This situation occurs when the overall speed of the cursor is lower than the speed of the target. However, when a corrective sub-movement is triggered, the cursor deviation continues to increase until the speed of the cursor is at least equal to the speed of the target. Therefore, for deviations behind the target, the visual information available immediately after the sub-movement is likely to represent more evidence for correction that at the time of the decision. This can be seen in the cursor deviation profiles of Figure 3-4A. This revised way of interpreting our ERP data can thus reconcile our findings with previous findings for discrete tasks.

Our model can additionally explain our ERP results in the perceptual discrimination task. Contrarily to most previous findings, we found a large ERN-like negative deflection after correct trials. Due to the time pressure,

subjects made decisions based on very little evidence. Whether in the case of correct, erroneous or uncertain responses, there is a high likelihood that the state of evidence drastically changed after the first decision. Indeed, non-decision times have been evaluated to be 200 ms for the visual information to start accumulating and 80 ms between the decision and the action (Resulaj et al., 2009). Relating these findings to our task for which average response time was 380 ms, the time left for evidence accumulation is 100 ms. At time of the ERN (40 ms after the motor response), subjects have had 120 ms more (40 + 80 ms) to process the stimuli since the decision time, i.e. more than twice as much time.

On the other hand, Boldt et al. did not observe a discernible ERN for uncertain responses because subjects had up to 1500 ms to respond (Boldt and Yeung, 2015), thus it was less plausible that large changes in the evidence occurred unless subjects made premature erroneous responses. Unfortunately, the authors did not report reaction times. Finally, our model could also explain why the ERN is considered as a fast alarm signal while the following positivity reflects the accumulated evidence (Steinhauser and Yeung, 2010) and confidence ratings (Boldt and Yeung, 2015). This was further corroborated by the results obtained in Chapter 2, where the confidence rating decoding based on EEG peaked together with the ERP positivity in both motor and observation conditions (Figure 2-3, C and D). Indeed, if the ERN is a comparison between the current state of evidence and the state of evidence at the decision time, then it cannot reflect the absolute strength of evidence.

The SMA is known to be a good candidate for the continuous monitoring of accumulated evidence. One monkey study has shown that the SMA has both a proactive and reactive role in the control of movements (Chen et al., 2010). It is therefore not constrained to a particular phase of motor planning and execution. Furthermore, Bonini et al. showed that the increase in LFP activity in the SMA after erroneous response could also be observed after incorrect signals that were inhibited early enough to be replaced by a correct response (namely covert errors). These findings argue for a continuous monitoring by the SMA for fast updates of motor plan (Hosaka et al., 2016). The SMA is also involved in the accumulation of temporal information and action control (Coull et al., 2016). Interestingly, self-paced movement were also suggested to rely on an accumulation of evidence reflected in the slow and gradual build-up of the Bereitschaftspotential in the SMA (Schurger et al., 2012). During visuo-motor tracking, the SMA is active (Picard and Strick, 2003) and its activity was linked to errors (Limanowski et al., 2017). This monitoring role of the SMA is consistent with its activation for both self-committed and observed errors. However, the presence of low frequency oscillations in the SMA that are time-locked to the sub-movement and the source localization of the ERP during the visuo-motor tracking task in the SMA suggest that motor actions could trigger the comparison process with previous evidence.

Our proposed model –although still in its infancy, allows us to predict data from established conflict response tasks as well as more recent perceptual decision-making tasks and continuous motor control by hypothesizing that the process underlying the ERP/ERN compares the current state of evidence to the state of evidence at the decision time instead of to the efference copy (Figure 1-1). We need however further experimental support as well as to apply it to more data to assess its explanatory power.

6.2 Intermittent control and performance monitoring

Following our proposition that decision making processes occurs periodically during continuous motor control under visual guidance in order to scale the sub-movements and evaluate cursor deviation (i.e. evidence for correction) after the sub-movement, it comes as no surprise that the brain uses an intermittent motor controller for such behaviors.

Intermittent motor control was originally proposed based on the observation of sub-movements during visuo-motor tracking (Craik, 1947; Navas and Stark, 1968; Miall et al., 1985), isometric force tasks (Slifkin et al., 2000; Vaillancourt et al., 2006) or drawing (Doeringer and Hogan, 1998). These observations are hard to explain in the framework of continuous, optimal feedback control (Todorov, 2004). Rather, intermittent motor control theory posits that sub-movements are planned intermittently based on sensory feedback but then unfold in an open-loop manner (Gawthrop et al., 2014). This open-loop time interval could provide time for the planning of the next sub-movement, a possibly serial processing step that could thus have a refractory period preventing continuous control (Vince, 1948; Neilson et al., 1988). Intermittent control has received support from computational models (Hanneton et al., 1997; Ben-Itzhak and Karniel, 2008; Bye and Neilson, 2010; Loram et al., 2012). However, there is still no agreement on whether the brain uses such a control mechanism (Karniel, 2011).

One argument against the existence of a refractory period in intermittent control comes from double step paradigms. In such paradigms, a target is shown (first step), triggering a reaching movement. During a subset of movements, the target is displaced (second step), triggering a corrective (sub-)movement. Reaction time to the second step were not longer than for the first step (Archambault et al., 2009). These results were interpreted as evidence that no central bottleneck delayed the processing of the second step and the authors argued against a refractory period in such tasks. However, when the same steps were applied repeatedly during visuo-motor tracking, there was an increase in response times for the second of two steps when both occurred in less than 200 ms (van de Kamp et al., 2013).

We propose that there is no refractoriness in motor planning *per se* but in the decision-making process that transforms the current state of evidence for *correction* (i.e. performance monitoring) to an up-scaling of the next sub-movement. This hypothesis implies that the motor planning of the first movement in the double step paradigm does not show refractoriness since there is no error detection. Nonetheless, the error detection and subsequent corrective action generated in response to the second step could be refractory. However, reaching movements are fast enough that no further error detection is likely to happen in time for a second correction (that would be a triple step paradigm). This is not the case for sustained visuo-motor tracking for which error detection and correction occurs periodically, as suggested by our results and proposed in our model. This process could thus be serial and show refractoriness, similarly to other cognitive processes (Marois and Ivanoff, 2005).

In Chapter 3, we showed that sub-movements are coupled with an ERP that encodes cursor deviation. In other words, performance monitoring occurs repetitively after each sub-movement. Behaviorally, sub-movements were shown to be scaled by cursor deviation (Miall et al., 1986; Selen et al., 2006). Sub-movements were also shown to couple to cortical oscillations (Gross et al., 2002; Jerbi et al., 2007). Our findings suggest a link between these two parallel lines of research: sub-movements are coupled to a network of oscillations that serve to synchronize the motor system with an intermittent performance monitoring and correction process. In Chapter 4, we show that sub-movements are not only coupled to cortical oscillations -and thus possibly to a periodic modulation of neuronal excitability (Lakatos et al., 2005)-, but also to high-gamma activity reflecting spiking activity. Our findings also put forward the complexity of the planning of sub-movements and monitoring of feedback in the medial frontal cortex, with some electrodes showing high-gamma activity coupled to sub-movements and some other electrodes showing high-gamma activity coupled to theta oscillations. Finally, in Chapter 5, we observed a transient activation of the ipsilateral sensorimotor cortex after large corrective sub-movements. All three chapters thus uncovered correlates of neural processing that depend on the phase of the sub-movements, implying that sub-movements are not just a consequence of intrinsic muscular properties driven by a continuous neural signal but are processed in an intermittent way in the brain.

Further experimental evidence is needed to find which neural processes show refractoriness during visuo-motor tracking. Some evidence comes from providing intermittent visual feedback of the cursor position at different frequencies (Slifkin et al., 2000). The authors showed that behavioral performance increased with increasing feedback rate until 6.4 Hz, after which performance reached an asymptote. This suggests that performance is not impaired if the motor system runs in open-loop every 150 ms (i.e at 6.4 Hz). Using this paradigm, one could observe how sub-movements are scaled depending on the phase of the sub-movement at which the visual feedback is provided. Such a paradigm could also answer interesting questions such as: do sub-movement couple to the intermittent feedback? And if not, do theta oscillations couple to the intermittent feedback or to the sub-movements?

From a evolutionary perspective, an additional argument in favor of intermittent control lies in the fact that it is implausible that we evolved any neural process specifically for continuous movements under visual feedback. Indeed, in a competitive world in which survival depends on fast actions that should not be predictable by preys or predators, we cannot think of any evolutionary advantages for slow visuo-motor tracking before humans started hunting with bows and arrow. With this in mind, it is logical that such behaviors result from the concatenation of so-called motor primitives (i.e. sub-movements) (Thoroughman and Shadmehr, 2000) and show intermittency.

6.3 Future work

To conclude this thesis, we summarize the next steps that could be carried out to continue this research. During this thesis, we collected a large amount of valuable data. Firstly, in the EEG-fMRI study, our goal was to use the EEG data to infer the timing of the activation of the different brain regions that contribute to the ERP. In a very near future, we plan on using single-trial BOLD estimates in regions-of-interests to regress the EEG at every time-point, as in (Hauser et al., 2015). We also plan to conduct connectivity analyses using the fMRI data to understand the functional connectivity between brain regions in order to gain insight on the role of the network that showed common activation for both committed and observed actions. We also wish to verify our preliminary model of performance monitoring using both EEG and ECoG/LFP recordings during continuous visuo-motor tracking as well as during reaching movements (Torrecillos et al., 2014) and discrete perceptual decision tasks during which the strength of evidence can be modulated experimentally in single-trials (Herz et al., 2016).

Finding sub-movements was challenging since positional data had to be differentiated twice to obtain hand acceleration, thus introducing temporal variability. Our goal was to make the visuo-motor task engaging for the subjects and simple to record (thus the use of a computer mouse). Nonetheless, future work would benefit from simpler paradigms, such as one-dimensional tracking using radial wrist movements and time-locking the ERP analysis to electromyographic correlates of agonist / antagonist muscular activations. Ideally, wrist position should be acquired with a movement tracker to reduce friction. Assuming that muscular correlates of sub-movements are sufficiently predictable in a window of around one second, one could imagine predicting the occurrence of sub-movements and providing feedback at different phases of the sub-movements. Using the paradigm from (Slifkin et al., 2000), we could provide intermittent feedback of cursor positions at different phase of the sub-movement and study differences in behavioral performance as a function of the phase of the sub-movement at which the visual feedback is provided. In discrete movements, there are oscillations in behavioral performance depending on the time between stimulus onset and movement initiation (Tomassini et al., 2017). Interestingly, these oscillations in behavior occur at theta frequency. We would expect similar findings during continuous movements. One could also imagine applying TMS pulses to provoke virtual lesions of the SMA at consistent phases of the sub-movement. We could then assess how this interference impairs tracking performance as a function of the phase of the sub-movement at which the SMA is stimulated. One study elegantly showed that applying transcranial alternating current stimulation (tACS) over the motor cortex at a specific phase delay of Parkinsonian tremor reduced tremor by 50% (Brittain et al., 2013). What would happen if we could couple the tACS stimulation to sub-movements?

6.3.1 Implications for brain-machine interfaces

Finally, we discuss how studying the neural bases of performance monitoring during continuous tasks could have implication for the design of brain-machine interfaces (BMI). BMIs aim at decoding brain signals to control devices (Wolpaw et al., 2002) such as robots, wheelchairs or virtual keyboards without involving muscles or the peripheral neural system (Millán et al., 2010). While non-invasive approaches have mainly focused on delivering discrete commands, various invasive BMI decode motor signals to control a robot arm or a computer cursor. This was shown in rodents (Chapin et al., 1999) and then in monkeys (Serruya et al., 2002; Taylor et al., 2002; Carmena et al., 2003). More recently, a tetrapledgic human subject was able to move a neuroprosthethic limb (Hochberg et al., 2006, 2012; Collinger et al., 2013) or to recover grasping capabilities through the use of neuromuscular electric stimulation (Bouton et al., 2016). These BMIs have relied on the idea that single neurons encode motor parameters such as hand direction (Georgopoulos et al., 1986) or velocity (Georgopoulos et al., 1988; Moran and Schwartz, 1999). However, newer theories of motor cortex argue for a paradigm shift towards population-wide encoding of motor parameters and dynamical systems approaches to motor control (Churchland et al., 2012; Shenoy et al., 2013; Panzeri et al., 2015) which are being tested in new BMIs (Kao et al., 2015).

Recently, some groups have started to assess how the brain's performance monitoring system could be used to glean additional information about the performance of the BMI decoder. Discrete erroneous events were decoded from ECoG data (Milekovic et al., 2013). Using scalp EEG, erroneous cursor directions were decoded in real-time to guide a robotic arm using discrete steps (Iturrate et al., 2015) and gradually unfolding cursor deviations can also be detected (Omedes et al., 2015). Using spiking activity in the motor cortex, Even-Chen et al. were able to improve decoding performances by automatically correcting decoder errors (Even-Chen et al., 2015). The same group recently showed that error-related spiking activity in the motor cortex was orthogonal to the space spanned by output-relevant activity (Stavisky et al., 2016). This implies that at the population level, error-related activity in the motor cortex does not directly affect motor output but is isolated to only later be integrated into the ongoing movement. However, the integration of performance monitoring correlates in continuous BMI control is still in its infancy.

However, current BMIs decoders are based on a linear time-invariant mapping of cortical activity either directly onto an output space that can then either be used continuously to move a cursor or a prosthetic arm, or thresholded to issue discrete decisions. When BMIs are used to continuously control cursors on the screen, or during the learning of neuroprosthetic control, the behavior will resemble continuous movements under visual-guidance. Our results suggest that during continuous motor output, subjects monitor their performance in an intermittent manner, after periodic motor actions (sub-movements). It would therefore be interesting to have a better mechanistic insight about the way the brain controls each sub-movement to develop BMI decoders that generate commands intermittently, possibly phase-locked to theta oscillations and decode correlates of performance monitoring in an integrated manner. In this regard, one study has already shown that phase-amplitude coupling in the ACC can be used as features to decode movement execution versus rest (Combrisson et al., 2017).

Chapter 7 References

Alegre M, de Gurtubay IG, Labarga A, Iriarte J, Malanda A, Artieda J (2004) Alpha and beta oscillatory activity during a sequence of two movements. Clin Neurophysiol 115:124–130.

Alegre M, Labarga a, Gurtubay IG, Iriarte J, Malanda a, Artieda J (2003) Movement-related changes in cortical oscillatory activity in ballistic, sustained and negative movements. Exp Brain Res 148:17–25.

Alexander WH, Brown JW (2011) Medial prefrontal cortex as an action-outcome predictor. Nat Neurosci 14:1338–1344.

Allain S, Hasbroucq T, Burle B, Grapperon J, Vidal F (2014) Response monitoring without sensory feedback. Clin Neurophysiol 115:2014–2020.

Allen PJ, Josephs O, Turner R (2000) A method for removing imaging artifact from continuous EEG recorded during functional MRI. Neuroimage 239:230–239.

Archambault PS, Caminiti R, Battaglia-Mayer A (2009) Cortical mechanisms for online control of hand movement trajectory: The role of the posterior parietal cortex. Cereb Cortex 19:2848–2864.

Archambault PS, Ferrari-Toniolo S, Battaglia-Mayer A (2011) Online control of hand trajectory and evolution of motor intention in the parietofrontal system. J Neurosci 31:742–752.

Aron AR, Behrens TEJ, Smith S, Frank MJ, Poldrack RA (2007) Triangulating a cognitive control network using diffusion-weighted magnetic resonance imaging (MRI) and functional MRI. J Neurosci 27:3743–3752.

Aron AR, Fletcher PC, Bullmore ET, Sahakian BJ, Robbins TW (2003) Stop-signal inhibition disrupted by damage to right inferior frontal gyrus in humans. Nat Neurosci 6:115–116.

Babiloni C, Carducci F, Cincotti F, Rossini PM, Neuper C, Pfurtscheller G, Babiloni F (1999) Human movement-related potentials vs desynchronization of EEG alpha rhythm: A high-resolution EEG study. Neuroimage 10:658–665.

Bastin J, Deman P, David O, Gueguen M, Benis D, Minotti L, Hoffman D, Combrisson E, Kujala J, Perrone-bertolotti M, Kahane P, Lachaux J, Jerbi K (2017) Direct recordings from human anterior insula reveal its leading role within the error-monitoring network. Cereb Cortex 27:1545–1557.

Becker MPI, Nitsch AM, Miltner WHR, Straube T (2014) A single-trial estimation of the feedback-related negativity and its relation to BOLD responses in a time-estimation task. J Neurosci 34:3005–3012.

Belitski A, Gretton A, Magri C, Murayama Y, Montemurro MA, Logothetis NK, Panzeri S (2008) Low-frequency local field potentials and spikes in primary visual cortex convey independent visual information. J Neurosci 28:5696–5709.

Ben-Itzhak S, Karniel A (2008) Minimum acceleration criterion with constraints implies bang-bang control as an underlying principle for optimal trajectories of arm reaching movements. Neural Comput 20:779–812.

Berthier NE (1996) Learning to reach: A mathematical model. Dev Psychol 32:811–823.

Boldt A, Yeung N (2015) Shared neural markers of decision confidence and error detection. J Neurosci 35:3478–3484.

Bonini F, Burle B, Liégeois-Chauvel C, Régis J, Chauvel P, Vidal F (2014) Action monitoring and medial frontal cortex: Leading role of supplementary motor area. Science (80-) 343:888–891.

Bor D, Schwartzman DJ, Barrett AB, Seth AK (2017) Theta-burst transcranial magnetic stimulation to the prefrontal or parietal cortex does not impair metacognitive visual awareness. PLoS One 12:1–20.

Botvinick M, Nystrom L, Fissell K (1999) Conflict monitoring versus selection-for-action in anterior cingulate cortex. Nature:179–181.

Botvinick MM, Braver TS, Barch DM, Carter CS, Cohen JD (2001) Conflict monitoring and cognitive control. Psychol Rev 108:624–652.

Bouton CE, Shaikhouni A, Annetta N V., Bockbrader MA, Friedenberg DA, Nielson DM, Sharma G, Sederberg PB, Glenn BC, Mysiw WJ, Morgan AG, Deogaonkar M, Rezai AR (2016) Restoring cortical control of functional movement in a human with quadriplegia. Nature 0:1–13.

Brittain J, Probert-smith P, Aziz TZ (2013) Tremor Suppression by Rhythmic Transcranial Current Stimulation. Curr Biol 23:436–440.

Brown JW, Alexander WH (2017) Foraging value, risk avoidance, and multiple control signals: how the anterior cingulate cortex controls value-based decision-making. J Cogn Neurosci 29:1656–1673.

Brown JW, Braver TS (2005) Learned predictions of error likelihood in the anterior cingulate cortex. Science 307:1118–1121.

Buetefisch CM, Revill KP, Shuster L, Hines B, Parsons M (2014) Motor demand-dependent activation of ipsilateral motor cortex. J Neurophysiol 112:999–1009.

Buneo CA, Jarvis MR, Batista AP (2002) Direct visuomotor transformations for reaching. 416:632–636.

Burle B, Roger C, Allain S, Vidal F, Hasbroucq T (2008) Error negativity does not reflect conflict: a reappraisal of conflict monitoring and anterior cingulate cortex activity. J Cogn Neurosci 20:1637–1655.

Busch NA, VanRullen R (2010) Spontaneous EEG oscillations reveal periodic sampling of visual attention. Proc Natl Acad Sci 107:16048–16053.

Bye RT, Neilson PD (2010) The BUMP model of response planning: Intermittent predictive control accounts for 10Hz physiological tremor. Hum Mov Sci 29:713–736.

Canolty RT, Edwards E, Dalal SS, Soltani M, Nagarajan SS, Kirsch HE, Berger MS, Barbaro NM, Knight RT (2006) High gamma power is phase-locked to theta oscillations in human neocortex. Science 313:1626–1628.

Carmena JM, Lebedev MA, Crist RE, O'Doherty JE, Santucci DM, Dimitrov DF, Patil PG, Henriquez CS, Nicolelis MAL (2003) Learning to control a brain-machine interface for reaching and grasping by primates. PLoS Biol 1:193–208.

Carter CS, Braver TS, Barch DM, Botvinick MM, Noll D, Cohen JD (1998) Anterior cingulate cortex, error detection, and the online monitoring of performance. Science (80-) 280:747.

Cassim F, Szurhaj W, Sediri H (2000) Brief and sustained movements: differences in event-related (de) synchronization (ERD/ERS) patterns. Clin Neurophysiol 111:2032–2039.

Cavanagh JF, Frank MJ (2014) Frontal theta as a mechanism for cognitive control. Trends Cogn Sci 18:414–421.

Cavanagh JF, Zambrano-Vazquez L, Allen JJB (2012) Theta lingua franca: A common mid-frontal substrate for action monitoring processes. Psychophysiology 49:220–238.

Chapin JK, Moxon K a, Markowitz RS, Nicolelis M a (1999) Real-time control of a robot arm using simultaneously recorded neurons in the motor cortex. Nat Neurosci 2:664–670.

Charles L, Opstal F Van, Marti S, Dehaene S (2013) Distinct brain mechanisms for conscious versus subliminal error detection. Neuroimage 73:80–94.

Chavarriaga R, Millán JdR, Member S (2010) Learning from EEG error-related potentials in noninvasive brain-computer interfaces. IEEE Trans Neural Syst Rehabil Eng 18:381–388.

Chen R, Gerloff C, Hallett M, Cohen LG (1997) Involvement of the ipsilateral motor cortex in finger movements of different complexities. Ann Neurol 41:247–254.

Chen X, Scangos KW, Stuphorn V (2010) Supplementary motor area exerts proactive and reactive control of arm movements. J Neurosci 30:14657–14675.

Churchland MM, Cunningham JP, Kaufman MT, Foster JD, Nuyujukian P, Ryu SI, Shenoy K V (2012) Neural population dynamics during reaching. Nature 487:1–20.

Cisek P, Kalaska JF (2010) Neural mechanisms for interacting with a world full of action choices. Annu Rev Neurosci 33:269–298.

Clayson PE, Baldwin SA, Larson MJ (2013) How does noise affect amplitude and latency measurement of event-related potentials (ERPs)? A methodological critique and simulation study. Psychophysiology 50:174–186.

Cohen MX (2014) Analyzing neural time series data: Theory and practice. MIT Press.

Cohen MX (2016) Midfrontal theta tracks action monitoring over multiple interactive time scales. Neuroimage 141:262–272.

Cohen MX, Ridderinkhof KR, Haupt S, Elger CE, Fell J (2008) Medial frontal cortex and response conflict: Evidence from human intracranial EEG and medial frontal cortex lesion. Brain Res 1238:127–142.

Coles MG, Scheffers MK, Holroyd CB (2001) Why is there an ERN/Ne on correct trials? Response representations, stimulus-related components, and the theory of error-processing. Biol Psychol 56:173–189.

Colgin LL (2013) Mechanisms and functions of theta rhythms. Annu Rev Neurosci 36:295–312.

Collinger JL, Wodlinger B, Downey JE, Wang W, Tyler-Kabara EC, Weber DJ, McMorland AJC, Velliste M, Boninger ML, Schwartz AB (2013) High-performance neuroprosthetic control by an individual with tetraplegia. Lancet 381:557–564.

Combrisson E, Perrone-Bertolotti M, Soto JL, Alamian G, Kahane P, Lachaux JP, Guillot A, Jerbi K (2017) From intentions to actions: Neural oscillations encode motor processes through phase, amplitude and phase-amplitude coupling. Neuroimage 147:473–487.

Coull JT, Vidal F, Burle B (2016) When to act, or not to act: That's the SMA's question. Curr Opin Behav Sci 8:14–21.

Coxon JP, Stinear CM, Byblow WD (2006) Intracortical inhibition during volitional inhibition of prepared action. J Neurophysiol 95:3371–3383.

Craik KJW (1947) Theory of the human operator in control systems. I. The operator as an engineering system. Br J Psychol 38:56–61.

d'Avella A, Saltiel P, Bizzi E (2003) Combinations of muscle synergies in the construction of a natural motor behavior. Nat Neurosci 6:300–308.

Danielmeier C, Eichele T, Forstmann BU, Tittgemeyer M, Ullsperger M (2011) Posterior medial frontal cortex activity predicts post-error adaptations in task-related visual and motor areas. J Neurosci 31:1780–1789.

Danielmeier C, Ullsperger M (2011) Post-error adjustments. Front Psychol 2:1–10.

Danielmeier C, Wessel JR, Steinhauser M, Ullsperger M (2009) Modulation of the error-related negativity by response conflict. Psychophysiology 46:1288–1298.

Davare M, Duque J, Vandermeeren Y, Thonnard JL, Olivier E (2007) Role of the ipsilateral primary motor cortex in controlling the timing of hand muscle recruitment. Cereb Cortex 17:353–362.

Debener S, Ullsperger M, Siegel M, Fiehler K, Cramon DY von, Engel AK (2005) Trial-by-trial coupling of concurrent electroencephalogram and functional magnetic resonance imaging identifies the dynamics of performance monitoring. J Neurosci 25:11730–11737.

Dehaene S, Posner MI, Tucker DM, Dehaene S, Posner MI, Tucker DM (1994) Localization of a neural system for error detection and compensation. Psychol Sci 5:303–305.

Della-Maggiore V, Malfait N, Ostry DJ, Paus T (2004) Stimulation of the posterior parietal cortex interferes with arm trajectory adjustments during the learning of new dynamics. J Neurosci 24:9971–9976.

Desmurget M, Epstein CM, Turner RS, Prablanc C, Alexander GE, Grafton ST (1999) Role of the posterior parietal cortex in updating reaching movements to a visual target. Nat Neurosci 2:563–567.

Desmurget M, Grafton S (2000) Forward modeling allows feedback control for fast reaching movements. Trends Cogn Sci

4:423–431.

Dipietro L, Poizner H, Krebs HI (2015) Spatiotemporal dynamics of online motor correction processing revealed by high-density electroencephalography. J Cogn Neurosci:1–15.

Doeringer JA, Hogan N (1998) Intermittency in preplanned elbow movements persists in the absence of visual feedback. J Neurophysiol 80:1787–1799.

Dykstra AR, Chan AM, Quinn BT, Zepeda R, Keller CJ, Cormier J, Madsen JR, Eskandar EN, Cash SS (2012) Individualized localization and cortical surface-based registration of intracranial electrodes. Neuroimage 59:3563–3570.

Edwards BG, Calhoun VD, Kiehl K a (2012) Joint ICA of ERP and fMRI during error-monitoring. Neuroimage 59:1896–1903.

Even-Chen N, Stavisky SD, Kao JC, Ryu SI, Shenoy K V (2015) Auto-deleting brain machine interface: Error detection using spiking neural activity in the motor cortex. In: Proceedings of the 37th Annual Conference of the IEEE EMBS, pp 71–75.

Faivre N, Filevich E, Solovey G, Kühn S (2017) Behavioural, modeling, and electrophysiological evidence for supramodality in human metacognition. J Neurosci.

Falkenstein M, Hohnsbein J, Hoormann J, Blanke L (1991) Effects of crossmodal divided attention on late ERP components. II. Error processing in choice reaction tasks. Electroencephalogr Clin Neurophysiol 78:447–455.

Falkenstein M, Hoormann J, Christ S, Hohnsbein J (2000) ERP components on reaction errors and their functional significance: a tutorial. Biol Psychol 51:87–107.

Faul F, Erdfelder E, Lang A-G, Buchner A (2007) G * Power 3 : A flexible statistical power analysis program for the social, behavioral, and biomedical sciences. Behav Res Methods 39:175–191.

Ferrez PW, Millán JdR (2005) You are wrong! –Automatic detection of interaction errors from brain waves. In: Proceedings of the 19th International Joint Conference on Artificial Intelligence.

Fiebelkorn IC, Saalmann YB, Kastner S (2013) Rhythmic sampling within and between objects despite sustained attention at a cued location. Curr Biol 23:2553–2558.

Fiori F, Chiappini E, Soriano M, Paracampo R, Romei V, Borgomaneri S, Avenanti A (2016) Long-latency modulation of motor cortex excitability by ipsilateral posterior inferior frontal gyrus and pre-supplementary motor area. Sci Rep:1–11.

Flash T, Hochner B (2005) Motor primitives in vertebrates and invertebrates. Curr Opin Neurobiol 15:660–666.

Fleming SM, Daw ND (2017) Self-Evaluation of Decision-Making : A General Bayesian Framework for Metacognitive Computation. Psychol Rev 124:91–114.

Fleming SM, Huijgen J, Dolan RJ (2012) Prefrontal contributions to metacognition in perceptual decision making. J Neurosci 32:6117–6125.

Fleming SM, Maniscalco B, Ko Y, Amendi N, Ro T, Lau H (2015) Action-specific disruption of perceptual confidence. Psychol Sci 26:89–98.

Fleming SM, Weil RS, Nagy Z, Dolan RJ, Rees G (2010) Relating introspective accuracy to individual differences in brain structure. Science (80-) 329:1541–1543.

Frank MJ, Woroch BS, Curran T (2005) Error-related negativity predicts reinforcement learning and conflict biases. Neuron 47:495–501.

Franklin DW, Reichenbach A, Franklin S, Diedrichsen J (2016) Temporal evolution of spatial computations for visuomotor control. J Neurosci 36:2329–2341.

Fries P (2015) Rhythms for cognition: Communication through coherence. Neuron 88:220–235.

Friston KJ, Zarahn E, Josephs O, Henson RNA, Dale AM (1999) Stochastic designs in event-related fMRI. 619:607–619.

Galvin SJ, Podd J V, Drga V, Whitmore J (2003) Type 2 tasks in the theory of signal detectability: Discrimination between

correct and incorrect decisions. Psychon Bull Rev 10:843–876.

Gawthrop P, Gollee H, Loram I (2014) Intermittent Control in Man and Machine. arXiv Prepr arXiv14073543.

Gehring W, Goss B, Coles M (1993) A neural system for error detection and compensation. Psychol Sci 4:385–390.

Gehring WJ, Knight RT (2000) Prefrontal-cingulate interactions in action monitoring. Nat Neurosci 3:516–520.

Georgopoulos AP, Kettner RE, Schwartz AB (1988) Primate motor cortex and free arm movements to visual targets in three- dimensional space. II. Coding of the direction of movement by a neuronal population. J Neurosci 8:2928–2937.

Georgopoulos AP, Schwartz AB, Kettner RE (1986) Neuronal population coding of movement direction. Science 233:1416–1419.

Gherman S, Philiastides MG (2015) Neural representations of confidence emerge from the process of decision formation during perceptual choices. Neuroimage 106:134–143.

Giszter SF (2015) Motor primitives—new data and future questions. Curr Opin Neurobiol 33:156–165.

Gold JI, Shadlen MN (2007) The neural basis of decision making. Annu Rev Neurosci 30:535–574.

Goodale MA, Pelisson D, Prablanc C (1986) Large adjustments in visually guided reaching do not depend on vision of the hand or perception of target displacement. Nature 320:748–750.

Grafton ST, Tunik E (2011) Human basal ganglia and the dynamic control of force during on-line corrections. J Neurosci 31:1600–1605.

Gross J, Timmermann L, Kujala J, Dirks M, Schmitz F, Salmelin R, Schnitzler a (2002) The neural basis of intermittent motor control in humans. Proc Natl Acad Sci 99:2299–2302.

Hajcak G, Moser JS, Holroyd CB, Simons RF (2006) The feedback-related negativity reflects the binary evaluation of good versus bad outcomes. Biol Psychol 71:148–154.

Hall TM, DeCarvalho F, Jackson A (2014a) A common structure underlies low-frequency cortical dynamics in movement, sleep, and sedation. Neuron 83:1185–1199.

Hall TM, Nazarpour K, Jackson A (2014b) Real-time estimation and biofeedback of single-neuron firing rates using local field potentials. Nat Commun 5:5462.

Hanneton S, Berthoz a, Droulez J, Slotine JJ (1997) Does the brain use sliding variables for the control of movements? Biol Cybern 77:381–393.

Hauser TU, Hunt LT, Iannaccone R, Walitza S, Brandeis D, Brem S, Dolan RJ (2015) Temporally dissociable contributions of human medial prefrontal subregions to reward-guided learning. J Neurosci 35:11209–11220.

Hayashi MJ, Saito DN, Aramaki Y, Asai T, Fujibayashi Y, Sadato N (2008) Hemispheric asymmetry of frequency-dependent suppression in the ipsilateral primary motor cortex during finger movement: a functional magnetic resonance imaging study. Cereb cortex 18:2932–2940.

Heilbronner SR, Hayden BY (2016) Dorsal anterior cingulate cortex: a bottom-up view. Annu Rev Neurosci 39:149–170.

Herz DM, Zavala BA, Bogacz R, Brown P (2016) Neural correlates of decision thresholds in the human subthalamic nucleus. Curr Biol 26:916–920.

Hill H, Raab M (2005) Analyzing a complex visuomotor tracking task with brain-electrical event related potentials. Hum Mov Sci 24:1–30.

Hochberg LR, Bacher D, Jarosiewicz B, Masse NY, Simeral JD, Vogel J, Haddadin S, Liu J, Cash SS, van der Smagt P, Donoghue JP (2012) Reach and grasp by people with tetraplegia using a neurally controlled robotic arm. Nature 485:372–375.

Hochberg LR, Serruya MD, Friehs GM, Mukand JA, Saleh M, Caplan AH, Branner A, Chen D, Penn RD, Donoghue JP (2006) Neuronal ensemble control of prosthetic devices by a human with tetraplegia. Nature 442:164–171.

Holroyd CB, Coles MGH (2002) The neural basis of human error processing: Reinforcement learning, dopamine, and the error-related negativity. Psychol Rev 109:679–709.

Hosaka R, Nakajima T, Aihara K, Yamaguchi Y, Mushiake H (2016) The suppression of beta oscillations in the primate supplementary motor complex reflects a volatile state during the updating of action sequences. Cereb Cortex 26:3442–3452.

Huang R-S, Jung T-P, Delorme A, Makeig S (2008) Tonic and phasic electroencephalographic dynamics during continuous compensatory tracking. Neuroimage 39:1896–1909.

Hummel F, Kirsammer R, Gerloff C (2003) Ipsilateral cortical activation during finger sequences of increasing complexity: representation of movement difficulty or memory load? Clin Neurophysiol 114:605–613.

Iannaccone R, Hauser TU, Staempfli P, Walitza S, Brandeis D, Brem S (2015) Conflict monitoring and error processing: New insights from simultaneous EEG–fMRI. Neuroimage 105:395–407.

Imamizu H, Miyauchi S, Tamada T, Sasaki Y, Takino R, Pütz B, Yoshioka T, Kawato M (2000) Human cerebellar activity reflecting an acquired internal model of a new tool. Nature 403:192–195.

Ito S, Stuphorn V, Brown JW, Schall JD (2003) Performance monitoring by the anterior cingulate cortex during saccade countermanding. Science (80-) 302:120–122.

Iturrate I, Chavarriaga R, Montesano L, Minguez J, Millán JdR (2015) Teaching brain-machine interfaces as an alternative paradigm to neuroprosthetics control. Sci Rep 5:13893.

Jasper H, Penfield W (1949) Electrocorticograms in man: Effect of voluntary movement upon the electrical activity of the precentral gyrus. Arch Psychiatr Nervenkr 183:163–174.

Jerbi K, Lachaux J-P, N'Diaye K, Pantazis D, Leahy RM, Garnero L, Baillet S (2007) Coherent neural representation of hand speed in humans revealed by MEG imaging. Proc Natl Acad Sci 104:7676–7681.

Kao JC, Nuyujukian P, Ryu SI, Churchland MM, Cunningham JP, Shenoy K V (2015) Single-trial dynamics of motor cortex and their applications to brain-machine interfaces. Nat Commun 6:7759.

Karniel A (2011) Open questions in computational motor control. J Integr Neurosci 10:385–411.

Kerns JG, Cohen JD, MacDonald AW, Cho RY, Stenger VA, Carter CS (2004) Anterior cingulate conflict monitoring and adjustments in control. Science 303:1023–1026.

Kiani R, Corthell L, Shadlen MN (2014a) Choice certainty is informed by both evidence and decision time. Neuron 84:1329–1342.

Kiani R, Cueva CJ, Reppas JB, Newsome WT (2014b) Dynamics of neural population responses in prefrontal cortex indicate changes of mind on single trials. Curr Biol 24:1542–1547.

Kiani R, Shadlen MN (2009) Representation of confidence associated with a decision by neurons in the parietal cortex. Science (80-) 324:759–765.

Klimesch W, Sauseng P, Hanslmayr S (2007) EEG alpha oscillations: The inhibition-timing hypothesis. Brain Res Rev 53:63–88.

Kobayashi M, Hutchinson S, Theoret H, Schlaug G, Pascual-Leone A (2004) Repetitive TMS of the motor cortex improves ipsilateral sequential simple finger movements. Neurology 62:91–98.

Koch G, Fernandez Del Olmo M, Cheeran B, Ruge D, Schippling S, Caltagirone C, Rothwell JC (2007) Focal stimulation of the posterior parietal cortex increases the excitability of the ipsilateral motor cortex. J Neurosci 27:6815–6822.

Koelewijn T, van Schie HT, Bekkering H, Oostenveld R, Jensen O (2008) Motor-cortical beta oscillations are modulated by correctness of observed action. Neuroimage 40:767–775.

Kolling N, Behrens TEJ, Wittmann MK, Rushworth MFS (2016) Multiple signals in anterior cingulate cortex. Curr Opin Neurobiol 37:36–43.

Körding KP, Wolpert DM (2004) Bayesian integration in sensorimotor learning. Nature 427:444–247.

Körding KP, Wolpert DM (2006) Bayesian decision theory in sensorimotor control. Trends Cogn Sci 10:319–326.

Koriat A (2006) Metacognition and consciousness. In: The Cambridge Handbook of Consciousness, pp 289–326.

Krebs HI, Aisen ML, Volpe BT, Hogan N (1999) Quantization of continuous arm movements in humans with brain injury. Proc Natl Acad Sci 96:4645–4649.

Kvam PD, Pleskac TJ, Yu S, Busemeyer JR (2015) Interference effects of choice on confidence: Quantum characteristics of evidence accumulation. Proc Natl Acad Sci 112:10645–10650.

Lachaux JP, Rodriguez E, Martinerie J, Varela FJ (1999) Measuring phase synchrony in brain signals. Hum Brain Mapp 8:194–208.

Lakatos P, Shah AS, Knuth KH, Ulbert I, Karmos G, Schroeder CE, Shah AS, Knuth KH, Ulbert I, Karmos G, Schroeder CE (2005) An oscillatory hierarchy controlling neuronal excitability and stimulus processing in the auditory cortex. J Neurophysiol 94:1904–1911.

Landau AN, Schreyer HM, Van Pelt S, Fries P (2015) Distributed attention is implemented through theta-rhythmic gamma modulation. Curr Biol 25:2332–2337.

Lau H, Maniscalco B (2010) Should confidence be trusted. Science (80-) 329:6–8.

Levitt H (1971) Transformed up-down methods in psychoacoustics. J Acoust Soc Am:467–477.

Limanowski J, Kirilina E, Blankenburg F (2017) Neuronal correlates of continuous manual tracking under varying visual movement feedback in a virtual reality environment. Neuroimage 146:81–89.

Loram ID, van de Kamp C, Gollee H, Gawthrop P (2012) Identification of intermittent control in man and machine. J R Soc Interface 9:2070–2084.

Luu P, Tucker DM, Makeig S (2004) Frontal midline theta and the error-related negativity: Neurophysiological mechanisms of action regulation. Clin Neurophysiol 115:1821–1835.

MacDonald a. W (2000) Dissociating the role of the dorsolateral prefrontal and anterior cingulate cortex in cognitive control. Science (80-) 288:1835–1838.

Macmillan NA, Creelman CD (2004) Detection theory: A user's guide. Psychology Press.

Makeig S, Westerfield M, Jung TP, Covington J, Townsend J, Sejnowski TJ, Courchesne E (1999) Functionally independent components of the late positive event-related potential during visual spatial attention. J Neurosci 19:2665–2680.

Manganotti P, Gerloff C, Toro C, Katsuta H, Sadato N, Zhuang P, Leocani L, Hallett M (1998) Task-related coherence and task-related spectral power changes during sequential finger movements. Electroencephalogr Clin Neurophysiol 109:50–62.

Maniscalco B, Lau H (2012) A signal detection theoretic approach for estimating metacognitive sensitivity from confidence ratings. Conscious Cogn 21:422–430.

Maniscalco B, Lau H (2014) Signal detection theory analysis of type 1 and type 2 data: Meta-d' , response-specific meta- d', and the unequal variance SDT model.

Maniscalco B, Lau H (2016) The signal processing architecture underlying subjective reports of sensory awareness. Neurosci Conscious:1–17.

Maris E, Oostenveld R (2007) Nonparametric statistical testing of EEG- and MEG-data. J Neurosci Methods 164:177–190.

Maris E, Vugt M Van, Kahana M (2011) NeuroImage Spatially distributed patterns of oscillatory coupling between high-frequency amplitudes and low-frequency phases in human iEEG. Neuroimage 54:836–850.

Marois R, Ivanoff J (2005) Capacity limits of information processing in the brain. Trends Cogn Sci 9:296–305.

McAuley JH, Farmer SF, Rothwell JC, Marsden CD (1999) Common 3 and 10 Hz oscillations modulate human eye and finger movements while they simultaneously track a visual target. J Physiol 515:905–917.

McCurdy LY, Maniscalco B, Metcalfe J, Liu KY, de Lange FP, Lau H (2013) Anatomical coupling between distinct metacognitive systems for memory and visual perception. J Neurosci 33:1897–1906.

Miall RC, Christensen LOD, Cain O, Stanley J (2007) Disruption of state estimation in the human lateral cerebellum. PLoS Biol 5:e316.

Miall RC, Weir DJ, Stein JF (1985) Visuomotor tracking with delayed visual feedback. Neuroscience 16:511–520.

Miall RC, Weir DJ, Stein JF (1986) Manual tracking of visual targets by trained monkeys. Behav Brain Res 20:185–201.

Miall RC, Weir DJ, Stein JF (1993) Intermittency in human manual tracking tasks. J Mot Behav 25:53–63.

Milekovic T, Ball T, Schulze-Bonhage A, Aertsen A, Mehring C (2013) Detection of error related neuronal responses recorded by electrocorticography in humans during continuous movements. PLoS One 8:e55235.

Millán JdR, Rupp R, Müller-Putz GR, Murray-Smith R, Giugliemma C, Tangermann M, Vidaurre C, Cincotti F, Kübler A, Leeb R, Neuper C, Müller K-R, Mattia D (2010) Combining brain-computer interfaces and assistive technologies: State-of-the-art and challenges. Front Neurosci 4:1–15.

Miltner WHR, Braun CH, Coles MGH (1997) Event-related brain potentials following incorrect feedback in a time-estimation task: Evidence for a 'generic' neural system for error detection. J Cogn Neurosci 9:788–798.

Morales J, Lau HC, Fleming SM (2017) Domain-specific patterns of activity support metacognition in human prefrontal cortex. bioRxiv:1–40.

Moran DW, Schwartz AB (1999) Motor cortical activity during drawing movements: population representation during sinusoid tracing. J Neurophysiol 22:2693–2704.

Mukamel R, Ekstrom AD, Kaplan J, Iacoboni M, Fried I (2010) Single-neuron responses in humans during execution and observation of actions. Curr Biol 20:750–756.

Mulliken GH, Musallam S, Andersen R a (2008) Forward estimation of movement state in posterior parietal cortex. Proc Natl Acad Sci U S A 105:8170–8177.

Murphy PR, Robertson IH, Harty S, O'Connell RG (2015) Neural evidence accumulation persists after choice to inform metacognitive judgments. Elife 4:1–23.

Mussa-Ivaldi FA, Bizzi E (2000) Motor learning through the combination of primitives. Philos Trans R Soc Lond B Biol Sci 355:1755–1769.

Mutha PK, Stapp LH, Sainburg RL, Haaland KY (2014) Frontal and parietal cortex contributions to action modification. Cortex 57C:38–50.

Navas F, Stark L (1968) Sampling or intermittency in hand control system dynamics. Biophys J 8:252–302.

Neilson PD, Neilson MD, O'Dwyer NJ (1988) Internal models and intermittency: A theoretical account of human tracking behavior. Biol Cybern 58:101–112.

Nieuwenhuis S, Ridderinkhof KR, Blom J, Band GP, Kok a (2001) Error-related brain potentials are differentially related to awareness of response errors: evidence from an antisaccade task. Psychophysiology 38:752–760.

Niki H, Watanabe M (1979) Prefrontal and cingulate unit activity during timing behavior in the monkey. Brain Res 171:213–224.

Omedes J, Iturrate I, Minguez J, Montesano L (2015) Analysis and asynchronous detection of gradually unfolding errors during monitoring tasks. J Neural Eng 12:56001.

Oostenveld R, Fries P, Maris E, Schoffelen J (2011) FieldTrip: Open source software for advanced analysis of MEG, EEG, and invasive electrophysiological data. Comput Intell Neurosci 2011.

Overbeek TJM, Nieuwenhuis S, Ridderinkhof KR (2005) Dissociable components of error processing. J Psychophysiol 19:319–329.

Palva S, Palva JM (2007) New vistas for alpha-frequency band oscillations. Trends Neurosci 30:150–158.

Panzeri S, Macke JH, Gross J, Kayser C (2015) Neural population coding: Combining insights from microscopic and mass signals. Trends Cogn Sci 19:162–172.

Pasalar S, Roitman A V., Ebner TJ (2005) Effects of speeds and force fields on submovements during circular manual tracking in humans. Exp Brain Res 163:214–225.

Pfurtscheller G (2001) Functional brain imaging based on ERD/ERS. Vision Res 41:1257–1260.

Pfurtscheller G, Aranibar A (1979) Evaluation of event-related desynchronization (ERD) preceding and following voluntary self-paced movement. Electroencephalogr Clin Neurophysiol 46:138–146.

Pfurtscheller G, Berghold a (1989) Patterns of cortical activation during planning of voluntary movement. Electroencephalogr Clin Neurophysiol 72:250–258.

Picard N, Strick PL (2003) Activation of the supplementary motor area (SMA) during performance of visually guided movements. Cereb Cortex 13:977–986.

Picazio S, Veniero D, Ponzo V, Caltagirone C, Gross J, Thut G, Koch G (2014) Prefrontal control over motor cortex cycles at beta frequency during movement inhibition. Curr Biol 24:2940–2945.

Pisella L, Gréa H, Tilikete C, Vighetto A, Desmurget M, Rode G, Boisson D, Rossetti Y (2000) An 'automatic pilot' for the hand in human posterior parietal cortex: Toward reinterpreting optic ataxia. Nat Neurosci 3:729–736.

Pleskac TJ, Busemeyer JR, others (2010) Two-stage dynamic signal detection: A theory of choice, decision time, and confidence. Psychol Rev 117:864.

Rabbitt PM (1966) Error correction time without external error signals. Nature 212:438.

Rao SM, Bandettini PA, Binder JR, Bobholz JA, Hammeke TA, Stein EA, Hyde JS (1996) Relationship between finger movement rate and functional magnetic resonance signal change in human primary motor cortex. J Cereb Blood Flow Metab 16:1250–1254.

Ratcliff R, Smith PL, Brown SD, Mckoon G (2016) Diffusion decision model: Current issues and history. Trends Cogn Sci 20:260–281.

Ray S, Maunsell JHR (2011) Different origins of gamma rhythm and high-gamma activity in macaque visual cortex. Plos Biol 9:e1000610.

Reddy H, Lassonde M, Bemasconi N, Bemasconi a, Matthews PM, Andermann F, Arnold DL (2000) An fMRI study of the lateralization of motor cortex activation in acallosal patients. Neuroreport 11:2409–2413.

Reichenbach A, Franklin DW, Zatka-Haas P, Diedrichsen J (2014) A dedicated binding mechanism for the visual control of movement. Curr Biol 24:780–785.

Resulaj A, Kiani R, Wolpert DM, Shadlen MN (2009) Changes of mind in decision-making. Nature 461:263–266.

Ridderinkhof KR, Ullsperger M, Crone EA, Nieuwenhuis S (2004) The role of the medial frontal cortex in cognitive control. Science (80-) 306:443–447.

Rodriguez-Fornells A, Kurzbuch AR, Münte TF (2002) Time course of error detection and correction in humans: Neurophysiological evidence. J Neurosci 22:9990–9996.

Rohrer B, Fasoli S, Krebs HI, Hughes R, Volpe B, Frontera WR, Stein J, Hogan N (2002) Movement smoothness changes during stroke recovery. J Neurosci 22:8297–8304.

Rohrer B, Fasoli S, Krebs HI, Volpe B, Frontera WR, Stein J, Hogan N (2004) Submovements grow larger, fewer, and more blended during stroke recovery. Motor Control 8:472–483.

Roitman A V., Massaquoi SG, Takahashi K, Ebner TJ (2004) Kinematic analysis of manual tracking in monkeys: characterization of movement intermittencies during a circular tracking task. J Neurophysiol 91:901–911.

Rounis E, Maniscalco B, Rothwell JC, Passingham RE, Rounis E, Maniscalco B, Rothwell JC, Passingham RE, Lau H (2010) Theta-burst transcranial magnetic stimulation to the prefrontal cortex impairs metacognitive visual awareness. Cogn Neurosci 1:165–175.

Ruiz MH, Huebl J, Schönecker T, Kupsch A, Yarrow K, Krauss JK, Schneider GH, Kühn A a. (2014) Involvement of human internal globus pallidus in the early modulation of cortical error-related activity. Cereb Cortex 24:1502–1517.

Sakaguchi Y, Tanaka M, Inoue Y (2015) Adaptive intermittent control: A computational model explaining motor intermittency observed in human behavior. Neural Networks 67:92–109.

Saunders JA, Knill DC (2004) Visual feedback control of hand movements. J Neurosci 24:3223–3234.

Savitzky A, Golay MJE (1964) Smoothing and differentiation of data by simplified least squares procedures. Anal Chem 36:1627–1639.

Scheffers MK, Coles MGH (2000) Performance monitoring in a confusing world: Error-related brain activity, judgments of response accuracy, and types of errors. J Exp Psychol 26:141–151.

Schroeder CE, Wilson DA, Radman T, Scharfman H, Lakatos P (2010) Dynamics of active sensing and perceptual selection. Curr Opin Neurobiol 20:172–176.

Schubotz RI (2007) Prediction of external events with our motor system: Towards a new framework. Trends Cogn Sci 11:211–218.

Schultz W, Dickinson A (2000) Neuronal coding of prediction errors. Annu Rev Neurosci 23:473–500.

Schurger A, Sitt JD, Dehaene S (2012) An accumulator model for spontaneous neural activity prior to self-initiated movement. Proc Natl Acad Sci 109:E2904-13.

Sederberg PB, Kahana MJ, Howard MW, Donner EJ, Madsen JR (2003) Theta and gamma oscillations during encoding predict subsequent recall. J Neurosci 23:10809–10814.

Seidler RD, Noll DC, Thiers G (2004) Feedforward and feedback processes in motor control. Neuroimage 22:1775–1783.

Selen LPJ, Shadlen MN, Wolpert DM (2012) Deliberation in the motor system: Reflex gains track evolving evidence leading to a decision. J Neurosci 32:2276–2286.

Selen LPJ, van Dieën JH, Beek PJ (2006) Impedance modulation and feedback corrections in tracking targets of variable size and frequency. J Neurophysiol 96:2750–2759.

Serruya MD, Hatsopoulos NG, Paninski L, Fellows MR, Donoghue JP (2002) Instant neural control of a movement signal. Nature 416:141–142.

Shadmehr R, Mussa-Ivaldi F a (1994) Adaptive representation of dynamics during learning of a motor task. J Neurosci 14:3208–3224.

Shadmehr R, Smith M a, Krakauer JW (2010) Error correction, sensory prediction, and adaptation in motor control. Annu Rev Neurosci 33:89–108.

Shenhav A, Botvinick MM, Cohen JD (2013) The expected value of control: An integrative theory of anterior cingulate cortex function. Neuron 79:217–240.

Shenoy K V, Sahani M, Churchland MM (2013) Cortical control of arm movements: A dynamical systems perspective. Annu Rev Neurosci 36:337–359.

Shima K, Tanji J (1998) Role for cingulate motor area cells in voluntary movement selection based on reward. 282:1335–1339.

Siedlecka M, Paulewicz B, Wierzchoń M (2016) But I was so sure! Metacognitive judgments are less accurate given prospectively than retrospectively. Front Psychol 7:1–8.

Slifkin AB, Vaillancourt DE, Newell KM (2000) Intermittency in the control of continuous force production. J Neurophysiol 84:1708–1718.

Stavisky SD, Kao JC, Ryu SI, Shenoy K V (2016) Motor cortical visuomotor feedback activity is initially isolated from downstream targets in output-null neural state space dimensions. Neuron:195–208.

Steinhauser M, Yeung N (2010) Decision processes in human performance monitoring. J Neurosci 30:15643–15653.

Swann N, Tandon N, Canolty R, Ellmore TM, McEvoy LK, Dreyer S, DiSano M, Aron AR (2009) Intracranial EEG reveals a time- and frequency-specific role for the right inferior frontal gyrus and primary motor cortex in stopping initiated responses. J Neurosci 29:12675–12685.

Tan H, Jenkinson N, Brown P (2014a) Dynamic neural correlates of motor error monitoring and adaptation during trial-to-trial learning. J Neurosci 34:5678–5688.

Tan H, Zavala B, Pogosyan A, Ashkan K, Zrinzo L, Foltynie T, Limousin P, Brown P (2014b) Human subthalamic nucleus in movement error detection and its evaluation during visuomotor adaptation. J Neurosci 34:16744–16754.

Tass P, Rosenblum MG, Weule J, Kurths J, Pikovsky A, Volkmann J, Schnitzler A, Freund H-J (1998) Detection of n:m phase locking from noisy data: Application to magnetoencephalography. Phys Rev Lett 81:3291–3294.

Taylor DM et al. (2002) Direct cortical control of 3D neuroprosthetic devices. Science (80-) 296:1829–1832.

Tazoe T, Perez M a (2013) Speed-dependent contribution of callosal pathways to ipsilateral movements. J Neurosci 33:16178–16188.

Thoroughman K a, Shadmehr R (2000) Learning of action through adaptive combination of motor primitives. Nature 407:742–747.

Todorov E (2004) Optimality principles in sensorimotor control. Nat Neurosci 7:907–915.

Tomassini A, Ambrogioni L, Medendorp WP, Maris E (2017) Theta oscillations locked to intended actions rhythmically modulate perception. Elife 6:1–18.

Torrecillos F, Alayrangues J, Kilavik BE, Malfait N (2015) Distinct modulations in sensorimotor postmovement and foreperiod beta-band activities related to error salience processing and sensorimotor adaptation. J Neurosci 35:12753–12765.

Torrecillos F, Albouy P, Brochier T, Malfait N (2014) Does the processing of sensory and reward-prediction errors involve common neural resources? Evidence from a frontocentral negative potential modulated by movement execution errors. J Neurosci 34:4845–4856.

Trujillo LT, Allen JJB (2007) Theta EEG dynamics of the error-related negativity. Clin Neurophysiol 118:645–668.

Tzourio-Mazoyer N, Landeau B, Papathanassiou D, Crivello F, Etard O, Delcroix N, Mazoyer B, Joliot M (2002) Automated anatomical labeling of activations in SPM using a macroscopic anatomical parcellation of the MNI MRI single-subject brain. Neuroimage 15:273–289.

Ullsperger M, Fischer AG, Nigbur R, Endrass T (2014) Neural mechanisms and temporal dynamics of performance monitoring. Trends Cogn Sci 18:1–9.

Ullsperger M, von Cramon DY (2003) Error monitoring using external feedback: specific roles of the habenular complex, the reward system, and the cingulate motor area revealed by functional magnetic resonance imaging. J Neurosci 23:4308–4314.

Vaillancourt DE, Mayka MA, Corcos DM (2006) Intermittent visuomotor processing in the human cerebellum, parietal cortex, and premotor cortex. J Neurophysiol 95:922–931.

Vallbo AB, Wessberg J (1993) Organization of motor output in slow finger movements in man. J Physiol 469:673–691.

van de Kamp C, Gawthrop PJ, Gollee H, Loram ID (2013) Refractoriness in sustained visuo-manual control: Is the refractory duration intrinsic or does it depend on external system properties? PLoS Comput Biol 9:e1002943–e1002843.

Van Den Berg R, Anandalingam K, Zylberberg A, Kiani R, Shadlen MN, Wolpert DM (2016) A common mechanism underlies changes of mind about decisions and confidence. Elife 5:1–21.

van Schie HT, Mars RB, Coles MGH, Bekkering H (2004) Modulation of activity in medial frontal and motor cortices during error observation. Nat Neurosci 7:549–554.

VanRullen R (2016) Perceptual cycles. Trends Cogn Sci 20:723–735.

Verstynen T, Diedrichsen J, Albert N, Aparicio P, Ivry RB (2005) Ipsilateral motor cortex activity during unimanual hand

movements relates to task complexity. J Neurophysiol 93:1209–1222.

Vidal F, Hasbroucq T, Grapperon J, Bonnet M (2000) Is the 'error negativity' specific to errors? Biol Psychol 51:109–128.

Vince A (1948) The intermittency of control movements and the psychological refractory period. :149–157.

Vocat R, Pourtois G, Vuilleumier P (2011) Parametric modulation of error-related ERP components by the magnitude of visuo-motor mismatch. Neuropsychologia 49:360–367.

Wassermann EM, Pascual-Leone A, Hallett M (1994) Cortical motor representation of the ipsilateral hand and arm. Exp Brain Res 100:121–132.

Williams ER, Soteropoulos DS, Baker SN (2010) Spinal interneuron circuits reduce approximately 10-Hz movement discontinuities by phase cancellation. Proc Natl Acad Sci 107:11098–11103.

Williams ZM, Bush G, Rauch SL, Cosgrove GR, Eskandar EN (2004) Human anterior cingulate neurons and the integration of monetary reward with motor responses. Nat Neurosci 7:1370–1375.

Wokke ME, Cleeremans A, Ridderinkhof KR (2017) Sure I'm sure: Prefrontal oscillations support metacognitive monitoring of decision making. J Neurosci 37:781–789.

Wolpaw JR, Birbaumer N, McFarland DJ, Pfurtscheller G, Vaughan TM (2002) Brain-computer interfaces for communication and control. Clin Neurophysiol 113:767–791.

Wolpert DM, Ghahramani Z (2000) Computational principles of movement neuroscience. Nat Neurosci 3 Suppl:1212–1217.

Wolpert DM, Ghahramani Z, Jordan MI (1995) An internal model for sensorimotor integration. Science (80-) 269:1880–1882.

Wolpert DM, Landy MS (2012) Motor control is decision-making. Curr Opin Neurobiol 22:996–1003.

Yeung N, Summerfield C (2012) Metacognition in human decision-making: confidence and error monitoring. Philos Trans R Soc Lond B Biol Sci 367:1310–1321.

Ziemann U, Iahii K, Borgheresi A, Yaseen Z, Battaglia F, Hallett M, Cincotta M, Wassermann EM (1999) Dissociation of the pathways mediating ipsilateral and controlateral motor-evoked potentials in human hand and arm muscles. J Physiol 518:895–906.

Appendix A : Pre-registration of the EEG-fMRI study (Chapter 1)

Study Information

1. Title: Neural processing of self-committed and observed errors

2. Authorship, by alphabetical order
Olaf Blanke, Arnaud Desvachez, Nathan Faivre, Iñaki Iturrate, Stéphanie Martin, José del R. Millán, Michael Pereira, Luana Serafini, Dimitri Van de Ville.

3. Research Questions
Numerous behavioral and neuroimaging studies have documented the brain's error monitoring system (Ullsperger et al. 2014). Several lines of research indicate that error detection can rely on external feedback, for instance by observing the consequences of one's action. Yet, electrophysiological responses to errors in speeded response tasks occur sometimes too early to rely solely on sensory feedback (Rodriguez-Fornell et al. 2002). This implies that errors may be detected based on decisional signals preceding the motor response (Coles et al. 2001), for instance associating preparation of the motor command to the continuous processing of stimulus information. The capacity to detect one's error is a key aspect of self-monitoring. Recent studies on self-monitoring have shown that prefrontal structures of the human brain are activated during appraisal of task performance (metacognitive monitoring; Fleming et al., 2012) and that error detection and confidence appraisal share neural correlates (Boldt and Yeung, 2015). Here, we aim at disentangling the role of external feedback and decisional signals for error monitoring, by comparing error detection and confidence appraisal between errors that are self-committed, and errors committed by an agent that are simply observed. Our study aims at answering three main questions:

Q1: is metacognitive monitoring better for committed vs. observed errors?

Q2: what are the common and distinct brain regions involved for detecting committed vs. observed errors?

Q3: how do neural responses following committed vs. observed error unfold over time?

4. Hypotheses

Q1: is metacognitive monitoring better for committed vs. observed errors?

At the behavioral level, we will assess how participants calibrate their confidence judgments on self-committed vs. observed decisions (active vs. observation condition). We assume that the sense of confidence is informed by decisional cues occurring during metacognitive monitoring (e.g., motor preparation, reaction times; Yeung & Summerfield, 2012), and therefore expect that confidence will track performance more closely in the active vs. observation condition. More specifically, when quantifying performance as a function of confidence using logistic regressions (see below), we predict that errors will be better detected in the active condition (resulting

in lower asymptotes of smaller magnitude in the active vs. observation condition or higher confidence bias), and that accuracy will increase more as a function of confidence in the active condition, as reflected by a steeper slope in the logistic regression (see below).

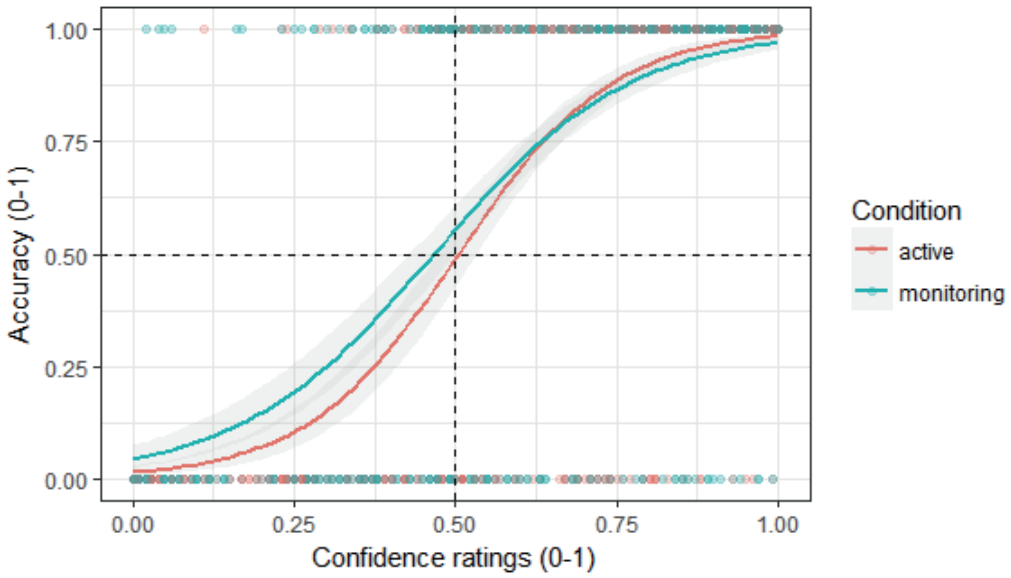

Figure 1: Logistic regression curve, illustrating the degree to which the confidence ratings predict the accuracy in the perceptual task, for the active and the observation condition. In particular, when formulating judgements about the computer's performance the participant is expected to be less accurate (i.e., less steep slope, indicating less correlation between confidence ratings and the actual accuracy), than when monitoring his/her own. More specifically, the participants are expected to better detect self-committed vs observed errors (i.e., lower asymptote of bigger magnitude for the observation condition, suggesting that the participant might be overconfident when detecting errors committed by the computer). The figure was derived from the behavioral data of the study pilots (n=9), and is displayed for illustrative purposes.

Besides these two key hypotheses, we will examine additional aspects of the data, and notably assess whether metacognitive monitoring in the two conditions correlate among subjects, in line with previous research showing the domain-generality of metacognition (Faivre et al., 2016). We will also examine how observed vs. committed reaction times are predictive of confidence, in line with decisional models of metacognition (Yeung & Summerfield, 2012). We will rely on previous measures developed in the laboratory to specifically quantify this link (Faivre et al., 2016). In particular, we expect to find a negative correlation between reaction times and confidence during correct active decisions (i.e., participants respond faster when sure to be correct), and a negative correlation between reaction times and confidence for active, self-committed errors (i.e., slower when sure to be incorrect). We predict weaker correlations for the observation condition.

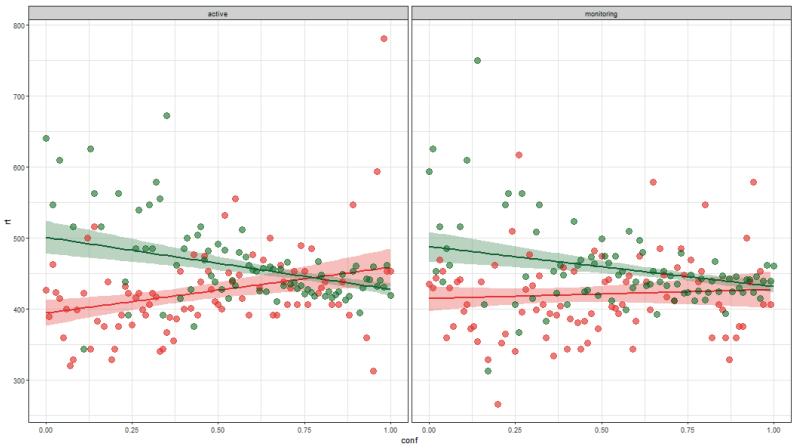

Figure 2: pilot data showing the linear regression between reaction times (y axis) and confidence (x axis) following correct (in green) and incorrect (in red) responses in the active and observation condition (n=10).

Q2: what are the common and distinct brain regions involved for detecting committed vs. observed errors?

In the active condition, comparing erroneous trials with low vs high confidence should highlight the brain regions responsible for the conscious detection of active errors, while performing the same contrast in the observation condition should uncover the brain regions responsible for the observed error monitoring mechanisms. The hypothesis to be tested is whether a common neural substrate between the two conditions can be found with fMRI. According to the literature the posterior frontomedian cortex (pFMC), in particular the rostral cingulate zone (RCZ), should be differentially activated during erroneous vs correct trials (Kiehl et al., 2000; Menon et al., 2001) and might represent the neural correlate of the error-related negativity, ERN (Dehaene et al., 1994; Gehring et al., 2000; Debener et al., 2005). A recent study dissociating response conflict and error monitoring showed that the later corresponded to more rostral activations (RCZ) than the former (pre-supplementary motor area; Iannaccone et al., 2015). The neural substrate of error monitoring in the case of observed errors was also more rostral (Hauser et al., 2014). We thus predict that the common neural substrate of error detection for both self-committed and observed errors will lie in the RCZ. Consequently, we also predict that differential activations will be found in more superior brain regions such as the supplemental motor area, since these regions are involved in conflict monitoring during the motor task (Bonini et al., 2012, Iannaccone et al., 2015) but not in the monitoring task. Finally, we also expect possibly indirect error-related activations in parietal and prefrontal regions (Danielmeier et al., 2011).

The RCZ is known to activate independently whether or not participants are conscious of their error (Klein et al., 2007). By contrast, we expect activity in the anterior insula to differ between conscious and unconscious errors, as shown previously (Ullsperger et al. 2010; Klein et al. 2007; Hester et al. 2005). The role of the anterior insula in mediating consciousness for errors could be understood in link with its the processing of interoceptive signals (Klein et al., 2007). Based on previous findings we expect observed errors to be partially subdued by similar neural correlates as committed errors, specifically dACC (van Schie et al. 2004; Shane et al., 2008; De Bruijn et al., 2009).

Q3: how do neural responses following committed vs. observed error unfold over time?

Previous results indicate that both self-committed and observed errors generate electrophysiological event-related potentials (ERP) along the anterior midline of the brain. Even if ERPs from self-committed and observed errors share similar patterns (Cavanagh and Frank, 2014), experimental evidence supporting a common neural substrate has been limited to EEG studies (Cavanagh et al., 2012). We aim at finding the neural generators of midline negativities originating from both self-committed and observed errors using simultaneous EEG-fMRI recordings. We will determine how brain regions found in the previous section with fMRI explain electrophysiological response to errors as measured with EEG. We expect to observe an electrophysiological response in the form of an event-related potential (ERP), time-locked to erroneous button-presses (active condition) or erroneous visual feedback (observation condition). For self-committed errors, an ERP over the frontal midline of the scalp has been reliably observed 50–100 ms after erroneous button presses in speeded response tasks: the error-related negativity (ERN; Falkenstein et al., 1991, Gehring et al., 1993). The ERN is followed by a positive potential called Pe, with maximum centro-parietal amplitude between 200-400ms after the erroneous response. Pe appears larger for error reported by the subject than unreported ones (Navarro-Cebrian et al., 2013) and seems to reflect adapting strategies. We thus expect to observe an ERN-Pe complex after (self-committed) erroneous button presses. We also consider ERN-Pe complex to be possibly involved in the observation condition. In addition, when external feedback (visual or auditory) indicates to the subject a worse outcome compared to what he expected, a feedback-related negativity (FRN) is observed 250 – 300 ms later (Miltner et al., 1997; Gehring and Willoughby, 2002). The FRN shows a similar shape and scalp topography compared to the ERN. The FRN is usually observed when the feedback is given related to a choice the subjects made themselves. Nonetheless, when subjects observe an external agent committed errors, a similar ERP is observed (Van Schie et al., 2004, Iturrate et al., 2015). We thus expect to observe an FRN-like ERP after erroneous feedback in the observation condition.

We will further investigate how confidence ratings modulates these ERPs amplitude, in accordance with a recent study of Boldt & Yeung (2015), showing amplitude modulation of the ERN-Pe complex as a function of confidence irrespective of response accuracy. In the present study we will try to replicate these findings for the active condition and we will investigate whether a similar modulation occurs also for monitoring-related ERPs. Besides amplitude Another electrophysiological correlate of confidence we will focus on is the alpha suppression, that is a decrease in alpha power, correlated to confidence ratings, taking place in parieto-occipital electrodes, from 300ms before to 200ms after the decision (Faivre et al., 2016), which might subserve attentional gating (i.e. Foxe & Snyder, 2011).

Sampling Plan

5. Existing data

Registration prior to creation of data: As of the date of submission of this research plan for preregistration, the data have not yet been collected, created, or realized.

6. Explanation of existing data

Not applicable.

7. Data collection procedures.

All participants will be right-handed, with normal hearing and normal or corrected-to-normal vision, and no psychiatric or neurological history. They will be naive to the purpose of the study and give informed consent, in accordance with institutional guidelines and the Declaration of Helsinki, and approved by the cantonal ethical

committee of Geneva. They will receive a monetary compensation in exchange of their participation (20 CHF per hour).

8. Sample size

A total of 25 participants from the student population in Geneva will take part in this study.

9. Sample size rationale

The sample size is determined based on power analyses conducted on the pilot behavioral data (n=9) for the main effects of interest. Using the R package "simr" (Green & MacLeod, 2016), we could test the effect of the interaction of confidence and condition on accuracy, based on a logistic mixed-effects model power calculation, with 100 simulations. We adopted a conservative approach by setting the effect size to -1.5 (instead of the observed -1.8) and α to 0.05. A 0.88 (95% CI = 0.80, 0.94) power was reached with a sample size of 25 participants. Besides this main effect of interest, we also performed power analysis for the interaction between accuracy and confidence on reaction times, based on a linear mixed-effects model power calculation. Using the same approach, the power for finding a significant effect size of -28.78 (observed) is 98% (95% CI = 93%, 99%) with a sample size of 25 participants. This sample size of 25 participants is equivalent or exceed what is typically used for EEG recordings (e.g., Charles et al., JoN 2015: 20 patients vs. 20 controls, resulting I n 13 vs. 13 after outlier exclusion; Boldt & Yeung: 16 participants) and fMRI recordings (e.g., Fleming et al., 2012: 26 participants).

10. Stopping rule

Data will be acquired until the predetermined sample size is reached.

Variables

11. Manipulated variables

Not applicable.

12. Measured variables

Behavioral variables

Type I task accuracy (binary: correct/incorrect on the visual discrimination task)
Type I reaction time (continuous: time to respond to the type I task in ms)
Confidence (continuous: visual analog scale)
Type II reaction time (continuous: time to report confidence in ms)

Physiological variables

fMRI (Siemens Prisma 3 Tesla)
Electroencephalogram (64ch. time-locked to type I response)
Heart rate (continuous: time-locked to type I response)
Pupil dilation (EyeLink 1000: time-locked to type I response)

13. Indices

See analysis plan section below

Design Plan

14. Study type

Observational Study - Data is collected from study subjects that are not randomly assigned to a treatment.

15. Blinding

No blinding is involved in this study.

16. Study design

The protocol includes two different conditions. For the active condition, a stimulus (two arrays of dots) is briefly (60 ms) shown after a random preparation period (fixation cross; 500 – 1500 ms). Subjects are instructed to indicate which of the two arrays contains the more dots by pressing a button with the left or right hand (type I task). The difficulty of the first order task will be titrated with a 1-up/2-down staircase procedure prior to the experiment, so that average task accuracy is 71% (Levitt, 1971). To ensure sufficient number of errors in the type I task, participants are instructed to respond in less than 500ms. An auditory feedback is played in case they take longer. Participants then report the confidence in their response (type II task) using a continuous scale ranging from 0 to 1 (0: I am sure I made a mistake; 1: I am sure I was correct). A random inter-trial interval of 1-2 seconds will be enforced, during which subjects can blink before the next trial.

During the observation condition, we replay the trials of the motor condition (identical timings and error distribution), permuting the trial order. The observation condition follows the exact same procedure as the motor condition, except that the first order task is performed by an avatar: participants see a hand pressing the right or left button, and have to indicate in the second order task the confidence they have that the hand was correct.

The protocol is divided into 6 runs with active/observation condition alternating every 12 trials. A run is composed of 48 trials, leading to 8 min runs. Altogether, we will record 144 trials in each condition. The total scanning time will be of approximately 1 hour, including breaks for the subjects to relax and rest.

17. Randomization

Trial order in the observation condition is randomly permuted.

Analysis Plan

18. Statistical models

Behavioral data (Q1)

Q1 (*is metacognitive monitoring better for committed vs. observed errors?*) will be answered using the behavioral data. Metacognitive performance will be primarily analyzed with binomial mixed-effects models between accuracy and confidence, with condition (active vs. monitoring) as a within-subject factor. Regression slope will be taken as an indicator of metacognitive performance and asymptotes as a marker of confidence bias (i.e., the tendency to report high or low confidence ratings independent of task performance, Rausch, et al., 2015). Significance will be assessed by likelihood ratio tests. Covariates of interest (e.g., reaction times) may be added to the model in a secondary analysis, after main differences between conditions are established.

All analyses will be performed with R (2016), using notably the afex (Singmall et al., 2015), BayesFactor (Morey & Rouder, 2015), ggplot2 (Wikham, 2009), lme4 (Bates et al., 2014), lmerTest (Kuznetsova, Brockhoff & Christensen, 2015), and effects (Fox, 2003) packages. In all ANOVAs, degrees of freedom will be corrected using the Greenhouse-Geisser method when needed.

fMRI data (Q2)

The answer to Q2 (*what are the common and distinct brain regions involved for detecting committed vs. observed errors?),* will be provided by fMRI results. We will compare error contrasts for the motor task (Error > Correct) with contrasts for the monitoring task (Error > Correct). The task differences (e.g. type I response vs. visual feedback) will cancel out in the Error > Correct contrast, leaving only the error-related activity.

Pre-processing: whole-brain 64 slices volumes will be acquired with a TR of 1.28 s using a multiband acceleration factor of four. B0 inhomogeneities will be corrected using field mapping, as long as the correction leads to improved images. Using SPM12 (Wellcome Trust Centre for NeuroImaging, UCL, London, UK), images will be realigned to the mean EPI and coregistred to individual T1 anatomical scans. After spatial normalization, a spatial smoothing will be applied.

Statistical analysis: our first goal is to find brain regions activated by errors during motor and monitoring. For this we will construct a first GLM with four regressors: correct and erroneous response during during the active and observation condition. Each regressor will be time-locked to the stimulus onset and will have a duration equal to the response time of the type I response. Each of the four regressors will additionally be parametrically modulated by the confidence ratings of the subjects, thus leading to a total of eight regressors. Finally, regressors of no interest will be added to the GLM: realignment parameters and a regressor with bad trials (late type I response, no type I response, no type II response). Different combinations of motion regressors will be tested (e.g., 6 regressors vs. Volterra expansion). Group-level analysis will be conducted using random-effect analysis and reported after correction for multiple comparisons.

Our contrasts of interest will thus be Error > Correct during the motor task and Error > Correct during the monitoring task. We can then perform two second-level analysis. First, the difference of error activity between tasks: (Error>Correct) motor > (Error-Correct) monitoring. Since low-level motor and visual-processing neural processes will cancel out in the first-level contrast, this analysis will not be confounded by task-related differences such as the type I response in the motor task versus the observation in the monitoring task. Second, we will perform a conjunction analysis to find the brain regions that are co-activated in both tasks in case of errors. Finally, we will repeat the previous two second-level analysis on the parametrically modulated regressors to find which brain regions covary with the confidence ratings. We will also use the slope of the logistic regression between confidence and accuracy as a covariate of interest, which will allow us to define the regions associated with metacognitive monitoring, as described in previous studies (e.g., Fleming et al., 2010; 2012). Analysis will be conducted using SPM12 (Wellcome Trust Centre for NeuroImaging, UCL, London, UK).

Electrophysiological data

To answer Q3 (*how does neural monitoring of committed vs. observed error unfold over time?*) we will first analyze how the event-related potentials (ERPs), previously described in the literature on error monitoring and confidence judgements are modulated by the experimental manipulation.

Preprocessing: continuous EEG will be acquired at 5000 Hz with a 64-channels MRI compatible Brainamp system. MR and pulse artifacts due to the simultaneous EEG and fMRI recording will be corrected using Brain-

Vision Analyzer 2.1. software. In particular, gradient artifacts will be detected and corrected using a sliding average template subtraction with 21 intervals (Allen et al., 2000). The pulse artifact correction will be performed with a semi-automatic mode, based on the pulse channel FT10 with no time delay, and manual check for correct peaks detection. Signal preprocessing will be performed using custom Matlab (Mathworks) scripts using functions from the EEGLAB toolbox. Following visual inspection, artifact-contaminated electrodes will be removed for each participant. A band-pass frequency filter between 1 and 10 Hz will be applied in order to remove residual scanner artifacts (present above 12 Hz), and the continuous signal will be re-referenced to the channels average. Epoching will be performed at type I response onset, and each epoch will be assigned the corresponding behavioral data. Epochs will be removed based on too long reaction times (>500 ms), or lack of response to type I or II task. For each epoch, a baseline correction will be performed based on an associated window belonging to the current trial, but prior to any stimulus presentation. Following visual inspection and rejection of epochs containing artifactual signal, independent component analysis on a number of principal components selected to explain 99% of the signal variance will be applied to individual data sets, followed by a semi-automatic detection of artifactual components (Chaumon et al., 2015). After artifacts rejection, artifact-contaminated electrodes will be interpolated using spherical splines (Perrin, Pernier, Bertrand, & Echallier, 1989).

Statistical analysis: voltage amplitude and oscillatory power within canonical frequency bands will be averaged within temporal windows (e.g., 20ms), and analyzed with linear mixed effects models using R together with the lme4 and lmerTest packages (lme4 and lmerTest packages: Bates et al., 2014; Kuznetsova et al., 2014). This method allows analyzing single trial data, with no averaging across condition or participants, and no discretization of confidence ratings (Bagiella, Sloan, & Heitjan, 2000). Models will be performed on each latency and electrode for individual trials, including raw confidence rating and accuracy as fixed effects, and random intercepts for subjects. In particular, two models will be generated: the first explaining the signal amplitude depending on the participant's accuracy (correct vs incorrect answers), and the second modeling the signal amplitude as a function of the raw confidence ratings. The two models will be performed for both active and observation condition separately. Statistical significance for electrophysiological data within regions of interest (e.g., fronto-central and parietal scalp regions) will be assessed after correction for false-discovery rate. When possible, cluster-based permutation tests will be used.

EEG-fMRI fusion (Q3)

To answer Q3 (*how do neural responses following committed vs. observed error unfold over time?*), we will quantify how the brain regions defined above (region of interest; ROI) explain the electrophysiological data at each time point (Hauser et al., 2015). Single trial BOLD activations will be estimated with a second GLM with one regressor per trial. The weights of the trial regressors will be averaged for each ROI and used as dependent variables to regress the EEG signal at every time point. This procedure will lead to as many models as samples in the epochs used to compute the ERP (see below). The weights of these models can then be averaged between subjects and tested against zero (one sample t-test, corrected for multiple comparisons using non-parametric cluster-based permutation tests (Maris and Oostenveld, 2008). The surviving weights will indicate a significant contribution of the corresponding ROI at the corresponding latency. This analysis will thus inform us about when ROIs contributing to the ERP are activated. Using the contrasts on parametric regressors from the first GLM (Q2), we will define which ROIs covary with confidence and which ROIs covary with error detection only and thus build a model of how confidence builds up over time.

19. Transformations

Data will be transformed in case they violate the assumption of normality (e.g., inverse reaction times).

20. Follow-up analyses

NA

21. Inference criteria

Two tailed tests with condition as within-subject factor will be used. The threshold for significance will be set to alpha = 5%. When possible, Bayes factors will be computed to support null findings, and set stopping rules (see above).

22. Data exclusion

The first trials of each condition will be excluded from analysis if they contain large variations of perceptual signal (e.g., staircase convergence issue).

Only trials with reaction times between 100 ms and 500 ms for the type I task will be kept for analysis.

Participants will be excluded in case they cannot reach 71% accuracy on the type I task, respond in more than 500ms in a majority of trials, or in case they do not use the confidence scale properly (e.g., no variance in confidence reports).

23. Missing data

The use of mixed models applied to behavioral and electrophysiological data will allow dealing with unbalanced datasets, so that data imputation will not be needed.

24. Exploratory analysis (optional)

Besides mixed logistic regressions, metacognitive performance will be analyzed using second-order signal detection theory: meta-d' will reflect the amount of perceptual evidence available when performing confidence judgments (Maniscalco & Lau, 2012). Confidence biases will also be computed with receiver operating characteristic curves (ROC): the area between the ROC and major diagonal will be divided by the minor diagonal, and confidence bias will be defined as the log ratio of the lower and upper area. Following previous studies (Schurger, Kim, & Cohen, 2015), we will examine gaze fixation and pupil dilation as a function of confidence ratings. Pupil dilation will be measured continuously (Eyelink). Pupil dilation has long been regarded as participating in decision making processes, specifically as a psychophysiological marker of decision uncertainty (Nassar et al., 2012; Preuschoff et al., 2011) and have recently been related to confidence ratings and metacognitive accuracy (Hauser et al., 2017; Lempert et al., 2015). In particular, Lempert et al., (2015) reported a negative correlation between pre-decisional pupil dilation and confidence ratings, as well as a modulation of metacognitive accuracy on the relationship between post-decisional pupil dilation and confidence ratings. We will try to reproduce the same findings and inspect possible differences between the active vs observation condition.

Cardiac pulse will be measured together with the EEG signal for motion and ballistocardiogram artifact removal. Besides this main purpose, it will allow us to quantify heart rate as a function of type II performance. Based on previous findings in healthy participants (Allen et al., 2016), we expect greater confidence to be associated with faster heart rate between stimulus onset and type II response. We will attempt to replicate these findings

following the same methods as Allen and colleagues, and compare this effect in the active vs. observation condition.

To explore time-varying functional connectivity between brain regions activated by errors, we will use co-activation patterns (Liu and Duyn, 2013, Karahanoglu and Van De Ville, 2015).

Curriculum Vitae

MICHAEL PEREIRA
Date of birth: 15. May 1985
Av. du Petit-Beaulieu 1
1004 Lausanne
(T) +41 79 409 97 46
(E) mpereira@riderules.com

Objectives

I have a strong experience in neuroimaging techniques, including EEG, ECoG and fMRI. As an engineer and neuroscience enthusiast, my goal is to bring the knowledge of signal processing and machine learning to neuroscience. I thus hope to contribute to our understanding of the interaction between motor control, cognitive processes and neurobiology with translational applications.

Core experience

2012-2017	***PhD in Electrical Engineering, EPFL, Lausanne (CH)***
	Using neuroimaging techniques to investigate interactions between cognitive processes and motor control during continuous visually-guided movements. (Co-)supervision of three Master thesis students and three interns. Teaching assistant for *brain-computer interfaces* (two semesters) and *data analysis* classes (two semesters).
2010-2012	***Junior research engineer at Sony Deutschland GmbH, Stuttgart (DE)***
	Signal processing and machine learning for speech and music. Supervision of two master projects.
2009-2010 (6 m)	***Master thesis at Sony Deutschland GmbH, Stuttgart (DE)***
	Speech enhancement for GSM communication (grade: 6/6)
2008-2009 (6 m)	***Internship at Sony Deutschland GmbH, Stuttgart (DE)***
	Speech enhancement for GSM communication
2007 – 2010	***Master in Communication Systems, EPFL, Lausanne (CH)***
	Focus on signal processing and cryptography (GPA: 5.33/6.00)
2000 – 2009	***Co-funder, Busimex, Lausanne (CH)***
	Website design and server maintenance

Technical skills

Neuroimaging:	EEG (incl. closed-loop decoding), fMRI (incl. combined EEG-fMRI), ECoG/LFP, tACS/tDCS
Technical:	Data analysis, signal processing, machine learning, brain-computer interaction, neuroprosthetics
Programming:	MATLAB, Python, C/C++, Java, Latex, HTML/PHP/MySQL

Selected scientific contributions

Accepted	**Pereira**, Sobolewski and Millán (2017), *Action monitoring cortical activity coupled to sub-movements*. eNeuro. (Journal paper)
Accepted	**Pereira**, Sobolewski and Millán (2016), *Theta phase coupling with rhythmic motor output during visuomotor tracking*. In Proceedings of the 6th International Brain-Computer Interface Meeting, Asilomar (CA), US. (conference paper).
Accepted	**Pereira**, Sobolewski and Millán (2015), *Modulation of the inter-hemispheric asymmetry of motor-related brain activity using brain-computer interfaces*. In Engineering in Medicine and Biology Society (EMBC), Milano, IT. (conference paper).
Under revision	Corbet, Iturrate, **Pereira**, Perdikis and Millán, *Sensory threshold neuromuscular electrical stimulation fosters motor imagery performance*. (Journal paper)
Under revision	Iturrate, Chavarriaga, Zhang, **Pereira**, Corbet, Leeb and Millán, *Dissociable neural imprints of hand grasping types from EEG. (Journal paper)*
In prep.	**Pereira**, Sobolewski and Millán, *Ipsilateral sensorimotor cortex activation correlates with hand kinematics during continuous visually-guided movements.* (Journal paper)
In prep.	**Pereira***, Iturrate*, Faivre*, Serafini, Martin, Desvachez, Blefari, Blanke, Van De Ville and Millán, *Performance monitoring during decision making and observation under uncertainty.* (Journal paper). (*shared authorship).
In prep.	Iturrate*, **Pereira***, Giraud and Millán, *Closed-loop decoding of EEG during transcranial alternating current stimulation.* (Journal paper). (*shared authorship).
Reviewer	Journal of Neural Engineering (IOP), 3 reviews (2017).

Languages

English (C2 TOEFL, fluent), French (native speaker), Spanish (excellent command), German (B2 certification, very good command)

Personal interests

Skiing (ski teacher in 2007), skitouring, mountaineering, surfing, kitesurfing, travelling and reading.